Directed Evolution of Lysine Deacetylases

Dissertation

zur Erlangung des akademischen Grades des Doktors der Naturwissenschaft

(Dr. rer. Nat)

Vorgelegt der Fakultät für Chemie und Chemische Biologie

der Technischen Universität Dortmund

Angefertigt am Max-Planck-Institut für molekulare Physiologie

in Dortmund

Vorgelegt von

Martin Spinck

mpi dortmund

technische universität dortmund

1st referee: Prof. Dr. Daniel Summerer

Chemical Biology, Chemical Biology of Nucleic Acid

Faculty of Chemistry and Chemical Biology

Technical University Dortmund

2nd referee: Prof. Dr. Andrea Musacchio

Mechanistic Cell Biology

Max-Planck-Institute of Molecular Physiology, Dortmund

Honorary Full Professor, University of Duisburg-Essen, Germany

Date of Submission: 02.06.2020

For my family.

Formal declaration

The work described in this dissertation was carried out between October 2016 and April 2020 under the guidance of Prof. Dr. Heinz Neumann at the Max-Planck-Institute of Molecular Physiology, Dortmund.

I hereby declare that I carried out the work independently and did not use any aid, other than the ones mentioned.

Eidesstattliche Erklärung

Die vorliegende Arbeit wurde in der Zeit von October 2016 bis April 2020 am Max-Planck-Institut für Molekulare Physiologie in Dortmund unter der Anleitung von Prof. Dr. Heinz Neumann durchgeführt.

Hiermit erkläre ich, dass ich die vorliegende Arbeit selbstständig und nur mit den angegebenen Hilfsmitteln angefertigt habe.

PUBLICATIONS AND CONTRIBUTIONS:

The work in this thesis was published and is available here:

Spinck, M., Neumann-Staubitz, P., Ecke, M., Gasper, R. and Neumann, H. (2020), Evolved, Selective Erasers of Distinct Lysine Acylations. Angew. Chem. Int. Ed.. Accepted Author Manuscript. doi:10.1002/anie.202002899

Spinck, M., Ecke M., Sievers S., and Neumann, H. (2018) Highly Sensitive Lysine Deacetylase Assay Based on Acetylated Firefly Luciferase Biochemistry 2018 57 (26), 3552-3555 doi:10.1021/acs.biochem.8b00483

Spinck, M., Ecke M., Schiller D., and Neumann, H. (*in press)* Directed Evolution of Lysine Deacetylases, Methods in Molecular Biology

Patent:

Neumann H., Spinck M., KDAC VARIANTS AND USES THEREOF, WO2019057925A1, applied: 2017-09-22, published: 2019-03-28

The figures used in this thesis are adapted and/or extended from the original publications.

I want to acknowledge the contribution to this work from Maria Ecke. She contributed greatly to the work on Sirt1 in the chapter “Creation of Acetyl-Selective Sirt1 Variants” and Petra Neumann for her help to carrying out the microscopy in chapter “Manipulations of Cellular Acylation Patterns using CobBac2”

Table of Contents

List of Abbreviations

5-FOA	-	5-fluoroorotic acid
ac	-	acetyl lysine (mutation)
AcK	-	acetyl lysine (amino acid)
ADP	-	adenosine di-phosphate
ADPr	-	adenosine diphosphate ribose
Arg	-	arginine
ATP	-	adenosine triphosphate
AUG	-	amber stop codon
boc	-	*tert*-butyloxycarbonyl -lysine
BSA	-	bovine serum albumin
bu	-	butyryl lysine (mutation)
BuK	-	butyryl lysine (amino acid)
CMV	-	cytomegalovirus
COMAS	-	Compound Management and Screening center
cr	-	crotonyl lysine (mutation)
CrK	-	crotonyl lysine (amino acid)
ddH20	-	double-distilled water
DLR	-	dual luciferase reporter
DNA	-	deoxyribonucleic acid
E. coli	-	escherichia coli
ESI	-	electrospray ionization
FACS	-	fluorescence activated cell sorting
Fluc	-	fierfly luciferase
GCE	-	genetic code expansion
GFP	-	enhanced) green fluorescent protein
gRNA	-	guid ribonucleic acid
HAT	-	acetyl-transferases
HDAC	-	histone deacetylase
HEK	-	human embryonic kidney
His	-	histidin
ID	-	identification
kDa	-	kilo dalton
KDAC	-	lysine deacetylases
LB	-	lysogeny broth
MS	-	mass spectrometry
MyK	-	myristoyl lysine
Myo	-	myoglobin
NAD	-	nicotinamide adenine dinucleotide
NAM	-	nicotinamide
NEB	-	new england biolabs
NLS	-	nuclear localisation signal
NTA	-	nitrilotriacetic acid
ON	-	overnight
ONC	-	overnight culture
OS	-	operating system
PCR	-	polymerase chain reaction
pr	-	propionyl lysine (mutation)
PrK	-	propionyl lysine (amino acid)
PylRS	-	pyrrolysyl-trna synthetase
RNA	-	ribonucleic acid
RT	-	room tempereture
SN	-	supernatant
tRNA	-	transfer ribonucleic acid
Ura	-	uracil
Ura3	-	orotidine 5'-phosphate decarboxylase
wt	-	wildtyp

For abbreviations of chemicals see chemical list.

ABSTRACT

Every cell in the human body contains the exact same genetic information in their nucleus but despite this cell function, structure and content can differs significantly. The reason for this is found in the epigenetic information, a complex code of chemical modification on the chromatin proteins and DNA which determines cellular identity. This code recently grew in complexity with the discovery of lysine acylation on histone proteins. Lysine acylation is related to lysine acetylation and spans a wide range of acyl-Coa derived modifcations like lysine propionylation, butyrylation, or crotonylation up to long chained myristoylation. All these modifications are installed and removed by a relatively small set of substrate promiscuous lysine acetyltransferases and deacetylases, respectively. The large extend of substrate promiscuity has hindered our understanding of acylation as part of the epigenetic code so far.

Here I present a directed evolution-based approach to alter deacylation selectivity of lysine deacetylases allowing for the manipulate of cellular acylation patterns and I developed novel methodology to rapidly measure deacylation activity. Both methods are based on genetic code expansion, a method to genetically encode unnatural amino acids in place of an amber stop codon into proteins, including various lysine acylations. I found that by acylation of the catalytic lysine of Orotidine 5'-phosphate decarboxylase (Ura3) its activity becomes dependent on deacylation and allows for selection of *E.coli* cells. Through the use of acylated firefly luciferase a highly sensitive KDAC deacylation assay was established.

The Ura3 selection system was able to select the *E.coli* Sirtuin CobB, and the human Sirtuins 1, 2, 3, 6 and 7 as well as the human histone deacetylase HDAC8. Selection of 40 million CobB mutants produced a wide range of acyl-selective mutants, as well as mutants exhibiting deallylation and boc- deprotection activity. Particularly interesting

was the $CobB_{ac2}$ mutant, which lost all decrotonylation activity but maintained all other deacylation activities. The crystal structure of $CobB_{ac2}$ revealed that crotonyl binding stabilized a novel conformation of the cofactor binding loop. Addition of NAD^+ caused the reaction to stop at intermediate 3, which could not be hydrolyzed due to the positioning of the cofactor binding loop. Expression of $CobB_{ac2}$ in mammalian cells removed all acylation except crotonylation, showing its potential to alter the epigenetic code. The same selection procedure was used to identify acetyl selective Sirt1 mutants and to isolate Sirt6 mutants with increased deacetylation activity.

The acylated firefly luciferase was further developed into an assay for drug discovery. In cooperation with the COMAS we identified novel scaffolds for Sirt1 inhibition, which is comparable in potency to Ex527 but more selective for Sirt1. Screening of activators could not identify potent chemical activators, but surprisingly we found that the native C-terminal lamin A peptide strongly activates Sirt1 decrotonylation.

In the future acyl-selective deacetylases will make an important contribution to a better the understanding of acylation in various biological processes such as aging, cell differentiation and metabolism.

ZUSAMMENFASSUNG

Jede Zelle im menschlichen Körper enthält genau die gleiche genetische Information in ihrem Zellkern, aber trotz dessen können sich Zellfunktion, Struktur und Inhalt erheblich unterscheiden. Der Grund dafür liegt in der epigenetischen Information, einem komplexen Code aus chemischen Modifikation der Chromatinproteine und der DNA, welcher die zelluläre Identität bestimmt. Dieser Code wurde kürzlich mit der Entdeckung der Lysinacylierung an Histonproteinen noch komplexer. Die Lysinacylierung hängt mit der Lysinacetylierung zusammen und umfasst einen weiten Bereich von Acyl-Coa-abgeleiteten Modifikationen wie Lysinpropionylierung, Butyrylierung oder Crotonylierung bis hin zur langkettigen Myristoylierung. Alle diese Modifikationen werden durch einen relativ kleinen Satz von promiskuitiven Lysinacetyltransferasen bzw. Deacetylasen des Substrats installiert und entfernt. Das große Ausmaß der Substrats Promiskuität hat unser bisheriges Verständnis der Acylierung als Teil des epigenetischen Codes behindert.

Hier präsentiere ich einen gerichteten evolutionären Ansatz zur Veränderung der Deacylierungsselektivität von Lysindeacetylasen, der die Manipulation zellulärer Acylierungsmuster ermöglicht, und entwickelte neue Methode zur schnellen Messung der Deacylierungsaktivität. Beide Methoden basieren auf der Erweiterung des genetischen Codes, einer kürzlich entwickelten Methode zur genetischen Codierung unnatürlicher Aminosäuren, einschließlich verschiedener Lysinacylierungen, anstelle des Bernstein Stopcodons in Proteine. Ich fand heraus, dass durch Acylierung das katalytische Lysin der Orotidin-5'-phosphat-Decarboxylase (Ura3) seine Aktivität von der Deacylierung abhängt und die Selektion von *E. coli*-Zellen ermöglicht. Mittels Acylierter Fierfly-Luciferase konnte ein hochempfindlicher KDAC-Deacylierungsassay etabliert werden.

Das Ura3-Selektionssystem war in der Lage das E. coli Sirtuin CobB und die humanen Sirtuine 1, 2, 3, 6 und 7 sowie die humane Histondeacetylase HDAC8 zu selektieren. Die Selektion von 40M CobB-Mutanten erzeugte eine breite Palette von Acyl-selektiven Mutanten sowie Mutanten, die aktivität für Deallylierung- und Boc-Entschützung zeigten. Besonders interessant war die $CobB_{ac2}$-Mutante, die jegliche Dekrotonylierungsaktivität verlor aber alle anderen Deacylierungsaktivitäten beibehielt. Die Kristallstruktur von $CobB_{ac2}$ zeigte, dass durch die Bindung von Crotonyl eine neue Konfirmation der Cofaktorbindungsschleife stabilisierte wird. Zugabe von NAD^+ führte dazu das die Reaktion am Intermediat 3 stoppte, welches aufgrund der Positionierung der Cofaktorbindungsschleife nicht hydrolysieren werden konnte. Die Expression von $CobB_{ac2}$ in Säugetierzellen entfernte alle Acylierungen mit Ausnahme der Crotonylierung und zeigte sein Potenzial den epigenetischen Code zu verändern. Das gleiche Selektionsverfahren wurde verwendet, um acetylselektive Sirt 1-Mutanten und Sirt 6-Mutanten mit erhöhter Deacetylierungsaktivität zu identifizieren. Die acylierte Glühwürmchen-Luciferase wurde zu einem Assay für die Wirkstoff-entdeckung weiterentwickelt. In Zusammenarbeit mit dem COMAS haben wir eine neue Leitstruktur für die Sirt1-Hemmung identifiziert, deren Wirksamkeit mit Ex527 vergleichbar ist jedoch für Sirt1 selektiver ist. Das Screening von Aktivatoren konnte keine wirksamen chemischen Aktivatoren für Sirt1 identifizieren, aber überraschenderweise fanden wir, dass das native C-terminale Lamin A-Peptid die Sirt1-Decrotonylierung stark aktiviert.

Insgesamt entwickelte ich neue Methoden zur Änderung der Sirtuin Deacylierungs-selektivität und zur Messung der verschiedenen Deacylierungsaktivitäten. In Zukunft werden acylselektive Deacetylasen einen wichtigen Beitrag zum besseren Verständnis der Acylierung in verschiedenen biologischen Prozessen wie Alterung, Zelldifferenzierung und Metabolismus leisten.

INTRODUCTION

Already in the 16th century alchemist discussed the origin of human live and its creation, at the time many alchemist strived to create a homunculus or miniature human (3). The idea of a homunculus as the origin of live was popularized in the following centuries by Anthonii Lewenhoeck who overserved germ cells for the first time using a microscope (4). He adapted the term homunculus to explain how a seemingly small cell could eventually develop into a complex human. At the time, he supported the preformation theory claiming that living organisms already exist in germ cells as fully formed miniature versions (homunculi). The homunculi would possess all features of a grown human and would simply grow in size with time (5). This theory has been long outlived, but the underlying question of how life truly unfolds remains to this day.

THE MISSING LINK BETWEEN GENETIC INFORMATION AND CELL FUNCTION

The foundation of the modern understanding of live was the discovery of the DNA structure and function in the in the middle of the 20th century, uncovering it action as the molecular carrier of genetic information. This discovery also let to the development of the “central dogma” in molecular biology, which states that strings of DNA (genes) are transcribed into RNA, which is translated into protein in a unidirectional process (6). This model could describe for the first time how information could be converted into the building blocks of live, but how this process is orchestrated to form complex organism remained elusive.

The human genome has been fully sequenced in 2004 (7), since then we know for certain that, with very few exceptions, every cell in the human body carries all genetic information required to recreate a full organism. But cells usually only use a fraction of

their genetic information to perform their individual, specific function and cellular identity is maintained even after division, changes in cell identity always occur in an well-defined process. When this process derails for any reason, it can have devastating consequences. One of the most visible examples is a rare type of cancer called teratoma. These cancerous masses can spontaneously form fragments of hair, bone, muscle and teeth (8), clearly showing the presence of the usually unused genetic information. In its most extreme form, this cancer is called homunculus (Fetiform teratoma) as it resembles a malformed fetus possessing partly formed organs and bones (9). While this is an extreme example, the loss of cellular identity is a hallmark of all types of cancer (10). The model of DNA as a simple string of information lacks the explanatory power to describe these dynamic changes observed throughout life.

THE ORIGIN OF EPIGENETICS

This discrepancy between the static nature of genetic information and the dynamic development of live was also recognized in the 1940s by the embryologist C. H. Waddington, which he termed epigenetic (11). The word epigenetic is a combination of epigenesis, a term used to describe the gradual development of an embryo, and genetics, with genes recently redefined as the heritable origin of proteins (12). The idea behind epigenetic was the existence of unknown non-genetic or environmental information that propagates together with genetic information and gives it its dynamic properties (13). Waddington died in 1975 before the molecular mechanisms behind epigenetic information were understood, but nowadays the picture of the DNA and genes has changed. Instead of being viewed as a simple string of information, the importance of different nuclear environments for gene expression and regulation is being recognized.

CHROMATIN AND POSTTRANSLATIONAL MODIFICATIONS

The nucleus does not solely contain DNA, instead it hosts a complex mixture of DNA and protein, known as chromatin. Epigenetics first gained traction with a better understanding of the interaction of histones, the major component of chromatin, with DNA. Inside the nucleus DNA is wrapped around nucleosomes, a complex of the histone proteins H1, H2A, H2B, H3 and H4 (14). The N-terminal tails of the histone proteins in the cylindrical nucleosome reach outwards into the wrapped DNA (15). It turns out that the strength of DNA binding by a nucleosome can be tuned by posttranslational modifications attached to the histone tails (16, 17). The nature of the modification has direct consequences for gene expression, with acetylation increasing and methylation decreasing RNA synthesis in general (18). This led to the proposal of a histone code as carrier of epigenetic information in addition to the genetic code. The histone code is a dynamic and complex pattern of posttranslational modifications which are installed on the histones and regulate the gene activity in their direct proximity (19). The epigenetic code was later extended to also include DNA modifications (20) and topological changes in chromatin superstructures (21). Deciphering the epigenetic code is a current objective in biomolecular research.

THE EPIGENETIC MACHINERY

The complexity of the epigenetic code is immense, because of the large variety of chemical modifications and the great number of residues on each histone that can be modified. Hence, billions of combinations are theoretically possible. But cells only contain a couple of thousand reoccurring epigenetic patterns, as it was found for a limiting set of 39 histone modifications (22). These patterns are controlled by various proteins responsible for the deposition, removal or recognition of the posttranslational

modifications on histones, generally referred to as “writer”, “eraser” or “reader”, respectively (23).

THE SURGE TO DECIPHER THE EPIGENETIC CODE

As the epigenetic code cannot be manipulated as freely as the genetic code can, the last decade was spent researching methods able to understand and manipulate the epigenome (24). The most common tools are small molecule inhibition of histone deacetylases or methyl transferases, which have been developed originally for treatment of cancer but also serve research purposes (25). A critical downside of this approach is the limiting selectivity of epigenetic drugs due to structural similarity and redundancy between the target proteins leading to pleiotropic effects (25). There have been attempts to artificially engineer isoform selective inhibitors using the bump-and-hole approach, which has been originally developed to address redundancy between kinases (26). The approach works by chemically modifying an isoform unspecific ligand to inactivate it and then place a compensating mutation into the target protein to enable binding of the modified ligand. For example, this allowed to differentiate the function of individual bromodomains (reader of acetyl-lysine) within the same protein (27) or to identify the cellular target of acetyl-transferases (HAT) using engineered enzymes and substrates (28). The bromodomain inhibitor was also further developed into a PROTAC resulting in the degradation of the target protein by targeting it to an E3 ligase and subsequent ubiquitylation (29).

These methods were developed to understand the function of the individual epigenetic writers, erases or readers but cannot address any intrinsic substrate promiscuity (30). This thesis aims to resolve this problem in the case of lysine deacetylases and resolve their substrate promiscuity towards different lysine acylations.

STRUCTURE AND FUNCTION OF LYSINE DEACETYLASES

Lysine deacetylases were initially found to erase the ε-acetyl groups of posttranslational modified lysine residues (31). In total, 18 different lysine deacetylases (KDAC) were identified in humans, which are divided into two families and 4 classes (32). The histone deacetylase family (HDACs) consists of 11 members of classes I, II and IV, which share a common ancestor and catalytic core domain (33). The catalytic site of HDACs possesses a metalloprotein α/β-fold with 8 parallel β-sheets surrounded by α-helices, which binds the catalytic Zn^{2+} or Fe^{2+} necessary for the hydrolysis of the acetyl amide bond (34).

The Sirtuin (Sir2-like proteins) family contains seven class III deacetylases. These enzymes developed independently of HDACs and were initially identified as potential ADP-ribose (ADPr) transferases by homology to the yeast Sir2 protein (35). The reason for the presumed ADPr transferase activity is the unique deacetylation mechanism of Sirtuins. In the reaction, the acetyl group from lysine is transferred to the ADPr moiety of NAD^+, producing a free lysine, nicotinamide and 2'-O-acetyl-ADP ribose in the process (36). The exact reaction mechanism (see **Figure 1**) is still disputed; in older models (reviewed Sauve AA. 2010) the deacetylated lysine is release from the bicyclic intermediate 2 before water enters the active site. A new model suggests that a conserved arginine catalyzes the collapse of the bicyclic intermediate by hydrogen bonding and causes a third intermediate to form, which than reacts with water and releases lysine in one step (37). The new model is supported by a crystal structure of Sirt2 in complex with NAD^+ and a thiol-lysine substrate analog. In this structure the deacetylation reaction stopped at a previously unreported 2`-hydroxy-bound lysine intermediate (38).

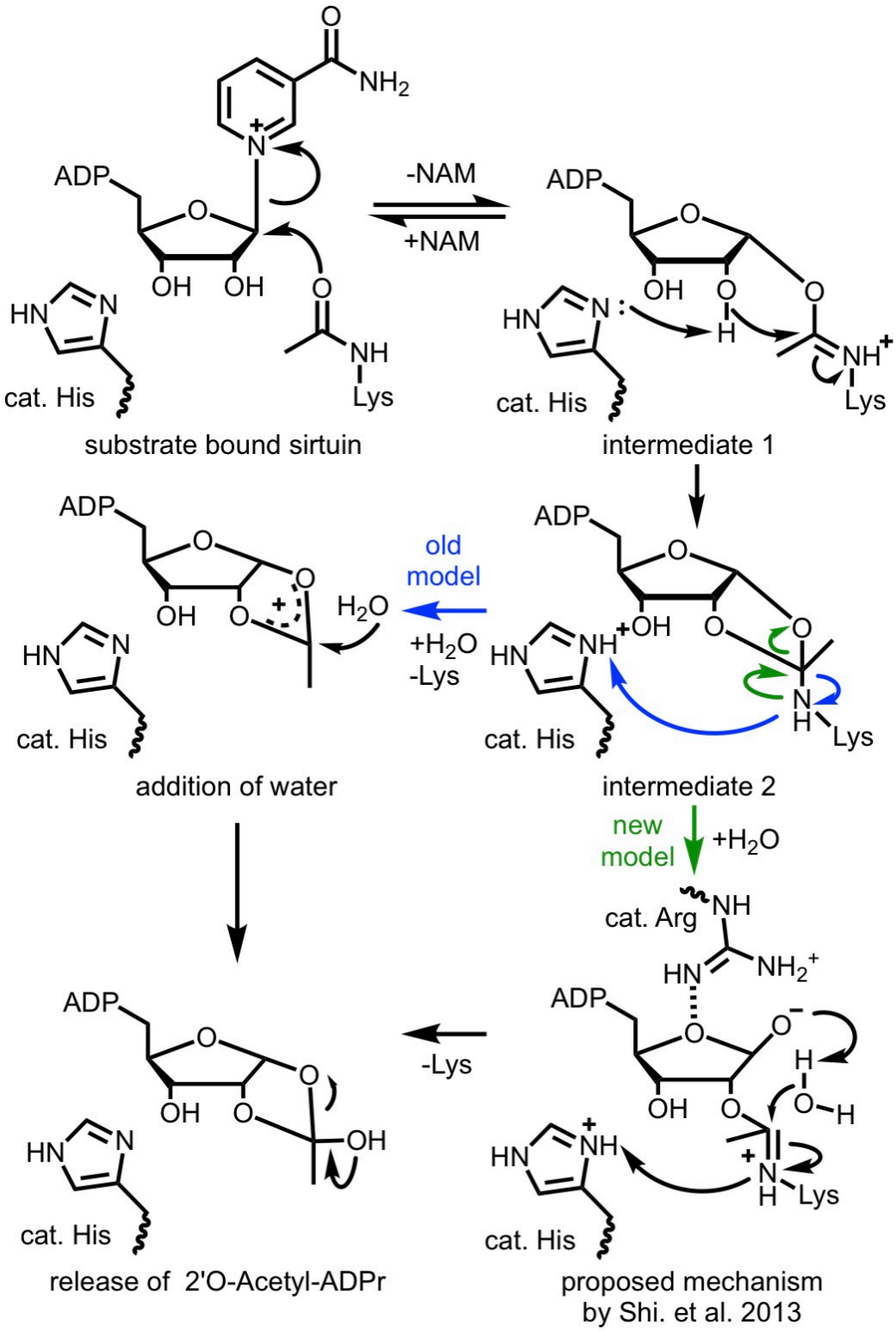

Figure 1: Proposed catalytic mechanisms for the Sirtuin deacetylation reaction. The reaction mechanism up to intermediate 2 is well characterized but two models exist how the intermediate is hydrolyzed. The older model adopted from Sauve AA. In 2010 (36) proposed that lysine is released from intermediate 2 followed by the formation of 2'O-Acetyl-ADPr. The new model proposed by Shi. et al. 2013 is based on molecular dynamic simulations and predicts a third intermediate (37). This stresses the importance of hydrogen bonding (dashed line) by a conserved arginine (Arg) for the reaction.

Even less is known about the ADP ribosylation activity. It has been suggested that ADP ribosylation occurs due to a substrate arginine reacting with the intermediate 1 (39). This is considered a side reaction in many Sirtuins, the only exception to this is the mitochondrial SirT4, which has very good ADP ribosylation activity but low deacetylation activity (40).

A NEW ADDITION TO THE EPIGENETIC CODE: ACYLATIONS

In fact, a lot of Sirtuin enzymes have relatively low to undetectable deacetylation activity, resulting in a controversy regarding Sirtuin function (41, 42). But with the discovery of several posttranslational lysine acylations, several Sirtuins were found to have better lysine deacylation activity than deacetylation (30). Lysine acylations is a broad group of posttranslational modifications chemically related to acetylation. The first acylations discovered were histone butyrylation and propionylation, which are longer acyl chain derivatives than acetyl (43). This was followed by a series of recently discovered acylations (**Figure 2A**) including the unsaturated crotonylation (44) or negatively charged malonylation and succinylation (45). To date, acylations have been identified ranging from polar 2-hydroxyisobutyrylation (46) or β-hydroxybutyrylation (47) to aromatic benzoylation (48) and long-chained acylations like myristoylation (49). How the plethora of modifications is regulated by the relative small number of Sirtuins is not understood but it can be expected that the acylation selectivity of Sirtuins is integral to their biological function.

SUBSTRATE PROMISCUITY IN SIRTUINS

The different isoforms of Sirtuins and HDACs differ quite substantially in their selectivity towards different acylations (50). For example, SirT1-3 were previously known to be the only Sirtuins with high deacetylation activity *in vitro* but they also have high activity for short uncharged acylations like butyrylation or crotonylation and SirT2 also has a

preference for long-chained acylations like myristoylation (51, 52). SirT5-7, for which previously no or low deacetylation activity was found, could now be linked to the removal of other acylations. SirT5 removes negatively charged lysine acylations (53), SirT6 long-chained fatty acids (50) and SirT7 has deacetylation and good debutyrylation activity (54). As diverse as the acylation selectivity of Sirtuins are also the biological functions and cellular localizations. Defects in Sirtuin function have been linked to diseases like cancer and aging (55). Sirtuins are found in the cell nucleus (Sirt1, 6 and 7), the cytoplasma (Sirt1 and 2) or the mitochondria (Sirt3-5), although some isoforms are present in multiple compartments, for example, splice variants of Sirt5 localizes to the cytoplasm and nucleus (56, 57). Due to the role of Sirtuins in cancer, metabolism and aging, they have been proposed to be valuable targets for inhibition or activation by drugs (58). Particularly, inhibitors for Sirt1 have been proposed for the treatment of breast cancer due the stabilizing effect of inhibition on p53 (59). The role of lysine deacylation in this context is unknown, it has been proposed that increased lysine crotonylation might decrease cancer proliferation and metastasis (60).

UNIQUE PROPERTIES OF LYSINE CROTONYLATION

Most acylations share part of the epigenetic machinery with acetylation, like the mentioned KDAC enzymes, but also acetylation-reader like bromodomains (61) and writer like histone acetyl-transferases (62) are promiscuous in their function towards different acylations. For some crotonylations the YEATS domain were discovered, which preferentially recognized crotonyl-lysine over acetyl-lysine and are structurally unrelated to the less specific bromodomains (63). Crotonylation was also one of the first acylations for which a specific function could be assigned during spermatogenesis, since it is highly enriched compared to all other acylations during this process (44).

Crotonylation has the unique property that it is more persistent towards removal by KDACs compared to other acylations and acts as a strongly activating epigenetic mark in the otherwise repressive environment during spermatogenesis (44). To allow decrotonylation, sperm cells have to actively deplete the crotonyl-CoA pool by oxidation to β-hydroxybutyryl-CoA (64). Lysine crotonylation has also been proposed to be involved in maintenance of stem cells pluripotency as well as telomere length, but here the exact mechanism is unclear (65).

The interplay between lysine acylation, like crotonylation, and KDACs in various cellular processes, such as gene expression, energy metabolism, differentiation or aging, has not been widely studied (32, 66, 67). So far these have been mainly linked to the deacetylation activity, but the discovery of other acylations raises the question how much of this function is due to deacylation. In the case of HDAC1 it was possible to separate the decrotonylation activity from the deacetylation activity by mutagenesis. This showed that decrotonylation is sufficient for inducing HDAC1-dependent stem cell differentiation and that crotonylation is required for self-renewal of stem cells (68). So far this has been the only case where acyl-selective mutants were employed to differentiate the acylation-dependent function of KDACs, but the study demonstrates that acyl-selective mutants can be a powerful tool to dissect the function of different acylations.

HOW CAN SUBSTRATE PROMISCUITY BE RESOLVED?

The group of W. Wei (2017) used rational mutagenesis to change the selectivity of substrate-unspecific HDAC1 by creating a chimeric mutant using a conserved sequence in the acetyl-selective class II HDACs (68). This unexpectedly resulted in a crotonyl-selective mutant, demonstrating the limitation of rational approaches. Rational mutagenesis is commonly used in biomolecular research and usually employed to

validate predictions based on structure or biochemical data (69). Such a method, using point mutations (usually substitution with alanine) at the active site, identified the catalytic histidine (70) or the residues responsible for shielding the reaction from water (37, 71) in Sirtuins. This approach also has been used to change the acyl-selectivity of the *E.coli* deacetylase CobB by removing the residues responsible for hydrogen bonding with negatively charged succinylation, yielding two mutants with 3-fold reduced deacetylation and 40-fold reduced desuccinylation activity (72). The mutated residues are not conserved in other Sirtuins, limiting this approach to CobB and succinylation. Such rational approaches are usually limited to specific proteins, which is a known problem in the development of biocatalysts as substrate selectivity is always determined by properties unique to individual enzymes (73). New methods are required to overcome this challenge and obtain acylation selective KDAC mutants of all types.

DIRECTED EVOLUTION AND ENZYME SELECTIVITY

To overcome this issue, I established a directed evolution-based approach to deconvolute the deacylation selectivity of KDACs. Directed evolution exploits diversification by random or site-saturated mutagenesis followed by screening and/or selection for mutants which have novel, desired properties (74). Selection is usually preferred to manual screening as mutagenesis easily creates millions of variants, of which most will be inactive, making manual screening time and labor intensive. The most common ways of selection is affinity enrichment (75), fluorescence activated cell sorting (FACS), (76)) or self-amplification (77) commonly used to increase binding affinity of antibodies or to improve polymerases' transcription efficiency. Selection of enzymes, other than polymerases, requires a link of enzymatic activity to cell survival.

To turn deacetylation into a selectable, cell-survival property I used another method developed by directed evolution, namely genetic code expansion (GCE).

THE CONCEPT OF GENETIC CODE EXPANSION

Genetic code expansion summarizes all methods which allow for the translation of genetically encoded non-natural amino acids by utilizing engineered translational components (78). One of the first GCE systems is based on an unusual observation made when investigating the methane synthesis in methanogenic archaea. It was found by crystallography that the methylamine methyltransferase of *Methanosarcina barkeri* contained an unusual catalytic pyrrolysine residue required for the transfer of methyl groups (79). Surprisingly, the pyrrolysine is not the product of posttranslational modification, instead, it is encoded translationally by the ribosome through a pyrrolysine-charged $tRNA^{Pyl}$, which is complementary to the amber stop codon (AUG) (79). Utilizing directed evolution, it was possible to change the substrate selectivity of pyrrolysyl-tRNA synthetase (PylRS) to charge the $tRNA^{Pyl}$ with other unnatural amino acids. Enabling to genetically encode lysine derivatives opened a whole new research field for functionalizing reactive groups for click chemistry (80), chemical protecting groups (81) and also posttranslational modifications like acylations (82, 83). The PylRS/$tRNA^{Pyl}$ system is also fully orthogonal to the native translational machinery and able to produce quantitatively acylated protein in *E.coli* (84).

DIRECTED EVOLUTION OF LYSINE DEACETYLASES

Without the need for an acetyltransferase (HAT) and the capability to site-specifically acylate proteins in *E. coli* by GCE, it is possible to create a selection system for the directed evolution of lysine deacetylases. It is well documented that lysine acetylation can inactivate enzymatic activity which can be reversed by deacetylation, reactivating the enzyme (85). If the same concept can be mimicked using GCE on an essential

enzyme, it should be possible to make deacylation a selectable feature for the survival of *E.coli* (86). This would make it possible to select large pools of mutants to identify active and selective mutants rapidly (87). Mutant libraries of KDACs can be created based on the available well-described structural and mechanistic data (88). Since the generic approach only requires deacylation activity, it should be possible to select any KDAC active in *E.coli*, which includes all mammalian Sirtuins (89) and some class I HDACs (90). Creating acyl-selective erasers would allow to more systematically alter the epigenetic code and improve our understanding of lysine acylation as an epigenetic marker (**Figure 2**).

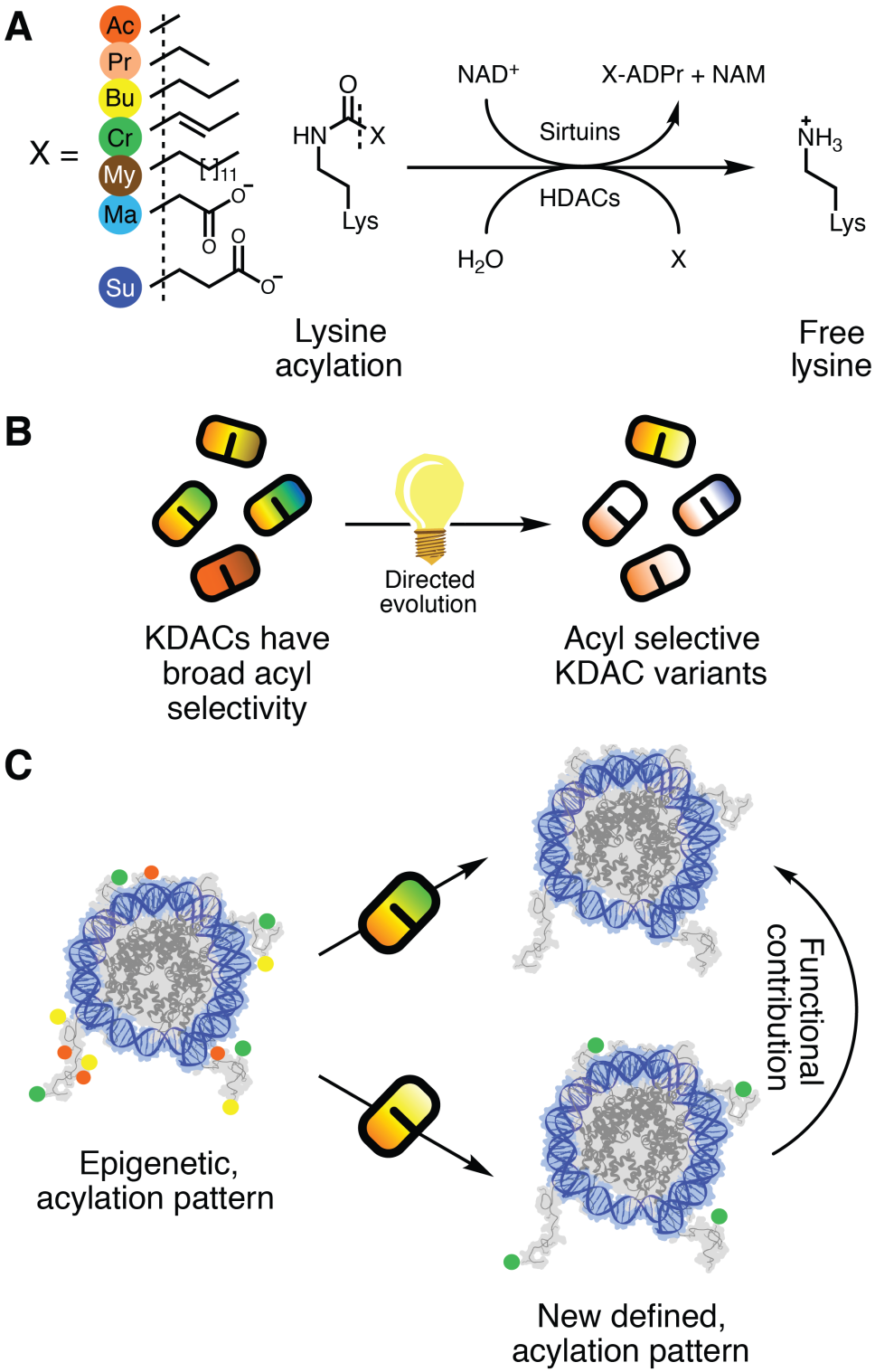

Figure 2: Background (A), objective (B) and prospect (C) for the directed evolution of lysine deacetylases (KDACs). A) Sirtuins and HDACs catalyze the removal of various lysine modifications, individual KDACs usually have a broad spectrum of modifications the are able to remove. The function of these acylation activities is unclear. B) This thesis' aim is to establish the methods necessary to evolve KDACs with designed acylation selectivity. C) Acylation selective mutants could be used to manipulate chromatin acylation patterns to deduce the function of individual acylation.

RESULTS

More and more distinct lysine acylation modifications are identified, however, their impact on transcription rate or cellular functions remains mainly unknown. This is because suitable and straightforward methods are not available to study single lysine acylation or distinct lysine acylation pattern in a cellular context. The key work of this thesis was to establish new methods to address lysine deacylation *in vivo*. I introduced the use of evolved acyl-selective deacetylases as a new method to alter cellular acylation states, either by co-expressing the evolved enzyme or by replacing the endogenous one. In order to do so, I developed a directed evolution selection system based on genetic code expansion, capable of identifying acyl-selective deacetylases from millions of mutants. The directed evolution system consists of a selection system, a novel deacylation assay for high throughput screening and independent validation of the obtained mutants, as well as their biochemical and cellular characterization.

LYSINE DEACYLATION SELECTION SYSTEM

A bacterial selection system is one of the most powerful engineering tools to obtain mutants with new properties. To create a selection system for lysine deacetylases, I used genetic code expansion to express a selectable marker protein, whose activity was inactivated by encoding of an acetyl lysine instead of an essential lysine residue at the active site: The uracil auxotrophic marker Ura3 (Orotidine 5'-phosphate decarboxylase) was used, since it has an essential lysine (K93) which reduces the catalytic efficiency by more than five orders of magnitude when mutated (91). By replacing the lysine 93 by an amber codon, using GCE for expression, Ura3 K93ac will be fully acetylated and therefore totally inactive.

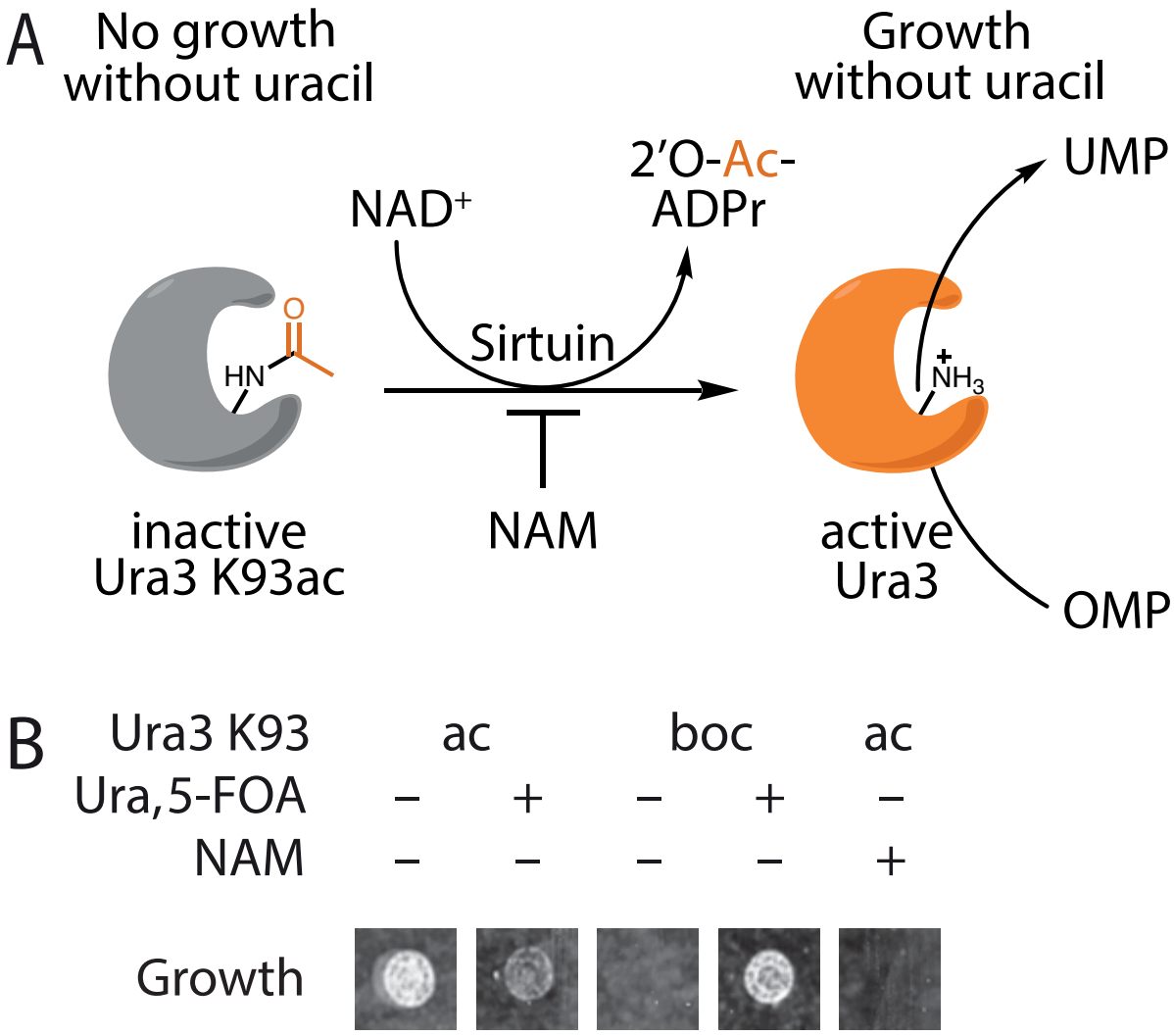

Figure 3: Proof of concept for a lysine deacetylase selection system using genetically encoded lysine acetylation in the Ura3 (Orotidine 5'-phosphate decarboxylase) active site. A) Expression of Ura3 with genetically encoded acetyl lysine at the catalytic lysine 93 fully inactivates the Ura3, thus preventing growth when cells starve of uracil. Enzymes able to remove the active site modification, like Sirtuin deacetylases, should be capable to reactivate the Ura3, enabling growth under starvation conditions. Inhibition of the Sirtuin by its natural inhibitor nicotinamide (NAM, 50 mM) should also prevent growth, as growth is proportional to the Sirtuin activity. B) Patch growth assay of uracil auxotrophic DB6656 *E.coli* (ΔPyrF), which were transformed with a plasmid encoding the amber suppression machinery and a Ura3 K93TAG (ID: 10H6 or 10H7). Growth in the absence of uracil (Ura) was only observed, when acetyl lysine (ac) was encoded at K93. Growth was inhibited by nicotinamide (NAM) and confers sensitivity to 5-fluoroorotic acid (5-FOA), a toxic Ura3 substrate. The reverse is true when a non-cleavable lysine is encoded (*tert*-Butyloxycarbonyl - lysine, boc).

An enzyme capable of removing the acetyl group should reactivate Ura3 and, hence, allow for selection by growth on uracil deficient medium (**Figure 3A**). The consequences of this is that under auxotrophic selection, the growth of individual *E. coli* cells is causally linked to their deacylation activity. This was tested by expressing Ura3 with an amber codon at K93 in an uracil auxotrophic *E.coli* strain (DB 6656). When an acetylated lysine is encoded, cell growth can be observed due to deacetylation by the endogenous CobB. When under the same conditions nicotinamide, a natural inhibitor of Sirtuins, was added, bacterial growth was fully suppressed (**Figure 3B**). This proves that growth is dependent on Sirtuin activity. The addition of 5-fluoroorotic acid (5-FOA) should enable negative selection using the Ura3 marker, since upon conversion by Ura3 it produces the toxic fluorouridine monophosphate (92). Indeed, addition of 5-FOA to the selection system leads to suppression of growth in the presence of uracil (Ura) (**Figure 3B**). This could be circumvented by encoding a non-cleavable lysine modification (*tert*-butyloxycarbonyl - lysine, boc) which confers resistance to 5-FOA and allows growth on plates containing uracil, since Ura3 is inactive due to the modified lysine (**Figure 3B**).

Taken together, my designed selection system, which exploits genetic code expansion to genetically encode an inactive Ura3, worked well for the endogenous *E.coli* deacetylase (CobB). Further, the same marker can be utilized for positive and negative selection by including 5-FOA and uracil in the selection scheme. If the encoded amino acid at K93 is not a Sirtuin substrate, growth does not occur under starvation condition but it conveys resistance to 5-FOA. To test if this system can be applied to other deacetylases, I created a knockout strain of the endogenous CobB (sole E. coli deacetylase) and PyrF (Ura3 homolog).

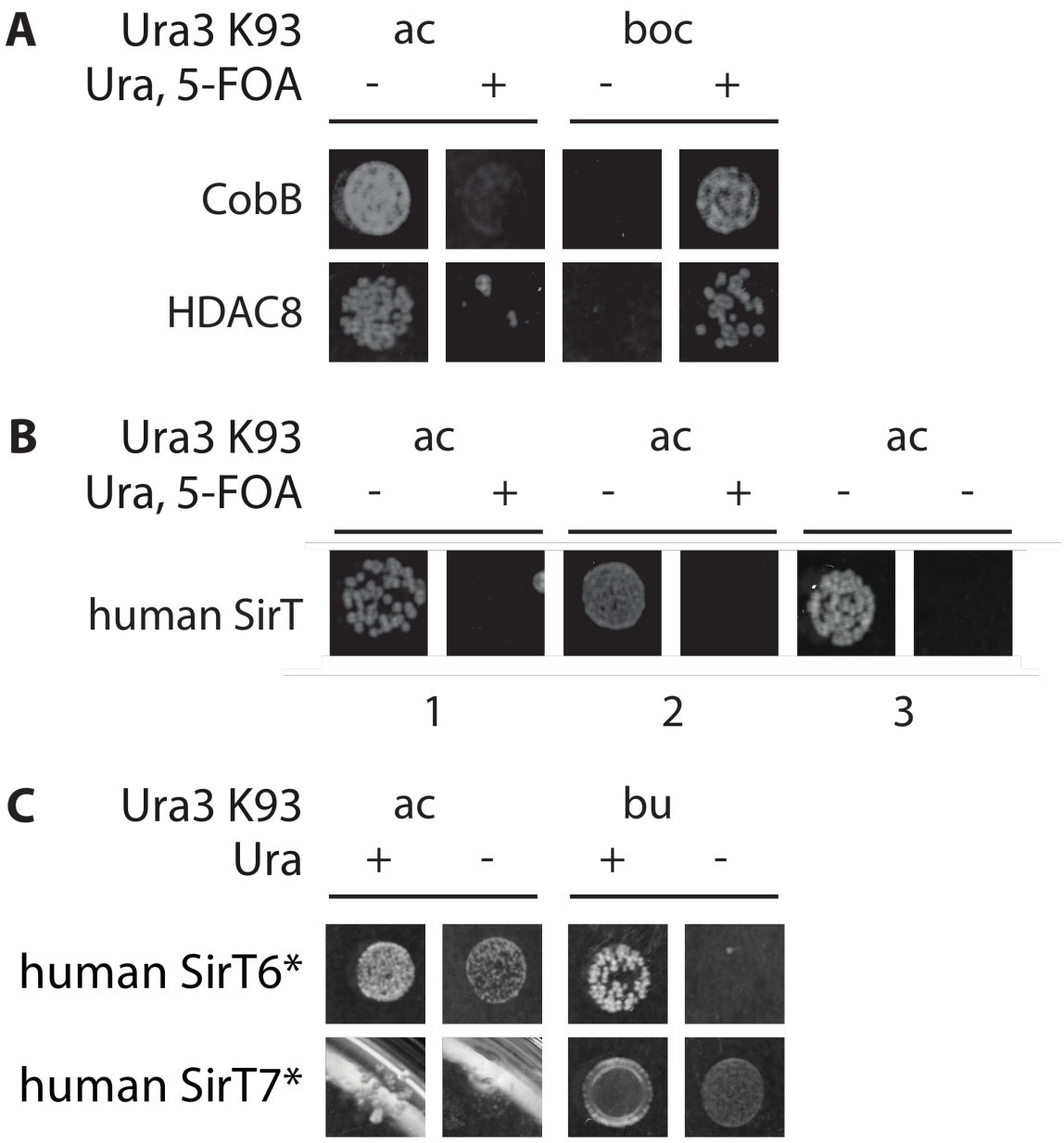

Figure 4: **Patch drop assay of the DH10β ΔPyrF ΔCobB transformed with expression plasmids for different Sirtuins or HDAC8 and the selection system for the indicated Ura3 K93 modification (ac: acetylation bu: butyrylation, or boc: tert-butyloxycarbonyl–lysine).** A) Positive and negative selection of CobB or HDAC8 in the created ΔΔ strain is possible on minimal medium (-) or plates containing uracil (Ura) and 5-fluoroorotic acid (5-FOA), respectively (all plates Sup. Figure 2). B) Positive and negative selection using of Sirt1-3 on acetylation. C) Positive selection of Sirt6 and Sirt7 is possible using acetylated or butyrylated Ura3, respectively. Negative selection was not possible. *slow growth over 3 days.

GENERAL APPLICABILITY OF THE SELECTION SYSTEM

The DH10β (Thermo Fisher) strain was used for the creation of the selection strain, since it is optimized for high transformation efficiency and DNA purifications.Particularly, transformation efficiency is the major bottleneck when screening large mutant libraries (93). The double knockout of PyrF and CobB was created by iterative CRISPR/Cas9 mediated mutagenesis and its identity was confirmed by colony PCR and sequencing of the genomic region in the plasmid cured strain (see **S. Figure 1**). Using the DH10β ΔPyrF ΔCobB strain (ΔΔ) I was able to confirm that selection is possible for various enzymes with deacetylation activity (**Figure 4**).

Initially, the selection for CobB deacetylation was repeated (Sirtuin, *E.coli,* **Figure 4A**) when expressing CobB from a plasmid in the knockout background. The same behavior as previously was observed, namely CobB enables growth on minimal medium when a cleavable acetyl-group was encoded in Ura3 K93 but not, when a non-hydrolysable Boc-group was incorporated. The opposite was true when 5-FOA and uracil were added. Confirming that positive and negative selection in the new strain is feasible, as expected from the initial experiment. Since the endogenous CobB is knocked out, selection of other deacetylases should be possible. This was confirmed for the histone deacetylase HDAC8 (human, **Figure 4A**), which showed the same behavior under the selection condition for CobB (growth when deacetylating Ura3 K93, or K93 carries a boc-group but 5-FOA is added, no growth with 5-FOA). Although HDAC8 is not a Sirtuin like CobB, but shows the same effect growth behavior, lead to the conclusion that selection only depends on deacetylation activity. Selection was also possible for other human promiscuous Sirtuins (Sirt1-3, **Figure 4B**), which was expected considering their strong, intrinsic deacylation activity. Selection for the less

active and more selective human Sirtuins 6 and 7 was possible, but both required longer growth time compared to CobB or Sirt1-3 (**Figure 4C**). Negative selection was tested (not shown) but did not lead to a significant decrease of cell growth, indicating that the amounts of 5-FOA converted by Ura3 is insufficient to cause cell death. Interestingly, Sirt6 could be selected only on acetyl-lysine, while Sirt7 expressing cells grow well on butyryl-lysine. This indicates that the intrinsic acyl preference might affect the screening outcome, both have previously been described to have deacetylation and debutyrylation activity (54).

Overall, the selection system can be used to select for deacetylation activity of all tested deacetylases (Sirtuins and HDAC8) showing general applicability to test for lysine deacylation. Of note is that, depending on the intrinsic activity and selectivity, some differences in growth rate and acyl-selectivity can be observed.

DIRECTED EVOLUTION OF ACYL SELECTIVE COBB MUTANTS

The basic selection system needs to be further developed for high throughput to test libraries of mutated KDACs. The *E. coli* deacetylase CobB was chosen as prove of concept for acyl-selective deacetylases and to establish the selection procedure. While the established selection system will form the core of the directed evolution approach, methods for rapid and quantitative deacylation activity are required. A selection protocol in general must be optimized to minimize the manual screening effort, this includes reducing the occurrence of false positive mutants and enabling the modulation of selection pressure to enrich for the most active mutants. The E. coli deacetylase CobB is highly substrate promiscuous and able to cleave most acyl groups regardless of the sequence context (94), making it an ideal candidate to establish the selection workflow. To generate mutants of CobB with altered acyl binding selectivity the active site of CobB (PDB: 1S5P) was targeted by site directed mutagenesis, randomizing

residues in direct contact to a bound acyl-lysine. (**Figure 5A**). The codons of the residues A75, Y62, R95, I131 and V187 were replaced by the NNK codons, thereby randomizing the amino acids. The final library had all 5 positions fully randomized (**Figure 5B)** and codes for 20^5 (3.2 million) mutants. Selection of the CobB active site library on positive selection plates containing different unnatural amino acids yielded large numbers of colonies on plates containing acetyl or crotonyl lysine, the natural substrates of CobB. Interestingly, E. coli expressing Ura3 K93 substituted by unnatural substrates alloc and boc-protected lysine, produced some colonies, which could indicate novel activity in these CobB mutants. Sequencing of the individual mutants from each plate revealed the presence of a large sequence diversity of CobB, with no mutant dominating the set. All sequenced plasmids were retransformed and retested in a patch drop assay, confirming that the observed growth is not the result of spontaneous strain mutation (S. Table 1 and S. Table 2). The following negative selection for the various mutant pools significantly reduced the overall diversity in the sequenced set, most strikingly for the mutants obtained after positive selection for decrotonylation followed by negative selection against deacetylation, resulting in only the mutant CobB A76H Y92F R95P I131V V187S being found in the final pool (8/8 sequencings, S. Table 2). The activity was again confirmed in a patch drop assay, where the mutant showed good growth on crotonylated but not on acetylated Ura3 K93. While many of the mutants were promising, we decided to further characterize the mutant pool obtained from positive selection for deacetylation activity and against decrotonylation activity. This pool was again selected for deacetylation in a third round of positive selection to enrich more active mutants (negative selection favors more inactive mutants). In total, plasmids from 60 colonies were sequenced, of which 14 different sequences were identified of which 4 dominated the set accounting for 60% of all sequences.

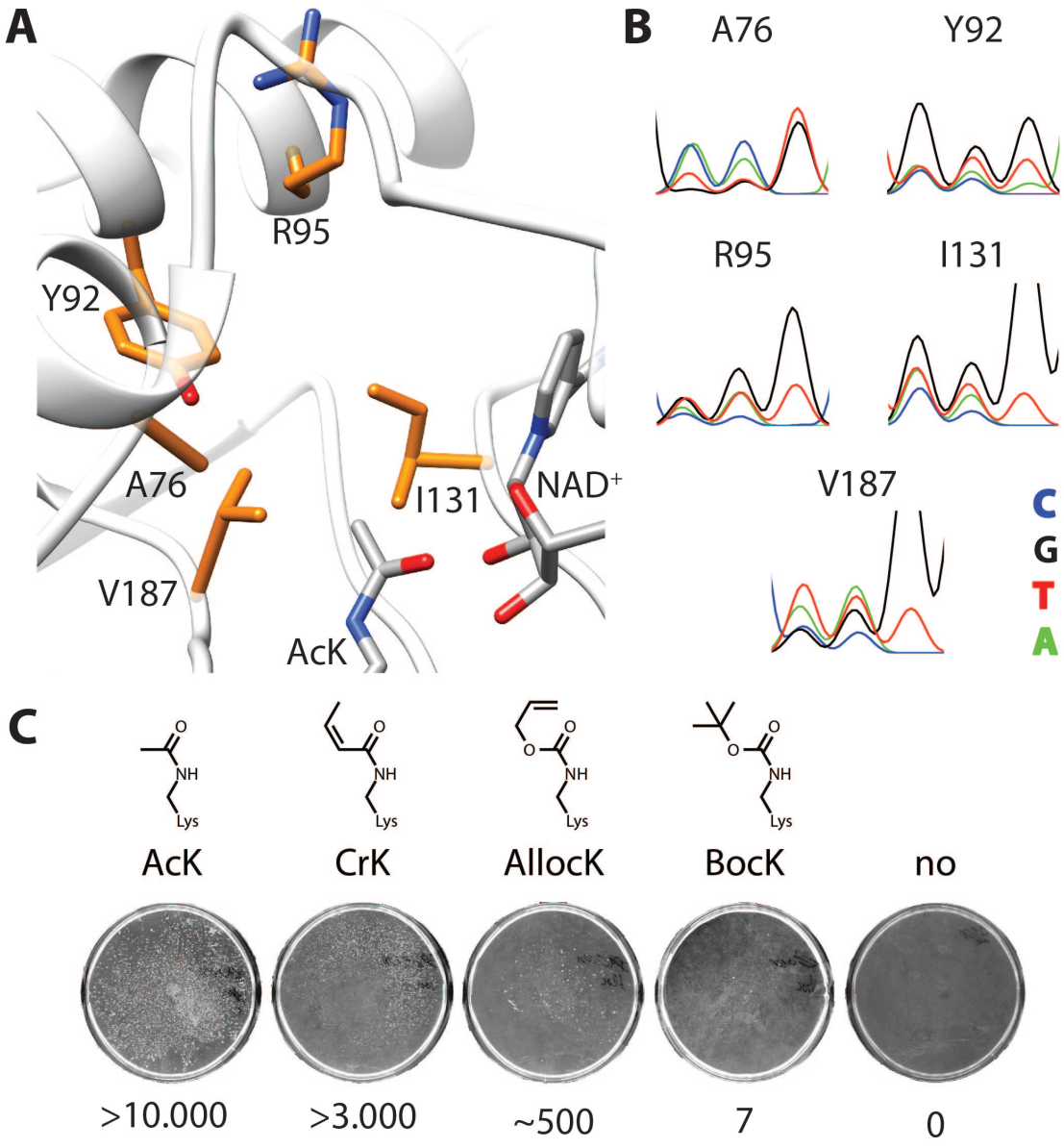

Figure 5: CobB active site library design and first positive selection for activity on natural or unnatural substrates. A) CobB active site with bound acetyl-lysine (AcK, 1S5P) and NAD+ (overlay 2H4F). The highlighted residues (orange) were randomized by site directed mutagenesis to all possible amino acids (NNK, codon). B) Sequencing traces of the final CobB active site library show the successful incorporation of the NNK codon in position of the 5 active site residues. C) Initial positive selection and estimated number of colonies for the CobB library, when different amino acids are encoded. No growth was observed when no amino acid was added.

All mutants were further characterized to better understand the screening outcome and to establish a workflow for future screenings. Since there were no well-established high throughput assays to measure deacylation, a new assay was developed, which will be discussed in the next part.

LYSINE DEACETYLATION ASSAY UTILIZING ACYLATED FIREFLY LUCIFERASE

Firefly luciferase is a commonly used reporter enzyme due to its high sensitivity. It was shown that the luciferase can be inactivated by genetic code expansion by modification of K529, which was used to determine the error rate of translation (95). Therefore, it might be possible to reactivate a K529 acylated firefly luciferase by deacylation (**Figure 6A**). When several of the identified mutated KDACs were co-expressed with dual Renilla-Firefly luciferase K529TAG fusion protein (95) they could reactivate the luciferase (**S. Figure 2**). However, mutants negatively selected for various acylations were found to have lost between 30-90% activity compared to the wt (**S. Figure 2E-F**). It should be noted that the loss was more severe for the deacylation activity they were selected against (See. S. Table 2). For example, CobB A76H Y92F R95P I131V V187S showed higher decrotonylation than deacetylation activity, as expected from the selection for decrotonylation and against deacetylation. To improve the assay, the possibility to use purified FLuc K529ac was tested as an alternative to coexpressing all components. This would only be possible, if the acylated luciferase is folded and soluble, unlike in a previously reported assay for sfGFP in which the acylation prevents fluorescence by preventing the folding of the protein unless rescued during expression by a deacetylase (96). To test this, cell lysate from ΔΔ cells expressing the dual-luciferase construct was treated with purified CobB in the presence and absence of nicotinamide.

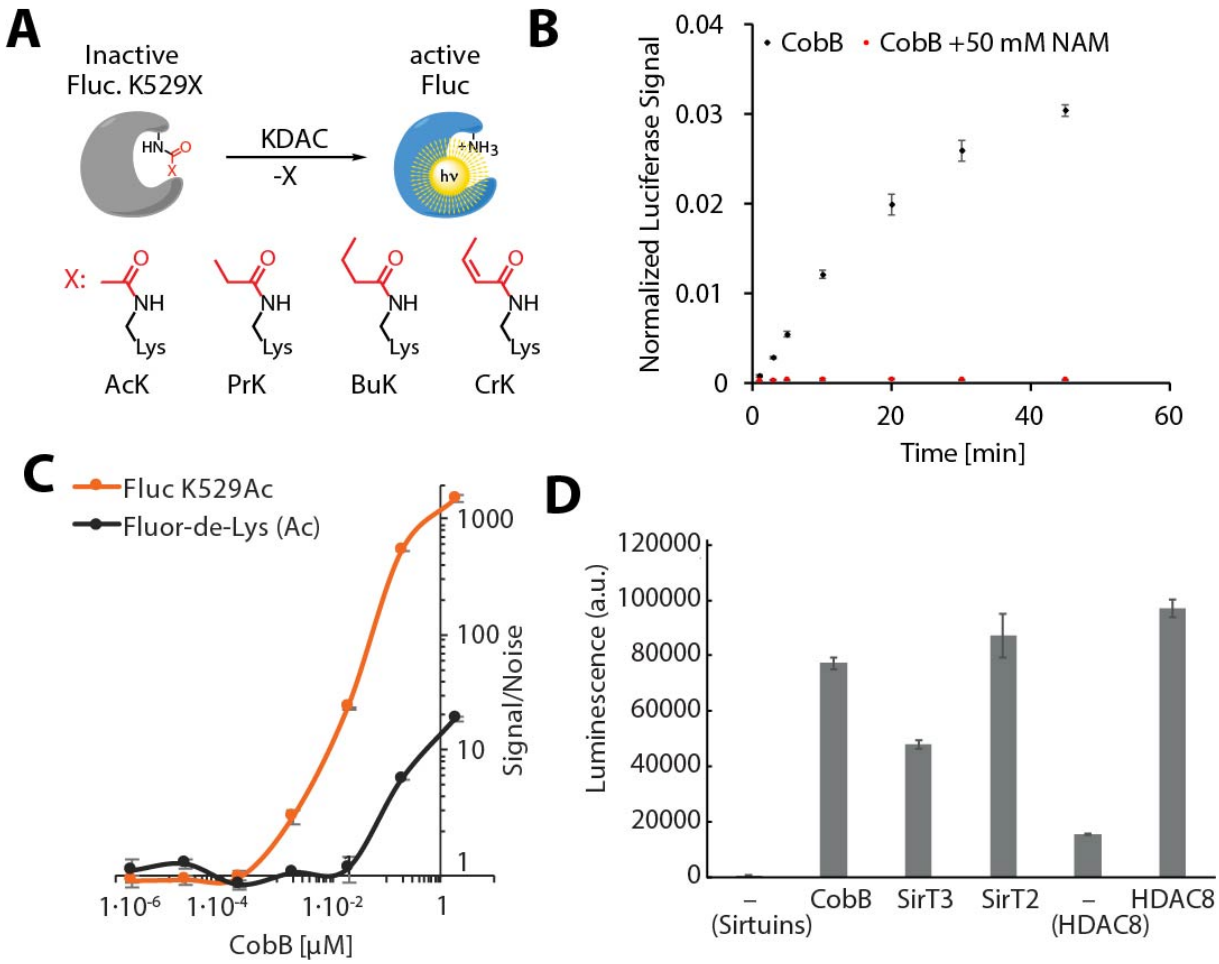

Figure 6 Proof of concept for an extremely sensitive deacylation assay based on K529 acylated firefly luciferase. A) Firefly luciferase (Fluc) is inactivated by encoding a modified lysine at K529, but the activity can be rescued by a lysine deacetylase (KDAC) and be detected as luminescence (hν). B) Cell lysate of *E.coli* expressing acetyl modified Firefly luciferase was treated with 20 µM purified CobB and the signal monitored over time in the absence and presence of 50 mM nicotinamide. C) Comparison of the signal to noise ratio for the purified K529Ac Firefly luciferase and the commercial Fluor-de-Lys deacetylation assay (97). Luminescence signal of firefly luciferase after adding 20 µg/mL of different Sirtuins and HDAC8 (requires different buffer).

The luciferase signal increase linearly over the first 20 min of the reaction before approaching saturation in presence of NAD^+ and CobB, no increase was observed when nicotinamide was included in the reaction (**Figure 6B**). This confirmed that the modified luciferase is soluble in cell lysate, and that its enzymatic activity can be recovered under these conditions by adding purified KDACs. Therefore, it was further optimized to use as a deacetylation assay. Acetylated firefly luciferase was purified via a C-terminal His_6-Tag and its performance compared with the commercial Fluor-de-Lys deacetylation assay. The luciferase-based assay has a 100-fold better signal/noise ratio compared to the Fluor-de-Lys assay and is capable of detecting Sirtuin activity at low nanomolar concentrations (**Figure 6C**). This makes it an exceptionally sensitive assay to measure deacetylation, which can easily be adaptable to detect other deacylation activities. Deacetylation was also determined for other Sirtuins and HDAC8, whereby HDAC8 required a different reaction buffer for optimal performance (**Figure 6D**).

BIOCHEMICAL CHARACTERIZATION OF THE ACETYL-SELECTIVE COBB VARIANTS

During the selection procedure 14 different CobB mutants could be enriched out of the initial pool of over 32 million variants. In the next step I set up a protocol for the biochemical characterization of such mutants with emphasis of deacylation activity for certain acyl groups. To test which of the 14 identified CobB mutants was the most active, a selection strategy with successively increased selection pressure was devised. Since the activated Ura3 is the limiting enzyme for the *E.coli* growth on the selection plates, addition of a Ura3 inhibitor like 6-azauridin (6-AU) should lower the effective Ura3 activity. This could be overcome by better deprotecting the acylated K93 of Ura3, required for growth, benefiting the more active mutants.

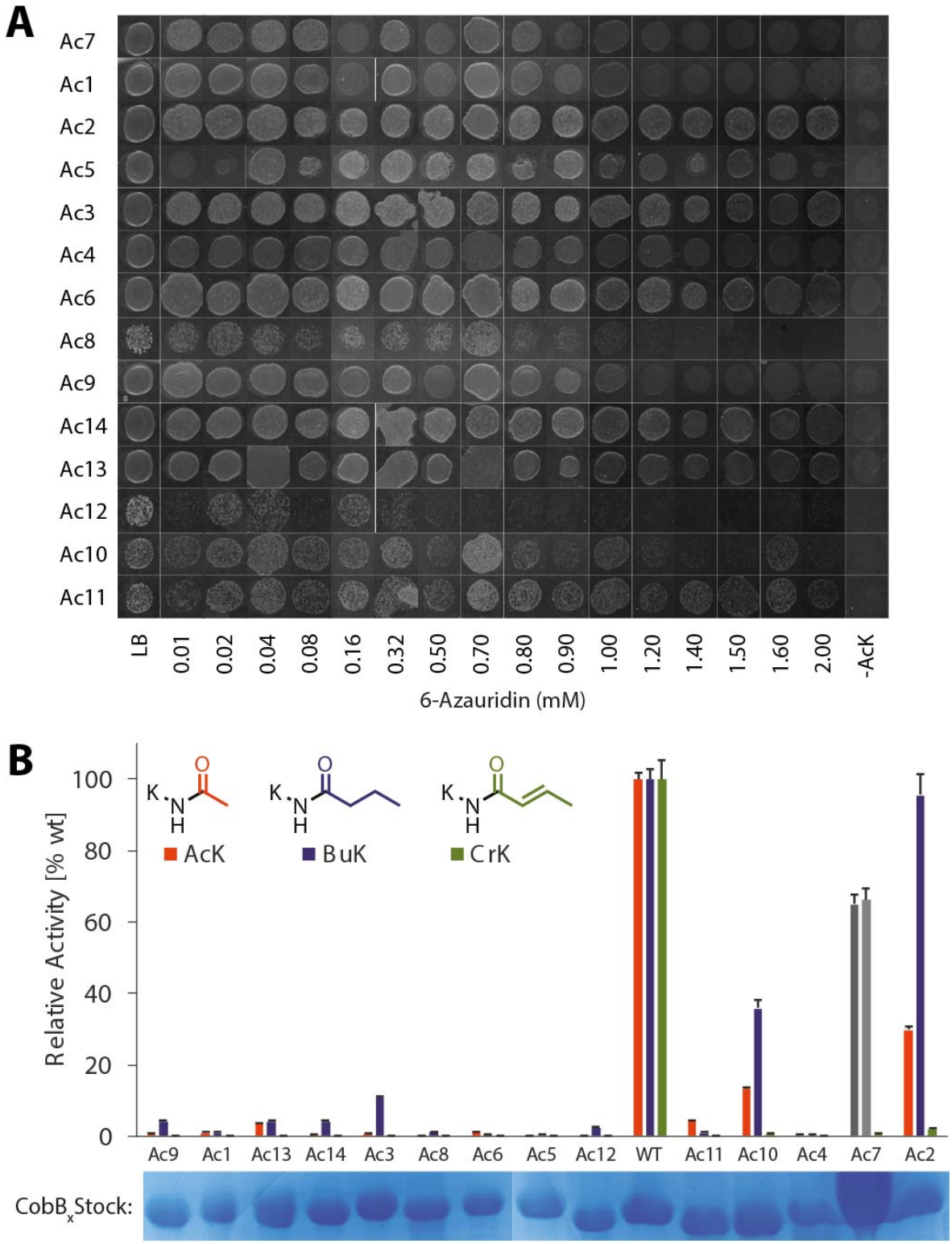

Figure 7: Characterization of the 14 acetyl-selective CobB mutants. A) Patch drop growth assay with increasing concentrations of the Ura3 inhibitor 6-azauridin (6-AU). More active mutants should show higher resistance to 6-AU than less active mutants. B) Fluc assay using K529 modified Firefly luciferase (AcK: acetyl-, BuK: butyryl- and CrK: crotonyl-lysine) and Ni^{2+}-NTA purified CobB variants. The mutants were diluted to a final concentration of 20 µM and the loading was controlled by SDS-PAGE. For the uncropped SDS-PAGE and activity of mutant Ac7 see **S. Figure 3**.

The *E. coli* each expressing one of the 14 CobB mutants identified in the selection process were arrayed in a patch drop assay, and growth on acetyl-lysine positive selection plates (Ura3 K93ac) with increasing concentrations of 6-azauridin (6-AU) was monitored. The resistance to 6-azauridin varied between 0.16 mM to 2 mM for the different mutants, particularly the mutant $CobB_{ac2}$ showed no reduction in growth even at 2 mM 6-AU. Also, the mutants $CobB_{ac3,6,\ 13\ and\ 14}$ showed significant resistance to 6-AU (**Figure 7A**). To compare the activity of the individual evolved CobB proteins in correlation to 6-AU resistance, all 14 mutants were Ni-NTA purified. The crudely purified mutant proteins were concentrated to about 100 µM, as judged by SDS-PAGE. Of note, the load of all proteins was the same except for $CobB_{ac7}$, which was measured separately (see**. S. Figure 3**). The deacetylation (AcK), debutyrylation (BuK) and decrotonylation (CrK) activity was measured using purified Firefly luciferase (FLuc) carrying the respective modification at K529 (**Figure 7B**). By comparing the purified mutant CobB protein activity to the growth assay, we confirmed that $CobB_{ac2}$ is the most active mutant with about 25% of the wt deacetylation activity. For other mutants, activity is severely reduced, closest in activity be $CobB_{ac10}$ with 15% of the wt deacetylation activity. This mutant did only show 6-AU resistance to about 1 mM in the patch growth assay and could not be further purified due to low solubility. The seeming discrepancy between the 6-AU resistance and activity in vitro is most likely the sum of several factors contributing possibly to it like protein folding, expression level, intrinsic activity or sensitivity to degradation. All other mutants had an intrinsic activity of <5% wt deacetylation activity in vitro, but in all cases the decrotonylation activity was even more severely reduced. Most interestingly, for many mutants the debutyrylation was not nearly as much reduced as the deacetylation activity, for example, the mutant $CobB_{ac2}$ maintained nearly wt debutyrylation activity.

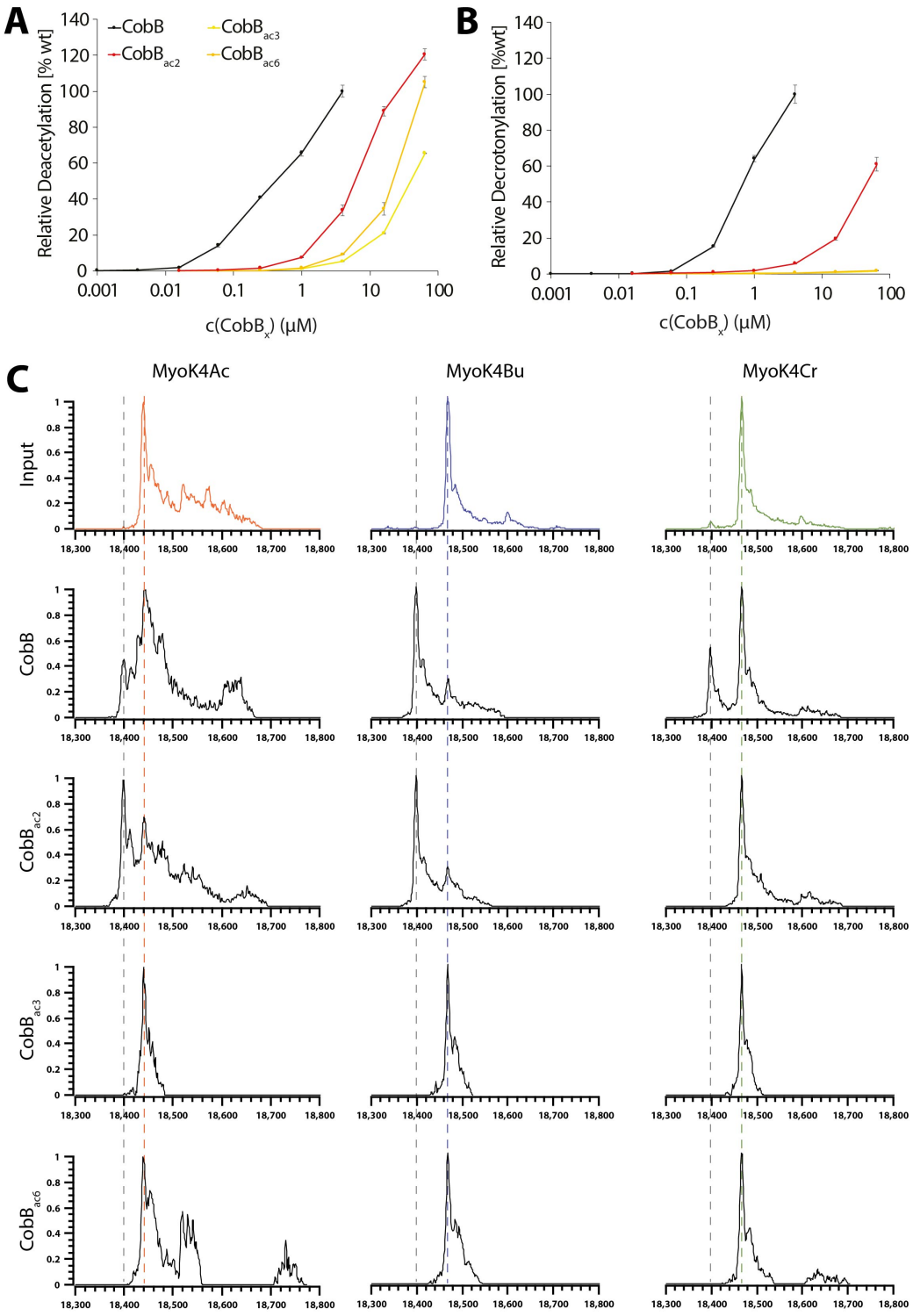

Figure 8: Characterization of CobB$_{ac2, ac3 and ac6}$ by FLuc deacylation assay and mass spectrometry using modified myoglobin (Myo). Deacetylation (A) and decrotonylation (B) activity of CobB wt and the acetyl-selective mutants measured with the Fluc assay. C) ESI-MS of K4 acylated Myoglobin (Ac: Acetyl, Bu: Butyryl or Cr: Crotonyl) before and after treatment with CobB or the acetyl selective CobB variants. The dotted lines show the expected mass for the acylated (colored) and deacylated (grey) myoglobin.

The library was designed with the idea that increasing the size of the active site residues would narrow the cavity and only allow binding of acetyl. Since butyryl and crotonyl have about the same size, it was assumed that activity against both would have been reduced to the same extent, but this was only the case for two mutants $CobB_{ac6}$ and $CobB_{ac11}$. Most mutants must have developed a mechanism to discriminate against crotonyl specifically. For further analysis the mutants $CobB_{ac2, 3 \text{ and } 6}$, of which $CobB_{ac2}$ was the overall most active mutant, and $CobB_{ac3}$ and $CobB_{ac6}$ were the most selective mutants, representing both types of selectivity were chosen for further analysis.

The CobB wt and the three acetyl selective mutants were purified, and their activity determined by titrating them against acetylated and crotonylated Firefly luciferase (**Figure 8A-B**). I could confirm that $CobB_{ac2}$ has about 25% of the wt deacetylation activity, while the crotonylation was reduced to about 2%. $CobB_{ac3 \text{ and } ac6}$ had lower deacetylation activity with 5% and 2.5% wt activity, respectively. But for both mutants the decrotonylation activity was reduced to nearly undetectable levels, which is a reduction by factor of more than 800. To examine if the remaining activity of the mutated CobB is still enough to cleave the respective acyl residues, we tested all mutants on myoglobin, modified with a respective acyl-lysine, where we could directly observe the change in mass upon cleavage by the CobB variants by ESI-MS (**Figure 8C**). The mutants $CobB_{ac3 \text{ and } ac6}$ were too inactive and produced no detectable product with any of the tested acylated myoglobins. $CobB_{ac2}$ could deacylate and debutyrylate myoglobin but not crotonylate modified myoglobin, unlike the wt CobB which converted all acylated myoglobins. Further experiments with $CobB_{ac3 \text{ and } ac6}$ showed that they have lost affinity for their binding of NAD^+, a likely explanation for their low activity (**S. Figure 4A**). Still, from a mechanistic point of view, these mutants are quite interesting, because both are highly inactive towards crotonylation but for $CobB_{ac3}$ the activity

increases from acetyl over propionyl to butyryl, while for $CobB_{ac6}$ the activity decreases (**S. Figure 4B**). So, while both mutants have experienced the same selection procedure, they evolved independent strategies to remove the decrotonylation activity. This signifies that the selection system will identify any mutant as long as it fulfills the selection criteria. Due to the low deacetylation activity of $CobB_{ac3/6}$ I focused on the mutant $CobB_{ac2}$, to show in further experiments that its activity could be used to manipulate histone acylation patterns.

MANIPULATIONS OF CELLULAR ACYLATION PATTERNS USING $COBB_{AC2}$

The mutant $CobB_{ac2}$ has lost most of its decrotonylation activity while maintaining activity for other acylations. It should be capable of shifting a cellular acylation state towards crotonylation. Initially, $CobB_{ac2}$ activity was tested on histone extract to see if it maintains its selectivity independent of the sequence context. When nuclear extract was incubated with CobB and $CobB_{ac2}$, I found that the decrotonylation activity of $CobB_{ac2}$ is reduced by a factor of 16, which is slightly lower than the 30 to 50-fold reduction observed in the Fluc assay (**S. Figure 5A**). A possible explanation is that the antibody used is not perfectly selective for crotonylation and recognizes butyrylation, which is removed by $CobB_{ac2}$ (**S. Figure 5B**). The deacetylation activity for H4 K16Ac was not decreased in $CobB_{ac2}$ in the concentration range tested (**S. Figure 5A**). From this experiment I concluded that the selectivity of $CobB_{ac2}$ is an intrinsic property of the mutant. Due to this, it should be possible to alter the acylation pattern of histones in living cells by simple expression of the mutant $CobB_{ac2}$. CobB and $CobB_{ac2}$ were fused with an NLS and a GFP and inserted in a mammalian expression vector under a constitutive promotor (CMV). In cells transfected (*) with CobB, all tested acylations were reduced to nearly undetectable level (**Figure 9A**), compared to the non-transfected cells.

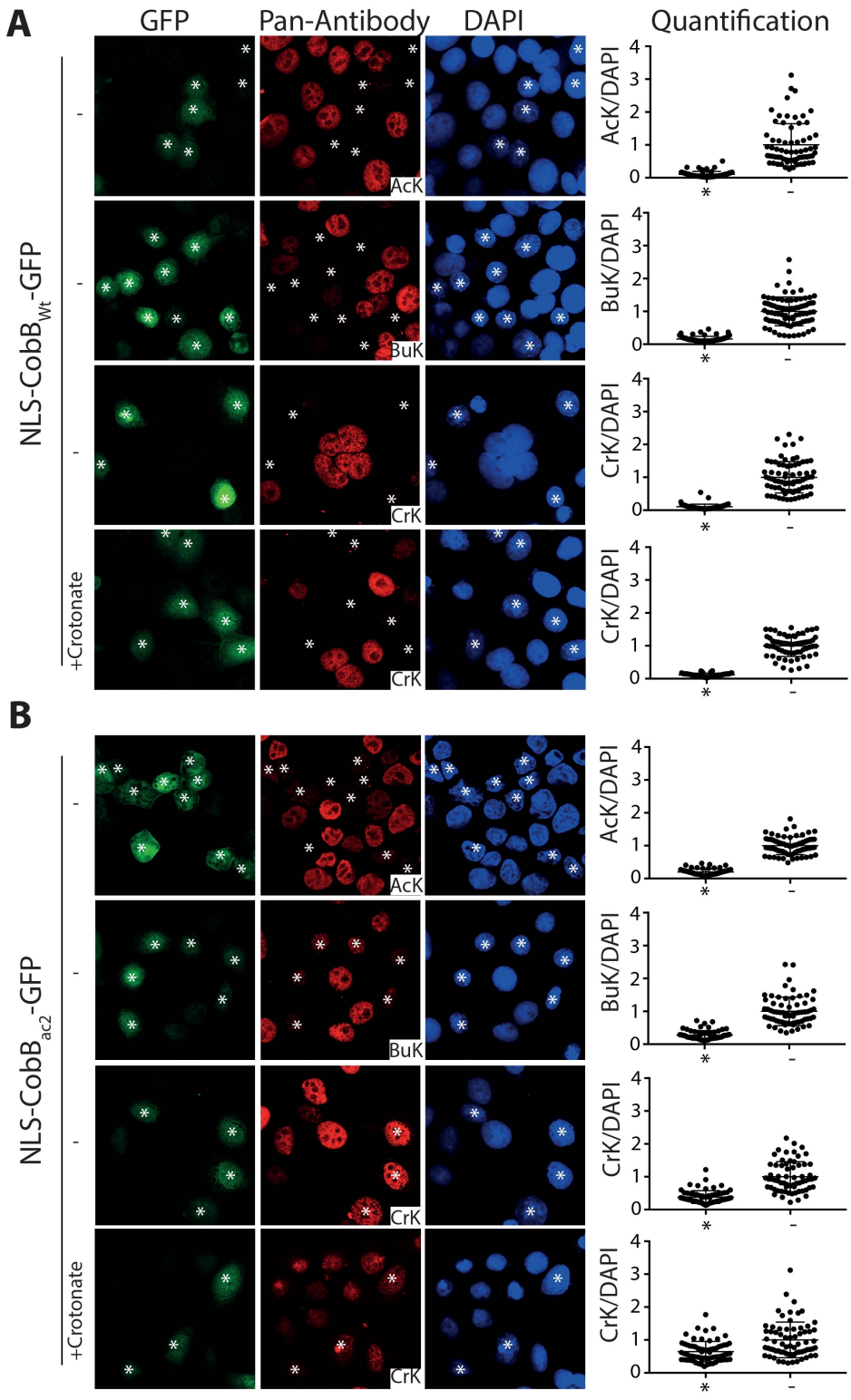

Figure 9: Expression of CobB and CobB$_{ac2}$ in HeLa cells alters the nuclear acylation pattern. CobB (A) and CobB$_{ac2}$ (B) were fused to a nuclear localization sequence (NLS) and GFP and transfected into Hela cells. After 24h of expression the nuclear acylation level for acetylation (AcK), butyrylation (BuK) and crotonylation (CrK) was detected by immune stain. The antibody signal in transfected (*) and untransfected cells was quantified and normalized on the DAPI signal for individual cells (n > 50). Shown are the individual measurements and the standard deviation of the mean.

In cells expressing $CobB_{ac2,}$ this enzyme reduced acetylation and butyrylation like cells expressing CobB. In contrast, crotonylation was only reduced to about 40% persisting signal. Since the antibody is not perfectly selective for crotonyl (**S. Figure 5B**), the reduction seen for crotonylation is likely due to the removal of butyrylation which is also recognized by the antibody. To test if this is the case, the cells were incubated with crotonate for 2 h before imaging the crotonylation. Crotonate should shift the acylation pattern towards higher crotonylation, and indeed the signal of the persistent crotonylation increased to about 60%. The addition of crotonate had no effect on crotonylation levels in cells expressing CobB. This confirmed that the persistent signal is indeed crotonylation.

To conclude, expression of $CobB_{ac2}$ significantly reduces nuclear acetylation and butyrylation while maintaining histone crotonylation. This confirms the intrinsic selectivity of $CobB_{ac2}$ and therefore shows that the selection system is indeed able to produce Sirtuins with altered acylation selectivity. The ability of the $CobB_{ac2}$ to discriminate against decrotonylation in a biological context, allows for targeted manipulation of the epigenetic landscape.

STRUCTURAL MECHANISM RESPONSIBLE FOR THE $COBB_{AC2}$ SELECTIVITY

$CobB_{ac2}$ has two active site point mutations, A76G and I131C. The two mutations have little to no effect on the deacetylation and debutyrylation but severely reduce the decrotonylation activity of the enzyme. To unveil the underlying mechanism, the mutants were crystalized bound to the different acylated peptides. The overall structure of mutant $CobB_{ac2}$ and wt CobB are very similar with a r.m.s.d. <0.5 Å. Most differences were found in the cofactor binding loop connecting the alpha helix 1 (α1) with alpha helix 2 (α2), which covers the active site on the opposing side of the mutations.

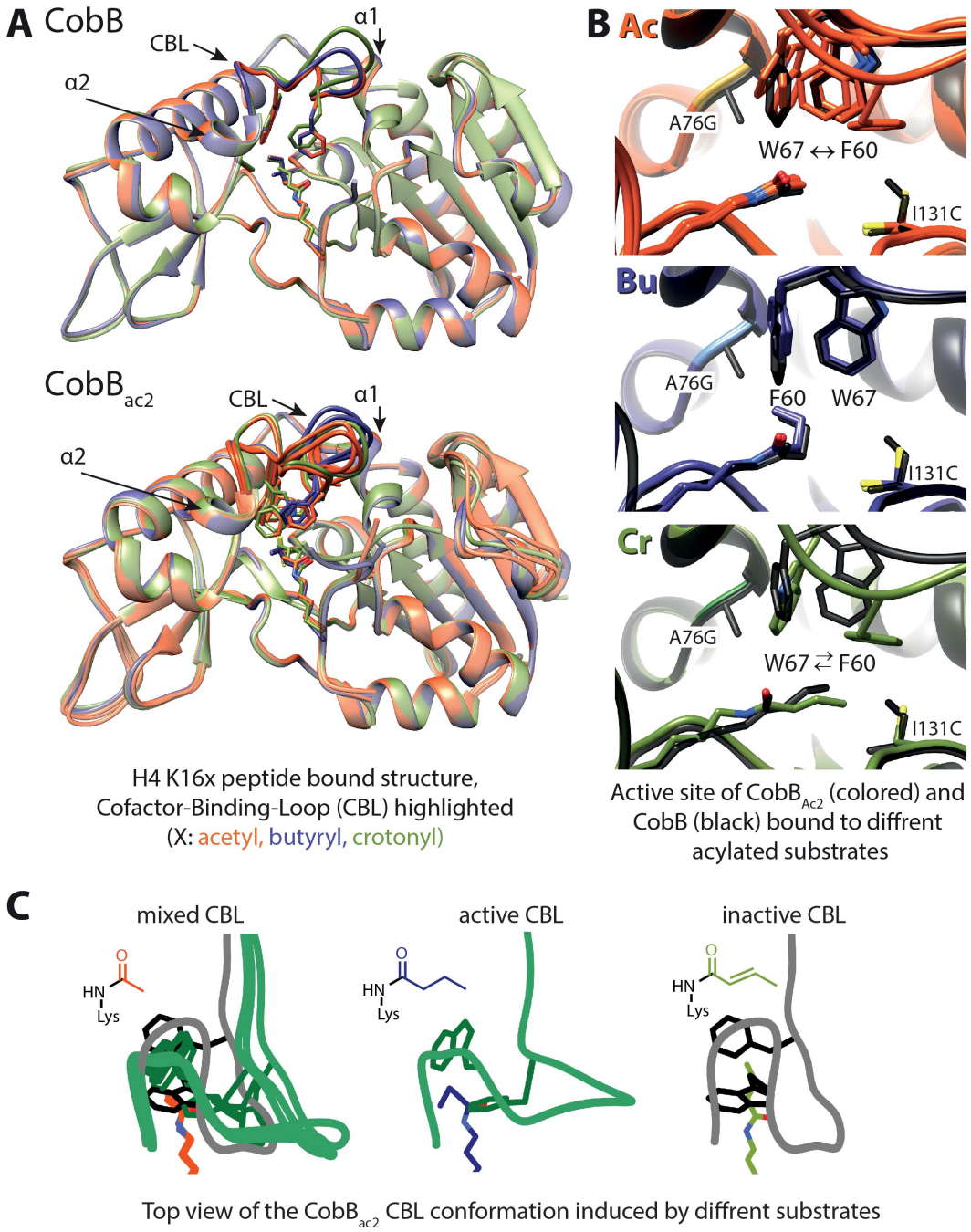

Figure 10: Crystal structure of CobB and CobB$_{ac2}$ bound to different acylated peptides showing a conformational change of the CBL in the acyl-selective mutant. A) Overlay of the peptide bound structures show little differences in their overall structure, the most significant difference is found in the cofactor-binding-loop of the CobB$_{ac2}$ mutant. B) Overlay of the CobB (black) and CobB$_{ac2}$ (colored) active site bound to the different acylated substrates (Ac: Acetyl-, Bu: Butyryl-, Cr: Crotonyl-lysine). The two point mutations allow for a conformational change of the CBL in response to the binding of crotonyl-lysine, swapping the position of W67 and F60. C) Conformational change of the CBL conformation shows that butyryl induces the active conformation (wt, green), and crotonyl (grey) presumes an inactive and acetyl a mixed conformation. For clarity some chains from the same unit cell were omitted see **S. Figure 6**.

Comparing the impact of the different acylated lysines on the CBL in the CobB structure, no change in response to the different acylations could be observed, all substrates show the same conformation. In the case of $CobB_{ac2}$ the CBL does adopt different conformations depending on the nature of the acylated lysine (**Figure 10A**). While binding of butyryl to $CobB_{ac2}$ showed now notable difference to the wt (**Figure 10B**, Bu), crotonyl induced a conformational change in the cofactor binding loop by swapping the relative position of W67 and F60 (**Figure 10B**, Cr). Why this conformation is inactive is not predicable from this structure. Acetyl-lysine does not induce a defined conformation upon binding $CobB_{ac2}$ and rather produces a mixed population of the native and crotonyl induced conformation (**Figure 10B**, Ac). Considering the biochemical data, I concluded that the two observed CBL conformations represent an active and inactive state of the protein. The mutant lost no activity for butyryl and the observed conformation is identical to the wt conformation, indicating that this represents the active state of the protein. Binding of crotonyl induces a new CBL conformation which I presume inactive due to the low activity of $CobB_{ac2}$ for crotonyl. The acetyl bound mutant showed a wide range of conformations covering active and inactive conformations, which matches with the partial loss of deacetylation activity in $CobB_{ac2}$ (**Figure 10C**).

While the CBL conformation in $CobB_{ac2}$ is clearly different for the crotonyl bound state, it is still unclear how this relates to the observed loss of decrotonylation activity. Hence, I attempted to solve the structure of $CobB_{ac2}$ in complex with crotonyl and NAD^+. Two different structures were obtained by co-crystallization of the reaction mixture (**Figure 11A**) or by soaking of preformed crystals with NAD^+ (**Figure 11B**). While both structures show that the reaction gets stalled at the Intermediate 3, the two structure differ in their CBL conformation, suggesting a conformational rearrangement of the CBL over time. The Intermediate 3 was proposed to be the last intermediate before

hydrolysis through water occurs (38). The CBL conformation found after 16 h of crystallization is still similar to the “inactive” conformation found for the $CobB_{ac2}$ H4 K16Cr complex, with F60 slightly less well resolved due to an increase in flexibility. In this structure, it becomes clear that W67 is positioned directly above the formed intermediate, preventing water from accessing the active site (**Figure 11A**). Access of water into the active site was observed in the structure after 36 h of soaking (**Figure 11B**), here W67 folded back into its original position opening the active site for water. There is no sign of hydrolysis of the Int. 3, suggesting that the mere presence of water is not sufficient and additional factors are required to hydrolyze the Int. 3. The mutant $CobB_{ac2}$ is still able to cleave crotonyl-lysine with low activity, so it can be assumed that Int. 3 hydrolyzes eventually. Also, it is possible that a fraction of the protein is not trapped in the inactive conformation and proceeds with the reaction normally, contributing to the crotonylation activity of $CobB_{ac2}$. This is supported by the presence of a mixed conformation of the active and inactive loop conformation in one chain of $CobB_{ac2}$ (**S. Figure 6B**).

Considering that most identified mutants shared this type of selectivity we hypothesized that the structural rearrangement of W67 and F60 is the defining feature of the butyryl over crotonyl-selectivity and any mutant sharing that phenotype should show a similar rearrangement. This was supported by the structure of $CobB_{ac3}$ in complex with H4 K16Ac peptide. It shows, despite completely different mutations, a similar rearrangement of F60 to the same position as in $CobB_{ac2}$ (**S. Figure 7A-B**), indicating that it gained selectivity through the same mechanism. Unfortunately, W67 was not resolved and no further structure bound to butyryl- or crotonyl-lysine could be obtained. To still test if the structural rearrangement is the main cause of selectivity, the residues F60 and W67 were swapped by mutagenesis creating CobB F60W W67F.

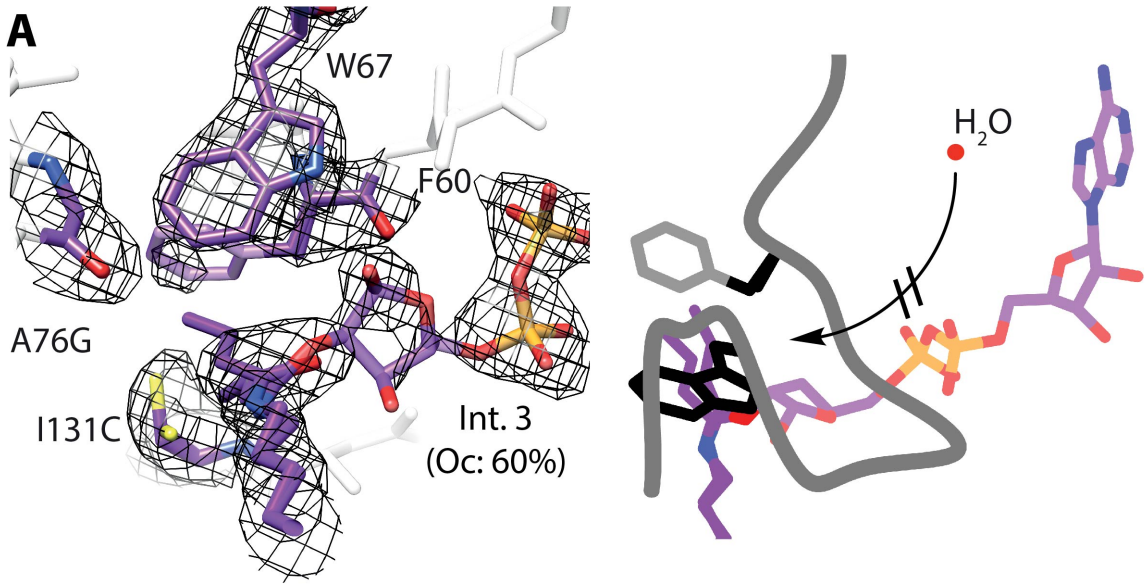

Structure of crotonyl-NAD⁺ Intermediate III after 16h of crystalisation.

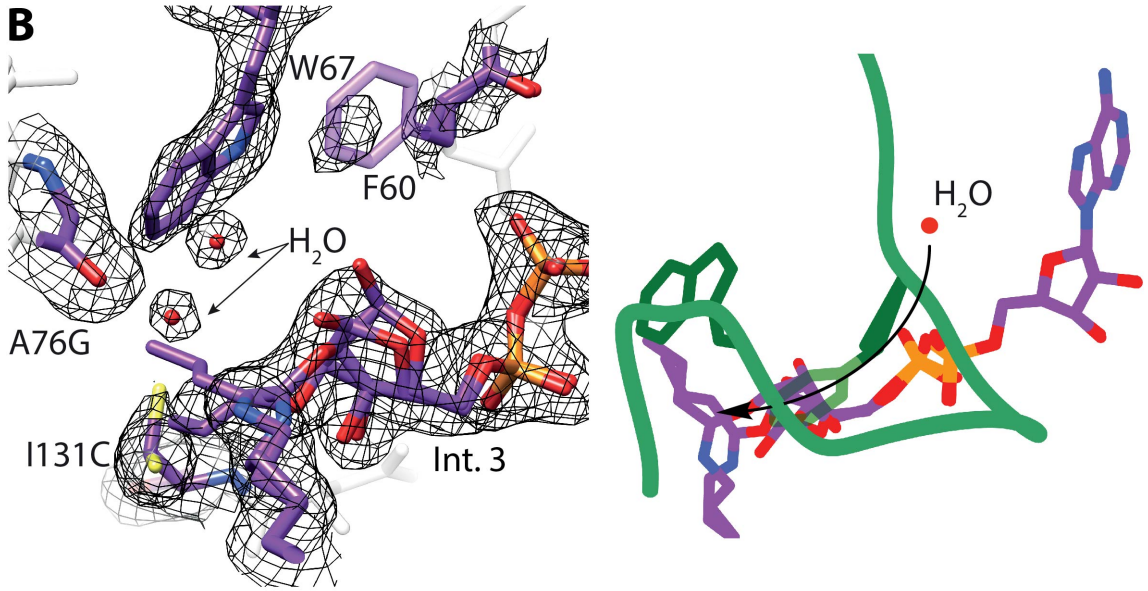

Structure of crotonyl-NAD⁺ Intermediate III after 36h of soaking.

Figure 11: When NAD^+ is added to start the decrotonylation reaction of $CobB_{ac2}$ the reaction is trapped at the Intermediate 3 (38) due to the novel CBL conformation. Two states of the Intermediate 3 (Int.3) were obtained either by co-crystalizing the reaction mixture overnight (16 h) (A) or by soaking preformed $CobB_{ac2}$/H4K16Cr crystals with NAD^+ for 36 h (B). For both, the active site with the $2F_o$-F_c omit map (black, 1σ) for key residues (purple) is shown, as well as the cartoon representation for the cofactor binding loop (CBL, active: green, inactive: grey). A) After 16 h of co-crystallization the crotonyl has reacted with NAD^+ but due to the positioning of W67 water is not capable of entering the active site, trapping the reaction at Int.3 (60% occupancy). F60 is not well resolved due to an increased flexibility of the CBL upon NAD^+ binding. B) After 36 h of soaking, the CBL reverted to the native-like conformation allowing water to enter the active site, nevertheless no hydrolysis of Int.3 is observed in this state.

This mutant should be inactive unless the native state is restored by the bound substrate. This predicts that the mutant should have a comparable selectivity to $CobB_{ac2}$, since binding of butyryl does not support the rearranged CBL conformation and should support formation of the native conformation. After purification, CobB F60W W67F was tested using the Fluc assay and, as expected, showed good debutyrylation activity, while activity for acetyl or crotonyl were severely reduced (**S. Figure 7C**). The butyryl induced rearrangement into the native conformation is also supported by its strongly stabilizing effect on CobB and $CobB_{ac2}$, in comparison to acetyl or crotonyl (**S. Figure 11A**).

To conclude, the identified mutants acquired their unique selectivity for debutyrylation over decrotonylation via an evolved, inactive CBL conformation, which is stabilized by the binding of crotonyl-lysine. The new conformation reduces the decrotonylation activity by blocking the access of water to the active site, preventing hydrolysis and stabilizes Int.3. Binding of butyryl-lysine stabilizes the native conformation and destabilizes the inactive conformation, supporting the debutyrylation activity.

CREATION OF ACETYL-SELECTIVE SIRT1 VARIANTS

Sirt1 is the major human Sirtuin responsible for regulating histone acylation levels (68). Acyl-selective variants would be of great value to dissect the contribution of individual acylations to cellular physiology. Using the same procedure as for CobB, we generated an active site mutant library of Sirt1 by randomizing 5 residues within the Sirt1 active site (**Figure 12A**). The library was subjected to the established selection procedure, consisting of three rounds of selection alternating between positive for deacetylation and negative against either decrotonylation, debutyrylation or depropionylation. From each selection round, plasmids of 32 colonies (see S. Table 4) were sequenced, and sequencing outcome was similar between the different negative selections.

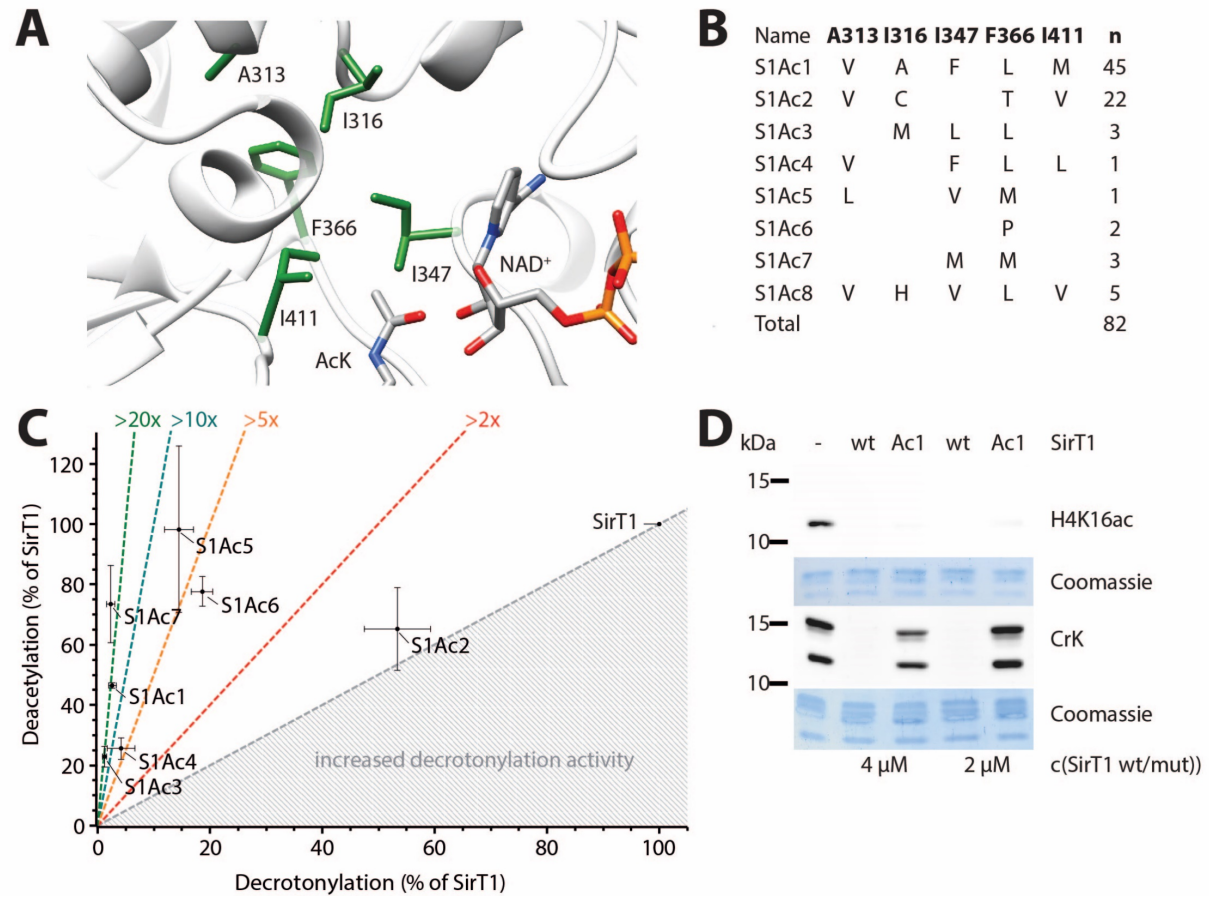

Figure 12: Creation of Sirt1 variants with AcK preference. A) Structure of the Sirt1 active site (4KXQ) with ligands NAD^+ and AcK imported from pdb-files 2H4F and 1S5P, respectively, shown as sticks. Residues highlighted in green were randomized to all possible combinations of natural amino acids in the mutant library. B) Sirt1 variants isolated after three rounds of selection from the library. C) Acyl-type preference of Sirt1 variants assayed on FLuc K529ac and K529cr. Dotted lines indicate the fold change in acetyl selectivity D) Sirt1 variant S1Ac1 deacetylates H4 K16ac but is compromised in histone decrotonylation. Activity of Sirt1 and $Sirt1_{Ac1}$ (2 µM or 4 µM) was measured by Western blot on isolated human histones using antibodies against H4 K16ac or pan-anti-CrK.

In total 82 plasmids were sequenced (**Figure 12B**), which resulted in 8 different mutants. Of the 8 mutants, the mutant S1Ac1 dominated the set, representing more than 50% of all sequenced plasmids, irrespective of the acylation used during the negative selection. This suggests that, unlike CobB, the Sirt1 mutants lost all deacylation activity except for deacetylation. 7 mutant Sirt1 proteins could be purified and the change in acylation preference was assayed using the Fluc assay for deacetylation and decrotonylation activity. All mutants, except S1Ac2, had their acyl preference shifted towards deacetylation. S1Ac1, S1Ac3 and S1Ac7 maintained between 20-70% deacetylation activity compared to wild-type, while showing an up to 20-fold increase in selectivity for Kac . All selective mutants were tested also for their activity towards butyryl- and propionyl-lysine (**S. Figure 8**). We found that, unlike in the CobB selection, all acetyl-selective mutants also lost their debutyrylation and, to a lesser extent, depropionylation activity, suggesting a reduction of the active site volume. We tested the evolved S1Ac1 on histone extract and found barely any decrotonylation activity up to a concentration of 4 µM of the Sirtuin variant, while the wt Sirt1 showed good decrotonylation throughout. Deacetylation of H4 K16Ac was only slightly reduced under the same reaction conditions (**Figure 12**).

In summary, the established selection system can identify acetyl-selective mutants of Sirt1. The mutants did not obtain selectivity through the same mechanism as for CobB, identifying the reason for selectivity of Sirt1 will require more in-depth structural analysis. The biochemical data suggest a reduction in the active site volume as major reason for the increased acetyl-selectivity.

EVOLVING SIRTUINS FOR IN VIVO LYSINE DEPROTECTION

During the selection of CobB some mutants could grow on boc- or alloc-protected lysine selection plates (**Figure 5**). This indicated that they gained the ability to deprotect these chemical protecting groups, which was confirmed in the dual-luciferase assay (**S. Figure 2**). Particularly mutant F7 showed enhanced activity for boc and alloc deprotection. I could confirm this in the Fluc assay using purified components, where F7 shows a 3-fold increase in deallylation and a 6-fold increase in boc deprotection activity *in vitro* (**Figure 12A**). The boc deprotection reaction is still sensitive to the inhibition by nicotinamide and dependent on NAD^+, with no difference in affinity between wt and mutant (**S. Figure 9A**). This suggested that the two point mutations of F7 (I131V and V187L) do not interfere with the reaction mechanism and rather just improved the affinity and binding pose of the Alloc substrate. The crystal structure of CobB F7 in complex with the H4K16Alloc peptide shows that the two mutations increase the active site size and allow for the alloc group to be accommodated in the active site (**Figure 12B**). The improved binding is reflected in an increase in thermal stability of CobB F7 when bound to H4K16Alloc, although the wt is also stabilized by H4K16Alloc binding to some extent. In contrast, the stabilizing effect of acetyl lysine on CobB F7 is reduced (**S. Figure 11B**), this also effects the activity of the mutant towards its natural substrates. The deacetylation activity is reduced by a factor of 8, while decrotonylation activity is only halved (**S. Figure 9B**). It also shows that the new bioorthogonal activities are, while detectable, at least 2 orders of magnitude lower than the deacetylation activity, leaving room for further improvements.

In summary, the selection system is capable to detect new activity in the evolved mutants for unnatural substrates. While the determined activity is low, it should be possible to further improve it by directed evolution.

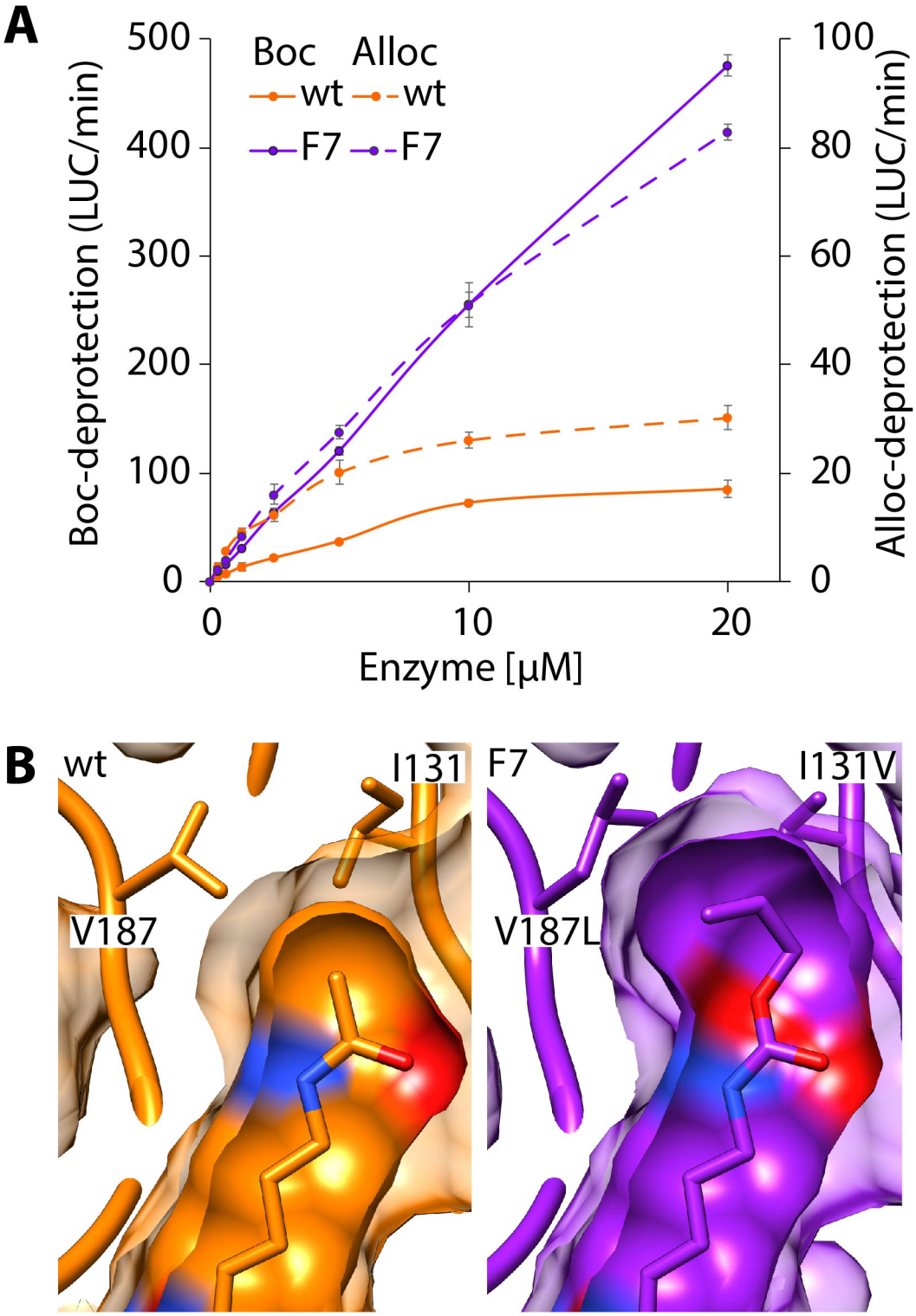

Figure 13: F7 shows enhanced deallylation and boc deprotection activity due to improved substrate binding. A) Continuous Fluc Assay (K529Alloc or Boc) for Alloc and Boc deprotection using mutant F7 and wt CobB. F7 shows a 3-fold increase in deallylation and 6-fold increase in boc deprotection activity compared to the wt. B) Crystal structure of CobB H4K16Ac complex (PDB: 1S5P) in comparison to the CobB F7 (I131V V187L) H4K16Alloc peptide complex. The mutation reshapes the active site, increasing its size allowing to accommodate the larger alloc group. (unpublished, see. S. Table 7 for refraction data)

DIRECTED EVOLUTION OF HDAC8

HDAC8 is a human histone deacetylase like Sirt1 but is distinct in its structure and deacetylation mechanism. Our initial experiments suggested selection of HDAC8 is possible with the developed selection system. Therefore, the selection strategy previously used for CobB and Sirt1 was applied to HDAC8. In the same fashion as before, five active site residues of HDAC8 in close proximity to the acetyl-lysine binding site were chosen (**Figure 14A**) for mutagenesis. Beside proximity to the target amino acid, also available data from previous mutagenesis studies were taken into account. This led to the exclusion of several stretches of glycine residues in direct proximity to the acetyl lysine as they have been described to not tolerate mutations (98, 99). The residues N136, C153, Q263 and L301 were not reported to be critical and were therefore fully randomized. W141 was replaced by a set of hydrophobic residues including tryptophan, as it is an important gate keeping residue. The resulting library was sequenced, confirming the successful randomization (**Figure 14B).** Positive selection of the library only resulted in around 50 colonies on the acetyl-lysine selection plate, all other amino acids yielded no colonies (**Figure 14C)**. When the plasmids isolated from the colonies were sequenced, only the wt sequence of HDAC8 and the single point mutation L301C were found. This indicates that the general selection was successful, but mutations at the chosen position lead to a loss of activity for all but one mutant. It was also expected to find the wt on the crotonyl-lysine selection plate, as wt HDAC8 has decrotonylation activity. Since no colonies were observed, it is unclear if the selection was successful; the same is true for both selections for unnatural amino acids. Considering the overall low number of viable mutants, the selection of HDAC8 was discontinued, as it would require a complete overhaul of the library.

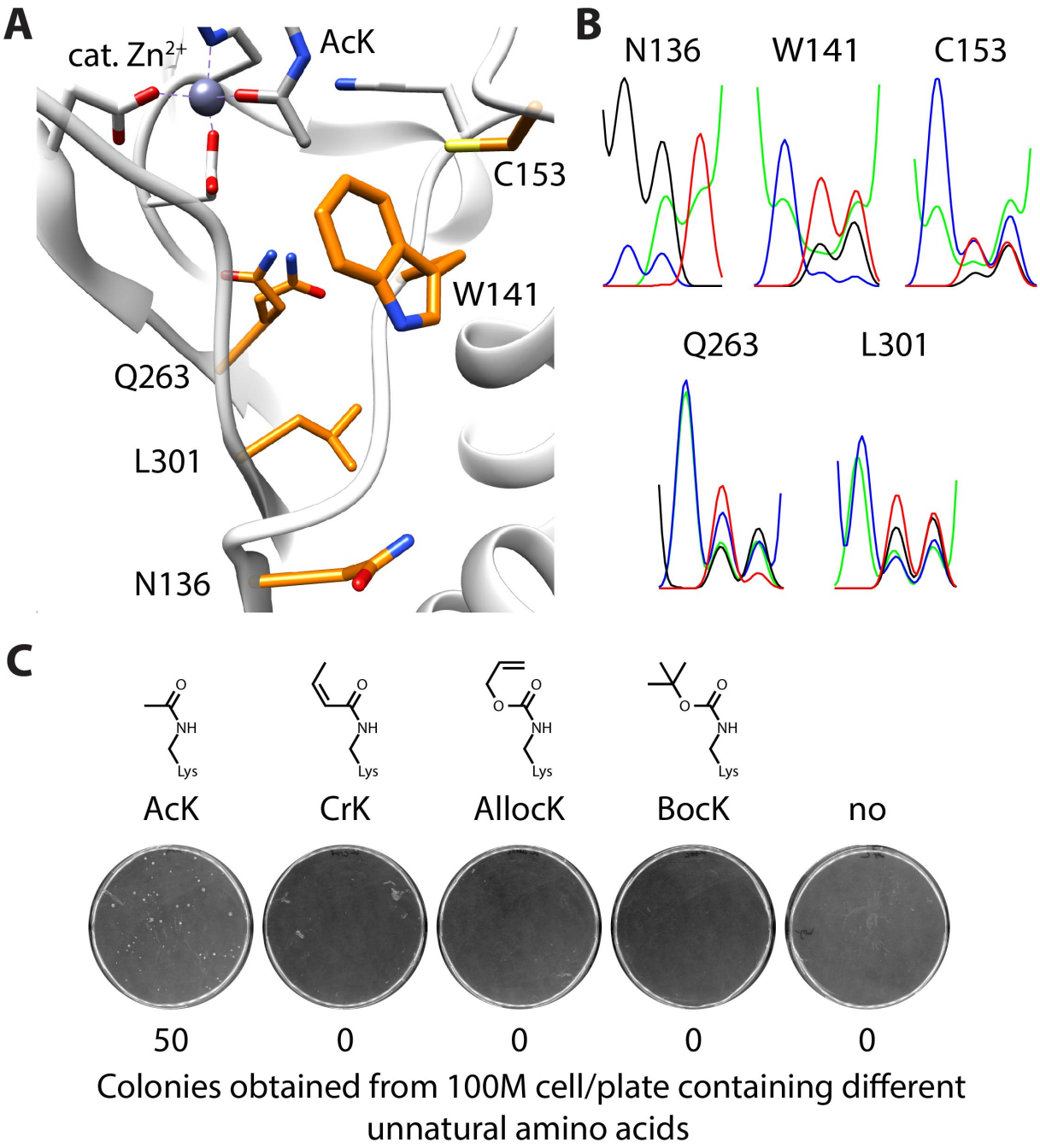

Figure 14: HDAC8 Library design and initial positive selection. A) The 5 residues (orange) in the HDAC8 active site were close to the binding site of acetyl-lysine (AcK, grey) and chosen for mutagenesis: N136, C153, Q263 and L301 were randomized to all proteinogenic amino acids (NNK), W141 was replaced with a set of hydrophobic or polar amino acids (WBS coding for C, F, I, L, M, R, W, T, S). B) The created HDAC8 library consists of 1.5 million mutants ($20^4 \cdot 12$), randomization of the individual positions was shown by sequencing of the pool (reverse primer). C) Initial positive selection and estimated number of colonies for the HDAC8 library when encoding different amino acids. No growth was observed when no amino acid was added.

It was found later that the critical residues controlling acylation selectivity in HDACs are located outside the active site in a flexible loop (68). Randomizing these residues might allow to evolve HDAC8 selectivity but this is outside the scope of my theses. Given better design it can be assumed that our directed evolution approach could yield acyl selective HDACs, as selection of HDAC8 in general worked flawless.

CREATION OF CONSTITUTIVELY ACTIVATED SIRT6 MUTANTS

The initial selection of Sirt6 showed that cells grow significantly slower under positive selection conditions compared to other Sirtuins. In cooperation with the group of John Denu we aimed to develop mutants with increased deacetylation activity. The Sirt6 deacetylation activity is an estimated 300-fold lower compared to its demyristoylation activity (49), but can be activated by several chemical compounds, mainly fatty acid-like molecules, have been described for this purpose (100). Our hypothesis was that it should be possible to create a mutant of Sirt6, which is constitutively activated for deacetylation activity. For this purpose, an active site mutant library based on the Sirt6 myristoyl-lysine/ ADP-ribose bound structure (PDB: 3ZG6) was designed, randomizing residues in contact with the myristoyl group (**Figure 15A**). The residues L9, V115, M157 and I185 were chosen to be fully randomized, while A53 and V70 were replaced with a smaller set of 8 amino acids (NYC codon, coding for A, F, I, L, P, S, T and V). To confirm the randomization, 8 colonies of the final library were randomly picked and sequenced (**Figure 15B**). The library was subjected to one round of positive selection, and after 2 (**Figure 15C**, S6.X) and 4 days (96 well plate) of growth, samples were collected and sequenced. The sequencing of the 96 well plate was incomplete and unusable. Instead of repeating the sequencing, the selection of the 96 well plate was repeated under increased selection pressure by the addition of 6-AU to focus our screening on more active clones.

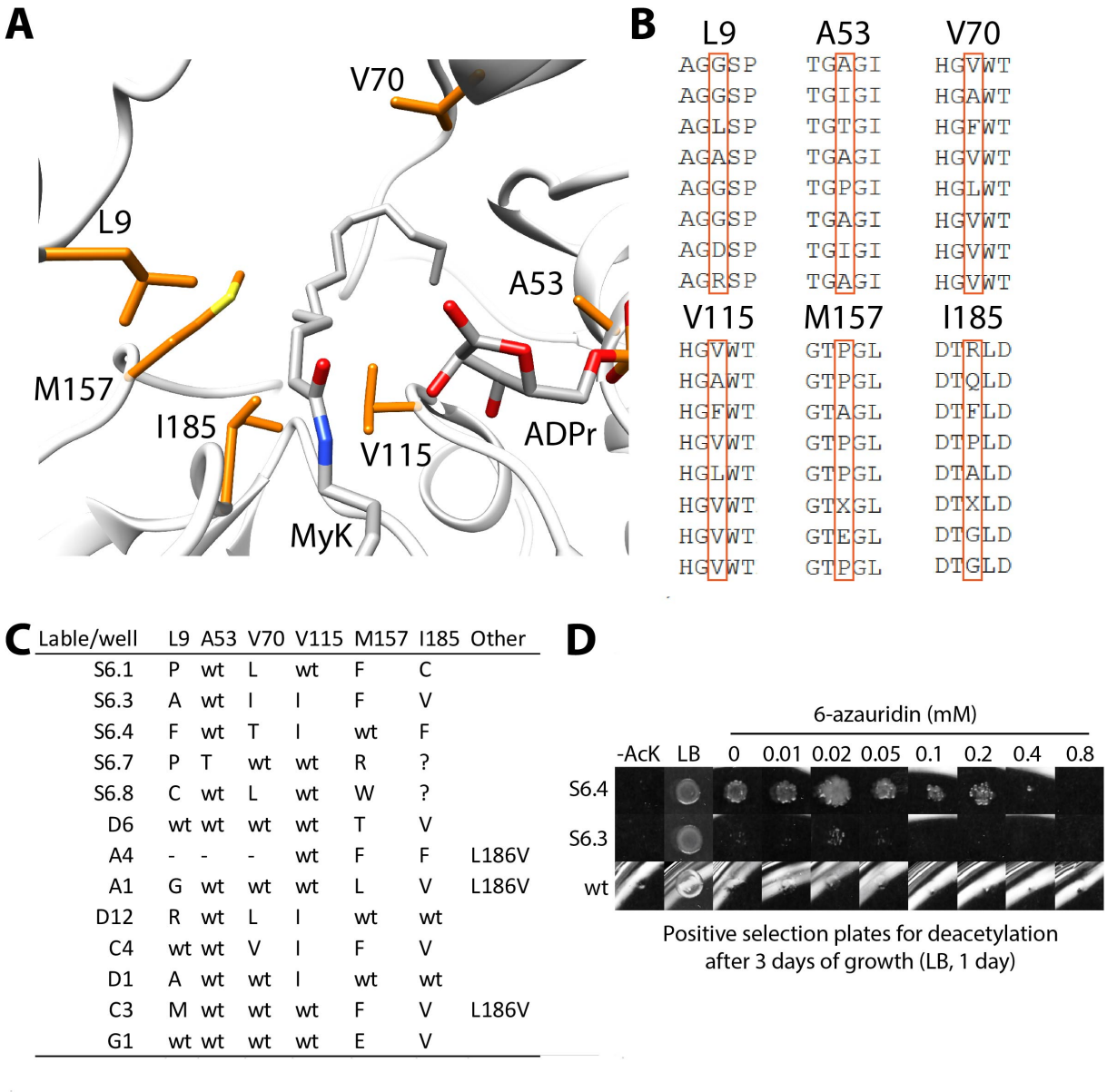

Lable/well	L9	A53	V70	V115	M157	I185	Other
S6.1	P	wt	L	wt	F	C	
S6.3	A	wt	I	I	F	V	
S6.4	F	wt	T	I	wt	F	
S6.7	P	T	wt	wt	R	?	
S6.8	C	wt	L	wt	W	?	
D6	wt	wt	wt	wt	T	V	
A4	-	-	-	wt	F	F	L186V
A1	G	wt	wt	wt	L	V	L186V
D12	R	wt	L	I	wt	wt	
C4	wt	wt	V	I	F	V	
D1	A	wt	wt	I	wt	wt	
C3	M	wt	wt	wt	F	V	L186V
G1	wt	wt	wt	wt	E	V	

Figure 15: Directed evolution of human Sirt6 for deacetylation selectivity. A) 6 residues of the Sirt6 active site (PDB: 3ZG6) near the bound myristoylated lysine (MyK) were chosen for mutagenesis. The residues L9, V115, M157 and I185 were fully randomized (NNK codon), while A53 and V70 were replaced by a small set of mainly hydrophobic amino acids (NYC coding for A, F, I, L, P, S, T and V) resulting in a library of about 10M mutants ($20^4 \cdot 8^2$). B) The randomization of the final library was confirmed by sequencing of 8 colonies without selection, the aligned position only shows expected amino acids in respect to the used codons. C) The library was subjected to one round of positive selection for deacetylation activity and individual clones were sequenced after 2 days (S6.X) and a 96 well plate was picked after 4 days. The 96 well plate was retransformed and reselected on selection plates containing 0.4 mM 6-azauridin. Cells from wells able to grow were sequenced (? not clear, - no sequence). D) 6-Azauridin selection of Sirt6, S6.4 and S6.3 after 3 days of growth. S6.4 showed clearly enhanced resistance to 6-azauridin. Sirt6 wt showed no growth on selection plates after 3 days under these conditions.

The 6-AU selection was previously tested for CobB and increased the selection pressure, benefiting more active mutants. I used the mutants grown after 2 days to determine the maximal 6-AU resistance of the current mutants. Only the S6.3 and S6.4 Sirt6 mutant regrew within 3 days on the 6-AU selection plates. S6.4 showed a 6-AU resistance of up to 0.4 mM (**Figure 15D**) and S6.3 showed some growth unlike the wt Sirt6. Therefore, the 96 well plate was retransformed and reselected on plates containing 0.4 mM 6-AU to enrich for more active mutants. Plasmids isolated from E. coli colony patches, which showed growth under the increased selection pressure, were sequenced (**Figure 15C**). From the collected mutants after 2 days or 4 days of selection no mutant was enriched, as was expected after just one round of selection. In both screenings, a Sirt6 M157 variant was identified, which was mutated to a larger hydrophobic amino acid, commonly phenylalanine. In turn this was accompanied by a reorganization of hydrophobic residues in the active site, commonly interchanging V, L; I, P, F or C at different sites and combinations. This kind of “hydrophobic shuffling” resembles the mutations previously observed in the selection of Sirt1, where they seemingly decreased the active site volume. Three mutants of Sirt6 showed usage of hydrophilic mutations, exchanging amino acids to R, T or E. These might use a different strategy to enhance deacetylation activity. The mutants require further biochemical characterization to determine their deacetylation activity. The developed Fluc assay showed no signal for Sirt6 (not shown), therefore all mutants were sent to our collaboration partner (Mark Klein at Denu Lab, Wisconsin) and await further analysis.

HIGH THROUGHPUT SCREENING FOR SIRT1 INHIBITORS AND ACTIVATORS

Sirt1 is central to a wide range of physiological processes and has been proposed as a potential target for activating (66) or inhibiting drugs (101), which could have beneficial effects in aging related diseases or cancer, respectively.

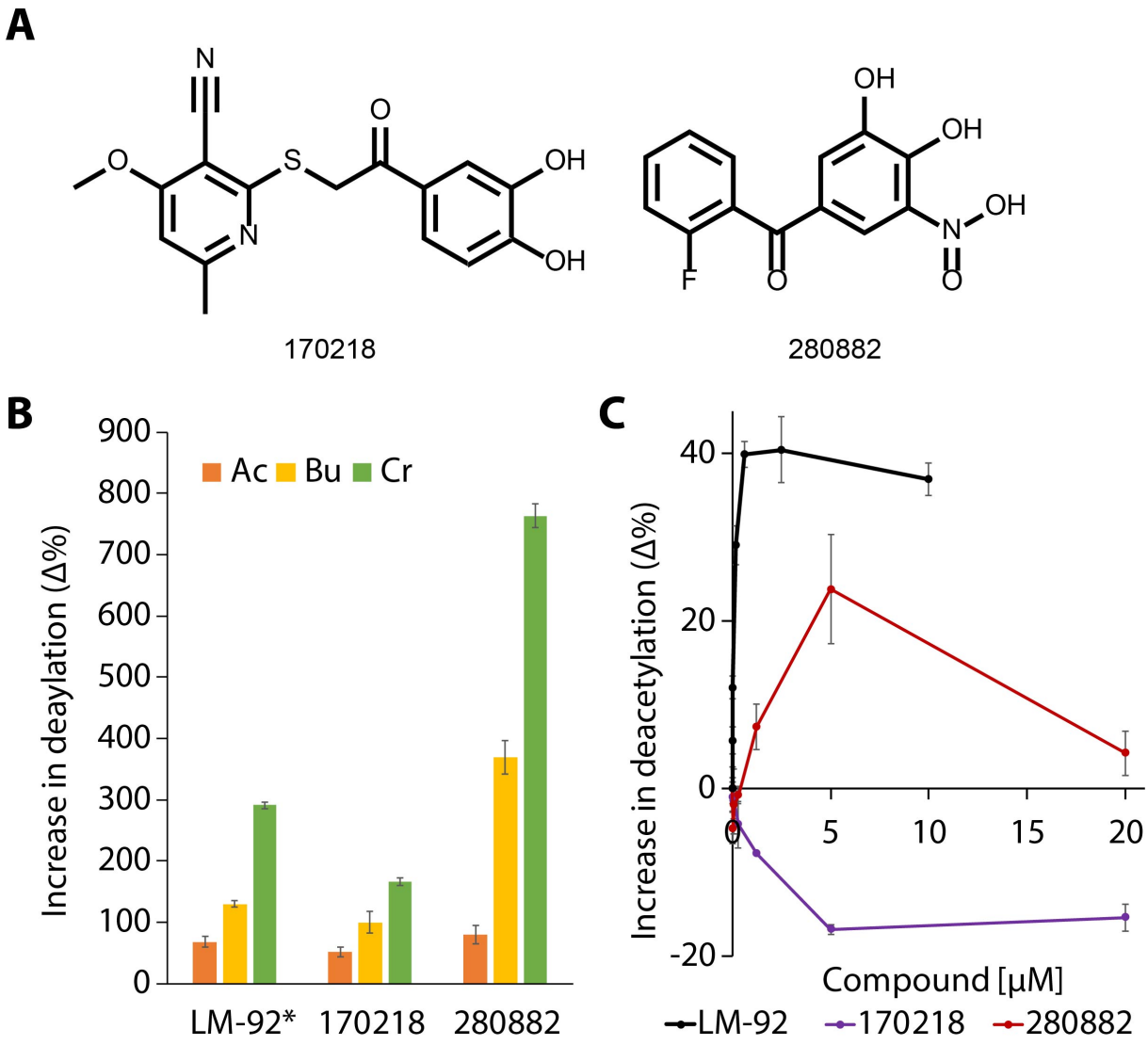

Figure 16: Validation of the activating effect of LM-92 peptide and two activators from the initial COMAS-screening. From the initial screening the two most potent compounds (A) were selected to be validated for activation of Sirt1. As a positive control an intrinsically disordered peptide from the nuclear lamina (LM-92) was purified (**S. Figure 10**). B) Change in deacylation activity in presence of 10 μM compound (* LM-92 estimated to be 1 μM). C) Titration of LM-92 (10 μM to 10 nM, AC50: 70 nM (102)) and the two compounds (20 μM to 20 nM).

In cooperation with the compound management and screening center (COMAS) we established the Fluc assay as a high throughput set up to identify Sirt1 activators or inhibitors within the COMAS-substance library, which consists of more than 240.000 molecules. The COMAS screening identified 21 potential activators and 114 inhibitors of Sirt1. To validate the activating compounds, the two most potent compounds were chosen (**Figure 16A**) and compared to a known Sirt1 activator. To date the most potent Sirt1 activator is the lamin A specific C-terminal region, which can activate Sirt1 *in vitro* at low nM concentrations (102). Since the original paper used solid phase synthesis to obtain the LA-80 peptide (80 aa of the lamin A C-terminus) I assumed that the peptide is intrinsically disordered. This led me to employ a protocol for expression and purification of intrinsically disorder proteins from *E.coli* (103) to express and purify the lamin A C-terminal peptide (here LM-92, 92 aa of the lamin A C-terminus). The LM-92 peptide was purified (**S. Figure 10**) and used as a positive control in the following experiments. It has to be noted that LM-92 was often used at lower concentration compared to the chemical compounds, as its solubility was often a limiting factor. Using the LM-92 peptide as a reference point, we tested the two activators for their ability to activate Sirt1 deacetylation and if the effect differs for other acylations. The LM-92 peptide increased deacetylation by about 50%, while debutyrylation and decrotonylation were increased by 125% and 300%, respectively. The same trend was observed for the two chemical compounds, particularly compound 280882 had a strong effect on decrotonylation by Sirt1 (**Figure 16B**). The correct level of activation cannot be determined and compared with each other since the activators were used in excess. Titration of LM-92 confirmed that it is a very potent activator and Sirt1 was 40% more active for deacetylating than without LM-92 at low nM concentrations. Activation with the chemical activators could only be reproduced for 280882, and it peaked with 20% higher activation of Sirt1 at 5 µM before the level of activation decreased at higher

concentrations. In summary, I could confirm the activating properties of LM-92, but both chemical activators are orders of magnitude less potent than LM-92. It is questionable if the compound 170218 has activating properties for deacetylation. Interestingly, activation is in all cases more efficient for crotonylation. It is possible that crotonyl removal is generally less efficient, compared to other acylation and benefits more from an overall activation of the enzyme (**S. Figure 4A;** shows CobB decrotonylation activity is more sensitive towards NAD^+ concentration than other acylations). The exact mechanism of activation remains unclear, and due to the low potency of the chemical compounds we decided to focus on characterization of the inhibitors.

The initial 114 inhibitors were tested for their selectivity towards Sirt1 over Sirt2 and Sirt3 by COMAS, including the commercial Sirtuin 1 inhibitor Ex527. Overall, this reduced the number of inhibitors to 8, which showed some level of selectivity or high potency (S. Table 5, green). To validate the potential candidate compounds as direct inhibitors of Sirt1, I tested them in an orthogonal assay inhibiting the deacetylation of extracted histone proteins by Sirt1. As a reference compound we used a commercial Sirt1 inhibitor Ex527, which served as a standard throughout the validation process. Acylation levels were detected by Western blotting and revealed that 149107 had some inhibitory effect on Sirt1 (**Figure 17A**). In the Fluc assay, IC50 of 149107 was around 10x higher compared to Ex527, but more selective for Sirt1 (**Figure 17B**). Titrating 149107 in the histone deacetylation assay showed a clear concentration dependent inhibition of Sirt1, but Ex527 is around 10x more potent in direct comparison (**Figure 17C**). Ex527 is known to be a noncompetitive inhibitor stabilizing the intermediate 2 during the deacetylation reaction (104). To test if 149107 acts in a similar way, we measured the impact of the compounds on protein stability in SYPRO Orange thermal shift assays.

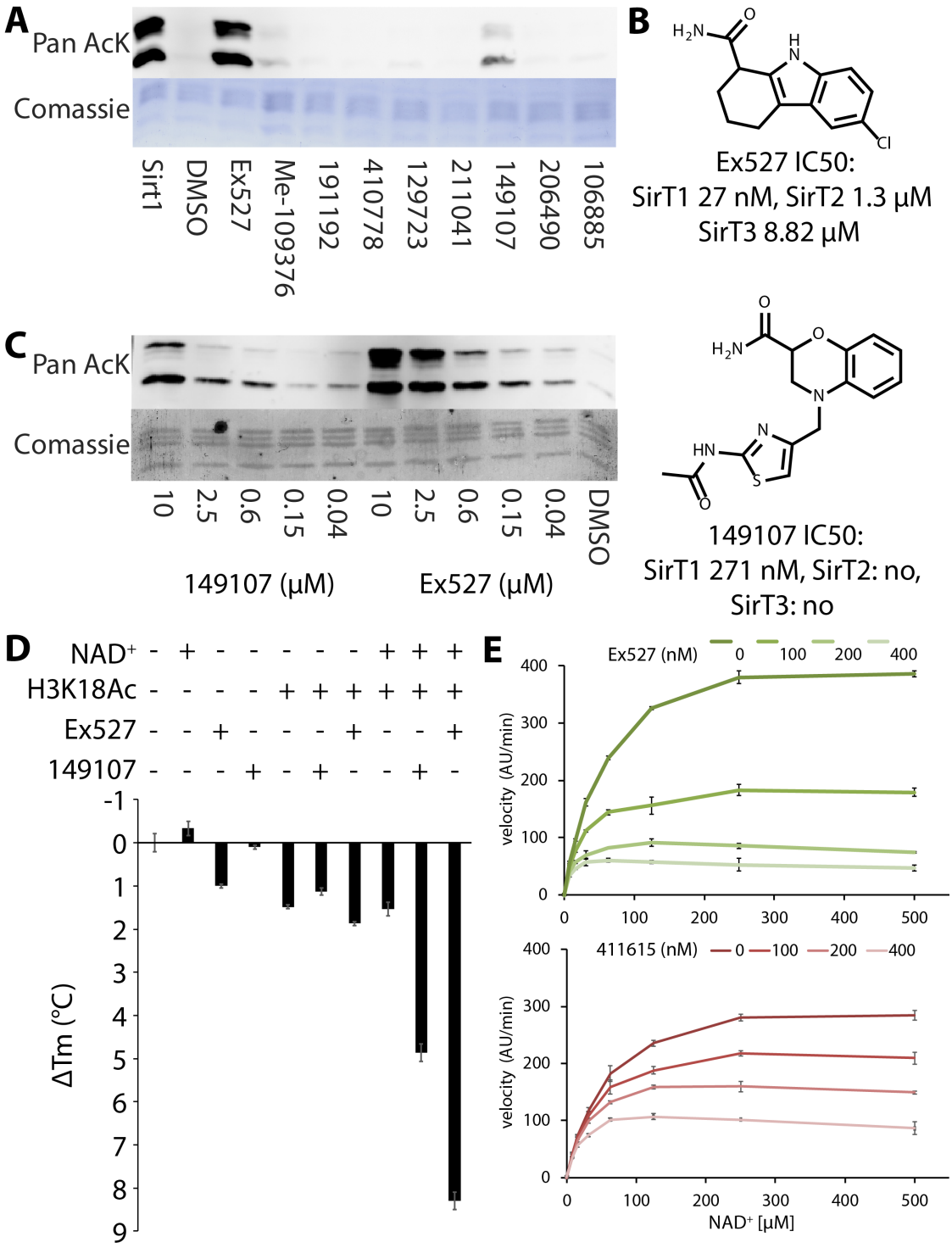

Figure 17: Characterization of 149107 and its optimized derivative 411615 as a Sirt1 inhibitor in comparison to the commercial inhibitor Ex527. A) Deacetylation of histones by Sirt1 in the presence of 10 µM of 8 compounds out of the COMAS screening and Ex527. B) Chemical structure and IC50 of Ex527 and 149107 for Sirt1-3. C) Deacetylation of extracted histone protein with decreasing concentrations of Ex527 and 149107. D) SYPRO Orange thermal shift assay of Sirt1 (1 mg/mL, Tm: 41.5 °C) bound to different combinations of NAD^+ (1 mM), H3K18Ac peptide (1 mM) and Ex527 or 149107 (0.1 mM). E) Michaelis–Menten kinetics of Ex527 and 411615 (new derivate of 149107) shows that both Inhibitors are non-competitive inhibitors (See S. Table 6 for Km and v_{max}).

The apo protein has a melting point (Tm) of 41.5°C, the addition of 149107 has little impact on the melting temperature. Only when NAD^+ and substrate peptide (H3K18Ac) are added, a drastic increase in melting temperature by 4.7°C can be observed. 149107 acts slightly different compared to Ex527, where Ex527 also has an impact on the apo protein. Both have in common that the most drastic increase is observed when all components are added to the reaction (**Figure 17D**). 149107 is therefore likely to be a non-competitive inhibitor, like Ex527. I could confirm this using a more potent chemical derivative of 149107 (411615), developed by COMAS. Using the continuous format of the Fluc assay, 411615 shows the same mode of inhibition as Ex527 (**Figure 17E**), reducing both Km and v_{max} (S. Table 6).

In sum, 149107 is a promising candidate for further optimization, particularly the high isoform selectivity is remarkable. To find the binding site of 149107 and mechanism of inhibition, the compound was send to our collaboration partner Michael Lammers for crystallization. This should allow for a more rational approach when optimizing the compound. If the compound acts differently to Ex527, both compounds might be additive due to their non-competitive nature.

DISCUSSION

The heart of this thesis it the concept for a novel selection system to determine deacylation activity based on genetic code expansion/amber suppression. In the past, genetic code expansion has been used to manipulate protein activity utilizing photolabile (105), photo switchable (106), enzymatically (107) or chemically cleavable protecting groups (108, 109) masking catalytically residues to reactivate protein function in living cells. Here this concept has been further exploited to develop a selection system, which is directly liked to cell survival: The Ura3 was expressed enzymatically inactive by a genetically encoded specific acyl-modified lysine (K93) and its reactivation is a direct consequence of the substrate specify by engineered lysine deacetylases (by directed evolution). Thus, one strength of this system is its broad range of possible KDAC substrates due to the powerful tool of GCE. Currently, these include lysine acetylation (82), propionylation (110), butyrylation (110), crotonylation (110, 111) and hydroxyisobutyrylation (112). This covers about half of the known Sirtuin substrates (113), the applicability of the selection system can be expected to grow in future when GCE is further extended to other lysine modifications, such as the negatively charged succinyl and glutaryl or long chained modifications like myristoylation. The latter modifications are not as abundant as the already available acyl residues (62) but they limit the use of acyl selective KDACs to investigate processes related to these acylation not available by GCE like ketogenesis (114) or membrane localization (115). Apart from the use in investigating lysine acylation the selection system could also facilitate other methods requiring selection, for example drug discovery using genetically encoded cyclic peptides (116). Under my supervision the use of the selection system in creating bump-and-hole Sirtuin 2 mutants was already successfully tested by my master student Damian Schiller (unpublished,

Masterthesis at TU Dortmund), showing its use in detection of small molecule protein interactions.

With the current selection system acyl-selective KDACs can be obtained for all available acylations in a straightforward manner by iterative rounds of selection, as demonstrated for CobB and Sirt1. Unlike rational approaches, as employed for the creation of a crotonyl-selective HDAC1 (68), directed evolution allows to identify mutants with the desired selectivity for any combination of acylations in large mutant pools without requiring detailed knowledge about the acylation binding. The selection system makes acyl-selective mutants available for a wide range of KDACs and acylations, which enables a new methodology to study lysine acylation and their contribution to the epigenetic code.

Using the crotonyl-selective HDAC1 mutants, Wei W et. al. (2017) were able to show the importance of HDAC1 in mouse stem cell differentiation and the genes regulated by HDAC1-dependent crotonylation. Like HDAC1, Sirt1 is essential for differentiation of neuronal cells (117) and in spermiogenesis (118) or osteogenesis (119). The deacetylation selective Sirt1 mutants created here could therefore be used to uncover the role of acylation in these processes. Also, it would be interesting to test if the selection for acylation-selective HDACs could be successful by mutating the residues Wei W et. al. (2017) used, as selection of HDAC8 was possible. This could greatly broaden the range of selective HDAC mutants available, as the rational approached is limited to crotonylation. Although activity for other acylations than acetylation has not been tested.

In general, the impact and interplay of most acylations other than acetyl is unknown. However, a few processes have been identified where acylations, like crotonylation, are essential. One of the first processes identified in which crotonylation plays a central role is the formation of sperm cells (44). One reason for why it was possible to

distinguish the effect of crotonylation in this process was that during spermatogenesis all other acylations are eventually removed. In other cells the acylation patterns are more complex and identifying the genes regulated by crotonylation is not easily possible. Here the mutant $CobB_{ac2}$ could be an interesting candidate to investigate the impact of lysine crotonylation specifically. Since $CobB_{ac2}$ removes all tested acylation except for crotonylation it can manipulate the epigenetic code in a unique manner. As we have shown in the cellular context of HeLa cells, expression of the mutant maintains histone crotonylation but removes all other acylations. This ability to precisely manipulate the epigenetic code might allow for the identification of crotonyl-specific gene expression and follow its interplay with other posttranslational modifications. For example, hardly anything is known about the interaction between butyrylation and crotonylation, which the mutant can differentiate very well.

The unique selectivity of $CobB_{ac2}$ is the consequence of two active site point mutations, A76G and I131C which specifically block deacylation of crotonyl-lysine. The crystal structures of $CobB_{ac2}$ showed that the mutations are do not influence the enzyme's ability to bind different substrates. Instead the mutations allow for a conformational change of the CBL spanning the active site. The conformational changes depend on the type of acylation bound to $CobB_{ac2}$. Butyryl-lysine induces the "active" conformation, while Crotonyl-lysine induces a new "inactive" conformation. This conformational change occurs due to an induced fit (120) upon binding of crotonyl. The induced nature becomes apparent in the acetyl lysine bound structure. This structure shows a complex mixture of different loop conformations bound to acetyl, demonstrating that substrate binding does not require a specific protein conformation and excluding the possibility of conformational selection (120).

The induced conformation ultimately results in the stabilization of the recently discovered Int.3, indicating a defect in the hydrolysis of the intermediate. The two key

residues, who swapped positions in the induced conformation, F60 (71) and W67 (37) have been so far manly be described to shield the intermediate 1 and 2 from hydrolysis. In a molecular dynamic simulation Shi et al. 2013 predicted the occurrence of a the Int. 3 (compare **Figure 1** and **Figure 11**) as a novel reaction intermediate. Accoring to the study a conformational change of the CBL is allowing the access of water to the active site through removal of the Y40 (W67, when positioned as in CobB wt) once Int.3 forms. This results in the hydrolysis of Int. 3 supported by the residue R34 (R61 in CobB, conserved in all Sirtuins) and product release. $CobB_{ac2}$ undergoes the same catalytic steps in the induced inactive conformation but when Int. 3 forms the new arrangement of W67 and F60 prevents the conformational change to allow water to enter the active site and initiate the hydrolysis reaction. The “inactive” CBL slowly refolds to a conformation resembling the native state, but despite the presence of water no hydrolysis of Int. 3 occurred. Most likely is this state is not truly equivalent to the native state, as for example the key R61 has not refolded into the predicted position.

Overall, the structures support the proposed mechanism by Shi et al. 2013 and that the previously found Intermediate 3 by Wang et al. 2017, using a non-hydrolysable substrate, is indeed a new reaction intermediate. That the CBL dynamic can respond to different acylation raises the question if natural changes to the CBL, for example posttranslational modifications or disease related mutations, could have consequences for the Sirtuin deacylation selectivity.

During our search for a Sirt1 activator, we found some evidence that manipulation of acylation selectivity in vivo might be possible. The reference compound LM-92 is a short intrinsically disordered peptide derived from lamin A, which is known to activate the deacetylation activity of Sirt1 (102). Our experiments could confirm that the peptide activated decrotonylation and debutyrylation even more strongly. This opens a new perspective on the role of the nuclear lamina and Sirt1 in diseases like aging and

progeria. The LAΔ50 mutation in the LM-92 (deletion of 50 aa) is one of the most common mutations causing progeria, but unlike other progeria mutations the lamina appears normal (121). Instead the mutation causes abnormal gene expression and influences the differentiation of adipocytes and osteoblasts (122), two processes related to Sirt1 (119). The newly developed mutants and methods might allow to unravel the interplay of Sirt1, lamin A and crotonylation.

The Sirt1 activators of our initial screening enhance decrotonylation in the same manner as LM-92, but their potency was several orders of magnitude lower compared to LM-92. Hence, none of them was pursued further. In future screening, it might be sensible to directly screen for activation of decrotonylation as the increase in signal is much more pronounced. Further, a better mechanistic understanding of Sirt1 activation would be beneficial for optimization of potential chemical activators.

Inhibition of Sirt1 is another interesting drug target due to its anti-cancer activity, and novel inhibitors with better clinical efficacy compared to Ex527 are still sought-after (123). The COMAS screening produced a novel chemical scaffold, which we confirmed to be a true Sirt1 Inhibitor *in vitro*. Like Ex527, 149107 is a non-competitive inhibitor, stabilizing the enzyme substrate complex. Compared to Ex527, our derivatives have lower affinity for Sirt1 but are more selective. Further cellular assays are necessary to test if the novel compounds are applicable in a cellular context. For instance, the effect of the compound on p53 K382 acetylation (124) can be tested as a intracellular Sirt1 target.

Sirt1 inhibition has shown promising results in treatment of breast cancer (125, 126). For our developed inhibitor to aid in these therapeutic approaches, further investigation in their mechanism of action and physiological properties are necessary. The initiated crystallization by the group of Prof. Dr. Michael Lammers and cellular experiments could aid future efforts to improve the inhibitor. In general, because of the strong

intrinsic selectivity and decent potency, the novel scaffold is a promising candidate for Sirt1 inhibition.

So far manly Sirt1 was discussed, as it is one of the best studied Sirtuins with well-defined enzymatic activity and physiological roles. But I was also interested, if the developed methods can address the role of emerging Sirtuins, like Sirt6 and Sirt7. While I confirmed that selection is possible with both, we aimed to address the function of Sirt6 activation in cooperation with the group of Prof. Dr. John Denu. There have been other attempts to use rationally designed ancestral Sirt6 mutant libraries (88 mutants) to create a more active version of Sirt6 (127). One variant showed higher *in vitro* demyristoylation activity but the deacetylation activity was reduced *in vivo*. Our approach is far less limited in number of mutants and the screening of more than 10 million mutants left a small amount of hit mutants, remarkably similar in sequence. Whether the mutants have enhanced deacetylation activity, as our 6-AU resistance assay suggests, is currently verified by collaborators. If one of the mutants is indeed constitutively activated for deacetylation, this can be a valuable tool to confirm the mechanism of activation (100) and can be used to closer examine the function of Sirt6 deacetylation vs demyristoylation *in vivo*. As Sirt6 possess several key targets which are acetylated lysines, as the deacetylation of H3K9Ac (128) or H3K56Ac (129) are depended on Sirt6.

Finally, I was able to identify CobB mutants with deallylation and boc-deprotection activity by selection. The crystal structure indicated that the two mutations, I131V and V187L, are supporting the binding of the new substrates, and the fundamental reaction mechanism remains the same as for acetylated substrates. This is consistent with the dependency of both reactions on NAD^+ and the sensitivity to nicotinamide. While the activity of the CobB F7 mutant is relatively low compared to the deacetylation activity a better understanding of the mechanism might allow for future optimization of the

initial activity, genetic code expansion also offers a wide range of protection groups which could also be tested (83). While the use of enzymes in chemical synthesis is still an exception (130) the evolved enzymes might find application in peptide synthesis, as they specifically deprotect lysines in a wide sequence context (94). The initial work here was already extended to human sirtuins by my master student Anto Filipovic, who was able to engineer robust deallylation activity into human Sirt2 (unpublished, master thesis at the TU Dortmund). These biorthogonal, human enzymes could find application in immunotherapies would, as they are likly non-immunogenic compared to other bioorthogonal enzymes (131). One current approach in cancer therapy uses CRISPR/Cas9 engineered immune cells to more specifically target cancer cells, but while the engineering and targeting was successful, the immune cells were unable to fully remove the cancer (132). Equipping the immune cell with a biorthogonal enzymes might allow to target the cancer cells without relying on the native immune response, as many malignant cancers developed survival strategies to escape the immune respons (133). The mutation necessary could be CRISPR/Cas9 edited into the immune cells, while a bioorthogonal inactivated toxic protein or peptide is externally added and catalytically reactivated in the proximity of the cancer.

In sum, I established new methodology to discover and characterize evolved lysine deacetylases utilizing genetic code expansion. The selection system has been shown to be compatible with HDAC8, Sirt1-3 and the less well characterized Sirt6 and Sirt7. The acyl-selective mutants of Sirt1 and CobB are capable of manipulating acylation patterns and could help to deconvolute the functions of lysine acylation in the future. The structural analysis of $CobB_{ac2}$ has shown experimentally the impact of the protein dynamics on acylation activity and aided in a better understanding of the Sirtuin deacetylation mechanism. The new Fluc assay simplifies measurement of different acylation activities immensely and could facilitate drug discovery. The drug screening

carried out at the COMAS facility using the Fluc assay produced novel drug scaffolds for activation and inhibition of Sirt1. I am confident that the directed evolution based approach to manipulate the epigenetic code, as it is portrayed in this thesis, will enable a better understanding of lysine acylation in the future.

MATERIAL AND METHODS

MATERIAL

CHEMICALS

Table 1: List of used chemicals, brackets contains their abbreviation or chemical formula.

Manufacture	Chemicals
ACROS Organics	Sodium butyrate
Alfa Aesar	Nicotinamide (NAM)
Applichem	Ampicillin, Bovine serum albumin, Chloramphenicol, Dipotassium phosphate (K_2HPO_4), Potassium dihydrogen phosphate (KH_2PO_4), Leucine, Spectinomycin, Tryptophan, Uracil, Valine
BACHEM	Acetyl-lysine (AcK), Alloc-lysine (AllocK), Boc-lysine (BocK)
Carbosynth	Butyryl-lysine (BuK)
Chem-impex	Crotonyl-lysine (BuK)
ChemCruz	4-(2-aminoethyl)benzenesulfonyl fluoride hydrochloride (AEBSF)
Difco Laboratories	Bacto trypton
Fischer	Ethanol, trichloroacetic acid (TCA)
Gerbu	Dithiothreitol (DTT), Glycerol, 3-(N-morpholino)propanesulfonic acid (MOPS), Disodium ethylenediaminetetraacetic acid (EDTA)
Gibco life technologies	DMEM+GlutaMAX™-I, fetal bovine serum (FBS)
ITW Reagents	Acetic acid, Hydrochloric acid (HCl), Sodium acetate (NaAc),
J.T. Baker	Iso-propanol, magnesium chloride ($MgCl_2$). Potassium chloride (KCl), Sodium bicarbonate ($NaHCO_3$)
Merck	Glutathione (GSH, reduced), Imidazole, Methanol, Sodium hydrogen phosphate (Na_2HPO_4), Zinc chloride ($ZnCl_2$)
ROTH	Aprotinin, Calcium chloride ($CaCl_2$), Glycine, Isopropyl β-d-1-thiogalactopyranoside (IPTG), Potassium acetate (KAc), Potassium hydroxide (KOH), Arabinose, Leupeptin hemisulfat, Phenymethylsolfonyl-fluorid (PMSF), Sodium dodecyl sulfate (SDS), Tetra-methylethylenediamine (TEMED), Tris (hydroxymethyl) aminomethane (Tris), Triton X-100
SERVA	Bromphenol blue, 4-(2-hydroxyethyl)-1-piperazineethanesulfonic acid (HEPES), Lysozyme
Sigma	6-Azauridine (6-AU), Agarose, Ammonium persulfate (APS), Adenosine triphosphate (ATP), 2-(hydroxymethyl)propane-1,3-diol (Bis-Tris), Dimethyl sulfoxide (DMSO), DNAse I, Isoleucine, Kanamycin, Nicotinamide adenine dinucleotide (NAD^+), Magnesium sulfate ($MgSO_4$), Manganese (II) chloride ($MnCl_2$), Polyethylene glycol (PEG3350, PEG400), Ponceau S, Rubidium chloride (RbCl), Skim milk, Tetracycline hydrochloride, TFA, Tricine, Tris(2-carboxyethyl)phosphine hydrochloride (TCEP), Trypsin
Thermo	D-Luciferin monosodium, Deoxy-nucleoside triphosphate (dNTP)
UKENNOR	Propionyl-lysine
VWR Chemicals	Sodium Clorid (NaCl), Tween-20
Waldeck	Sodium hydroxide (NaOH)
Zymo Research	5-Fluoroorotic acid (5-FOA)

CONSUMABLES AND COMMERCIAL KITS

Table 2: Manufacturer and product name of the commercial products used in this thesis.

Manufacture	Product name
Applichem	Acrylamide 4K solution (30 %) 37.5 : 1
BioRad	Electroporation Cuvettes 2 mm, Immuno-Blot PVDF Membrane, Poly-Prep chromatography column
Brand	96 well PCR plate
costar	96-deep well block
Eppendorf	combi tips (100, 200, 500, 1000, 2000, 5000 μL)
Expedeon	InstantBlue Protein Gel Stain

Manufacture	Product name
GE Healthcare	Amersham™ Protran™ NC Nitrocellulose-Membrane, Filterpaper Whatman No. 4
Gibco	Freestyle™ 293 Expressionsmedium
Greiner Bio-one	Petri dishes
Jena Bioscience	SuperClear™ Plates, pregreased
Merck	Centrifugal filter tubes
Millipore	Amicon Filter Concentrators
Nanotemper	Prometheus NT.48 Series nanoDSF Grade Standard Capillaries
NEB	6x Gel Loading Dye Purple, Various restriction enzymes
omega	E-Z 96® FastFilter Plasmid DNA Kit
PEQLAB	peqGOLD Plasmid Miniprep Kit
Promega	Dual-Luciferase® Reporter Assay System
QIAGEN	Midi & Maxi Plasmid Prep Kit, QIAquick PCR Purification Kit, QIAquick Gel Extraction Kit
Roche	Expand™ High Fidelity PCR System
Sarstedt	Falcon Tubes (15 mL, 50 mL), Cuvettes, Microreaction tubes (1.5 mL, 2 mL)
Thermo	T4 DNA Ligase, 96 Well Plate Microfluor 1 Black, Gene Ruler 1 kb GeneJET™, Glass Slides, Plasmid-Miniprep-Kit, Lipofectamine 2000, Ni-NTA HisPur Superflow Agarose, PageRuler™ Prestained Protein Ladder 10 to 180 kDa, Phusion High-Fidelity DNA Polymerase, Restriction enzymes, Taq DNA Polymerase,
VWR	GelRed DNA dye

BUFFER

Table 3: Chemical composition of all used buffers.

Buffer Name	Ingredients
2x luciferin buffer	40 mM Tricine, 200 µM EDTA, 7.4 mM $MgSO_4$, 2 mM $NaHCO_3$, 34 mM DTT, 0.5 mM ATP and 0.5 mM luciferin, pH 7.8
4x SDS-sample buffer	250 mM Tris, 100 mM DTT, 6% SDS,40% glycerin, 20% bromophenol blue
COMAS reaction buffer	25 mM Tris/HCl pH 8.0, 137 mM NaCl, 2.7 mM KCl, 1 mM $MgCl_2$, 1 mM GSH
ESI Buffer	40 mM Tris buffer, 50 mM NaCl, 1 mM DTT, 0.1 mM $ZnCl_2$, pH 8
gel filtration buffer	20 mM HEPES pH 7.5, 100 mM NaCl, 10 mM DTT
HDAC8 buffer	50 mM HEPES pH 7.4, 100 mM KCl, 0.001% Tween-20, 5% DMSO, 0.25 mM TCEP and 0.1 mM $ZnCl_2$
HEC293 lysis buffer	25 mM Tris pH 8, 300 mM NaCl, 10% glycerol, 1 mM TCEP, 1 mM EDTA, 5 µg/ml AEBSF, 5 µg/ml aprotinin, 5 µg/ml leupeptin
luciferase wash buffer	20 mM Tris/HCl pH 8, 10 mM imidazole, 200 mM NaCl, 10 mM DTT
LB medium	1% Bacto Trypton, 0.5% Yeast Extract, 1% NaCl, pH 7.4
LM-92 gel filtration buffer	20 mM Bis-Tris pH 6.8, 50 mM KAc, 10 mM DTT
LM-92 wash buffer	20 mM Bis-Tris pH 6.8, 300 mM KAc, 10 mM Imidazole, 1 mM DTT
luciferase storage buffer	20 mM Tris pH 8, 50 mM NaCl, 10 mM DTT or 1 mM TCEP
M9 minimal medium	33.7 mM Na_2HPO_4, 22.0 mM $KHPO_4$, 8.6 mM NaCl, 9.4 mM NH_4Cl, 1 mM $MgSO_4$, 0.4% glucose, 0.1 mM $CaCl_2$ pH 7.4
M9 selection plates	M9 minimal medium, 0.2% arabinose, 1% glycerol, 0.4% glucose, 0.1 mM tryptophan, 80 mg/L valine, 80 mg/L isoleucine, 80 mg/L leucine, 50 mg/mL kanamycin, 15 mg/mL tetracycline, ± 0.1 mM uracil, ± 10 mM acetyl-lysine or 1 mM other modifications
Ni-NTA wash buffer	20 mM HEPES pH 7.5, 200 mM NaCl, 20 mM imidazole, 1 mM DTT
PBS	13.7 mM NaCl, 2.7 mM KCl, 10 mM Na_2HPO_4,1.8 mM KH_2PO_4, pH, 7.4
Ponceau S Staining Solution	0.1% Ponceau S, 1% Acetic Acid
SDS running buffer	25 mM Tris, 192 mM Glycine, 0.1% SDS pH 8.3
SDS Seperation Gel buffer	1.5 M Tris, pH, 8.8, 0.4% SDS
SDS stacking gel Buffer	1 M Tris, pH, 6.8, 0.8% SDS
Sirtuin buffer	25 mM Tris/HCl pH 8.0, 137 mM NaCl, 2.7 mM KCl, 1 mM $MgCl_2$, 1 mM DTT, 1 mg/ml BSA
Sirtuin gel filtration buffer	20 mM Tris pH 8, 50 mM NaCl, 10 mM DTT
Sirtuin wash buffer	20 mM Tris pH 8, 200 mM NaCl, 20 mM Imidazole
sodium acetate solution	3 M NaAc, pH 5.2
TAE buffer	40 mM Tris, 100 µM EDTA, 20 mM Acetic acid
TBS	150 mM NaCl, 10 mM Tris, pH 7.5
TBST	TBS, 0.05% Tween-20
TFB1	100 mM RbCl, 50 mM $MnCl_2$, 30 mM KAc, 10 mM $CaCl_2$, 15% Gycerol, pH 5

Buffer Name	Ingredients
TFB2	10 mM MOPS, 10 mM RbCl, 75 mM $CaCl_2$, 15% Glycerol, pH 8
Towbin-transfer buffer	25 mM Tris, 192 mM Glycine, 20% methanol, pH 8.3

PLASMIDS

Table 4: Plasmids created and used throughout this thesis. Abbreviations for resistant marker genes: Tet: Tetracycline, Spec: Spectinomycin, Kan: Kanamycin, Cm: Chloramphenicol, Amp: Ampicillin

Vector	Insert	Resistance	Box Position
pPylT	URA3	Tet	10H5
pPylT-URA3 K93TAG	PylS	Tet	10H6
pPylT-URA3 K93TAG	AcKRS3	Tet	10H7
pCDF DUET-1	-	Spec	8
pMyo4TAG	PylT	Tet	112
pBK	PylS	Kan	147
pPylT	DLR TAG	Tet	191
pBK	AcKRS3	Kan	206
pKD46	non	Amp	11B4
pCRISPR	non	Kan	11B1
pCAS9	non	Cm&Tet	11B2
pdCAS9	non	Cm&Tet	11B3
pCRISPR	CobB-PAM clone #5	Kan	11C1
pETDuet1	Fluc K529TAG-His6	Spec	12C1
pBAD	CobB	Kan	M1A3
pBAD	HDAC8	Kan	M1A2
pCRISPR	PyrF	Kan	M1A4
pBAD	4	Kan	M1A5
pBAD	1	Kan	M1A6
pBAD	1N	Kan	M1A7
pBAD	4+2+3 full CobB library	Kan	M1A8
pBAD	4+2	Kan	M1A9
pCRISPR	Pyr_spec	Spec	M1B1
pMA7CR_2.0	non	Amp	M1B2
pACBB-TetT-LVA	non	Cm	M1B3
pMAZ-SK	non	Kan	M1B4
pREDTAI	non	Amp	M1B5
pCRISPER	non	Spec	M1B6
pMAZ-SK_User	non	Kan	M1B7
pCAS9_gRNA-Spec	gRNA_spec	Cm	M1B8
pMAZ-SK CobB	gRNA_CobB	Kan	M1C1
pMAZ-SK PyrF	gRNA_PyrF	Kan	M1C2
pCRISPER_I-Sec-I_1	non	Kan	M1C3
pCRISPER_I-Sec-I_2	non	Kan	M1C4
pCRISPER_I-Sec-I_1u2	non	Kan	M1C5
pRSF-Duet1-His6-Sirt1	Sirt1 cat	Kan	M1C6
pGEX-T5S-TEV-Sirt2	Sirt2 cat	Amp	M1C7
pGEX-T5S-TEV-Sirt3	Sirt3 cat	Amp	M1C8
pBK-His6-Sirt1	Sirt1 cat	Kan	M1D1
pBK-His6-TEV-Sirt2	Sirt2 cat	Kan	M1D2
pBK-His6-TEV-Sirt3	Sirt3 cat	Kan	M1D3
pBK-His6-trom-Sirt7	Sirt7_full	Kan	M1D4
pGFP (petra)	His6-NSirt1C wt	Kan	M1D5
pGFP (petra)	His6-NSirt1C B2	Kan	M1D6
pGFP (petra)	His6-NSirt1C G2	Kan	M1D7
pGFP (petra)	His6-NSirt1C F2	Kan	M1D8
pGFP (petra)	His6-NSirt1C H10	Kan	M1E1
pGFP (petra)	NSirt1C B2	Kan	M1E3
pGFP (petra)	NSirt1C G2	Kan	M1E4
pGFP (petra)	NSirt1C F2	Kan	M1E5
pGFP (petra)	NSirt1C H10	Kan	M1E6
pGFP (petra)	myc-NSirt1C B2	Kan	M1E8
pGFP (petra)	myc-NSirt1C G2	Kan	M1F1
pGFP (petra)	myc-NSirt1C F2	Kan	M1F2
pGFP (petra)	myc-NSirt1C H10	Kan	M1F3
pGFP (petra)	empty	Kan	M1F4
pECE	Flag-Sirt1 (full)	Amp	M1F5

Vector	Insert	Resistance	Box Position
pGFP (petra)	LMNA	Amp	M1F6
pGFP (petra)	LMNA 586	Amp	M1F7
pBK	CobB wt F60W W67F	Kan	M1F8
pBK	CobB wt F60Y	Kan	M1G1
pBK	CobB B1 F60W W67F	Kan	M1G2
pBK	CobB B1 F60Y	Kan	M1G3
pET15	Sirt5 A82W	Amp	M1G4
pET15	Sirt5 iso3 del189-206	Amp	M1G5
pET15	Sirt5 A82W	Amp	M1G6
pET28	Sirt7 Y119F	Kan	M1G7
pET28	Sirt7 C189I	Kan	M1G8
pET28	Sirt7 C189V	Kan	M1H1
10H5	Ura3 K93TAG	Tet	M1H2
pCDF	LM-92	Spec	M1H3
pCMV	NLS-CobB-GFP	Kan	M1H4
pCMV	NLS-CobBAc2-GFP	Kan	M1H5
10H5 (TAG)	Ura3 pylS(Z)	Tet	M1H6
pCMV	Sirt1-full-GFP	Kan	M1H7
pCMV	NLS-CobBAc3-GFP	Kan	M1H8
px459 (puro)	gRNA Position 3	Amp	M2A1
px459 (puro)	gRNA Position 4	Amp	M2A2
px459 (puro)	gRNA Position 5	Amp	M2A3
px459 (puro)	gRNA knockout	Amp	M2A4
px459 (puro)	gRNA cat His	Amp	M2A5
px458 (GFP)	gRNA Position 3	Amp	M2A6
px458 (GFP)	gRNA Position 4	Amp	M2A7
px458 (GFP)	gRNA Position 5	Amp	M2A8
px458 (GFP)	gRNA knockout	Amp	M2B1
px458 (GFP)	gRNA cat His	Amp	M2B2
pBAD	Sirt6	Kan	M2B3
pECF	Flag-Sirt1-B1	Amp	M2B4
pECF	Flag-Sirt1-H9	Amp	M2B5
pBK	His-Sirt7-C2	Kan	M2B6
PBK	His-Sirt7-E2	Kan	M2B7
pBK	His-Sirt7-A2	Kan	M2B8
pCDF	His6-Sirt1cat	Spec	M2C1
pCMV	NLS-Sirt1cat-GFP	Kan	M2C4
pCMV	NLS-Sirt1cat(VAFLM)-GFP	Kan	M2C5
pCMV	NLS-Sirt1cat(MM)-GFP	Kan	M2C6
pBK	Sirt6 act. Site library	Kan	M2C7
pBK	HDAC8 act. Site library	Kan	M2C8
pBK	Sirt1 acti site library	Kan	S1L 1.2

ANTIBODIES

Table 5: List of the used antibodies.

Antigen	Company	Typical conditions and dilution	Host
H4 K16ac	Abcam (ab109463)	3% Milk/TBS 1:15000	Rabbit
Pan-AcK	PTM biolabs (105)	5% BSA/TBST 1:2000	Rabbit
Pan-BuK	PTM biolabs (301)	5% BSA/TBST 1:1000	Rabbit
Pan-CrK	PTM biolabs (502)	5% Milk/TBST 1:2000	Rabbit
Rabbit-HRP	Sigma (A6154)	5% Milk/TBS 1:10000	Goat
Rabbit-Cy3	Jackson Immune Research (111-165-144)	3% BSA/PBS 0.1% Triton X-100 1:1000	Goat

CELL LINES AND *E. COLI* STRAINS:

Table 6: Genotype and source of the *E.coli* strains used in this study

Organism	Strain	Genotype	Source
E. coli	DH10B	F– *mcr*A Δ(*mrr-hsd*RMS-*mcr*BC) Φ80*lac*ZΔM15 Δ*lac*X74 *rec*A1 *end*A1 *ara*D139 Δ(*ara leu*) 7697 *gal*U *gal*K *rps*L *nup*G λ–	Invitrogen
E. coli	DB6656	F-, *lacZ624*(Am), *λ*-, *trpA49*(Am), *pyrF79::Mu*, *rpsL179*(strR), *hsdR27*	CGSC
E. coli	BL21 DE3 RIL	E. coli B F- ompT hsdS(rB- mB-) dcm+ Tetr E. coli gal λ (DE3) endA Hte [argU ileY leuW Camr]	Millipore
E. coli	DH10B Δ*pyrF* Δ*cobB*	F– *mcr*A Δ(*mrr-hsd*RMS-*mcr*BC) Φ80*lac*ZΔM15 Δ*lac*X74 *rec*A1 *end*A1 *ara*D139 Δ(*ara leu*) 7697 *gal*U *gal*K *rps*L *nup*G λ– *CobB PyrF*	This thesis
Human	HEK293	-	Inhouse
Human	HeLa	-	Inhouse

EQUIPMENT

Table 7:List of the used equipment an manufacturers

Purpose	Manufacturer	Product
Centrifuge	Beckman Coulter	Allegra X-22 R
		Allegra X-22 R
		Avanti J-26S XP
		J-25-50
		JLA-8.1
	Eppendorf	Centrifuge 5810 R
		Centrifuge 542-4
Chromatography	GE-Healthcare	HILoad™ 26/60 Superdex™ 200
		HILoadTM 26/60 SuperdexTM 75
Documentation	BMG Labtech	FluoStar Omega Microplate Reader
	Biostep	Imager Celvin® S 320
	BioRad	GelDoc XR
	Sony	Thermo printer UP-D895
	Epson	Perfection V850 Pro
Electroporation	BioRad	GenePulser Xcell
		+ PC Module
		+ CE Module
Incubator	Eppendorf	New Brunswick™ S41i
	Memmert	Universalschrank UN
Microscope	Zeiss	LSM800/510
		Primovert
PCR cycler	BioRad	C1000 Touch Thermal Cycler
		CFX96 Touch Real-Time PCR Detection System
	SensoQuest	Lab cycler
Photometer	NanoDrop	Spectrophotometer ND-1000
	biowave	WPA
Pipettes	Eppendorf	Multipette M4
		1000, 200, 100, 20, 10 µL Eppendorf res
	Hirschmann	Pipetus
Power source	BiorRad	PowerPaC 300
	Major Science	MP-250V
Purification	GE- Healthcare	Äkta Purifier 10
		Äkta prime
		Frac-950
	Hyland Scientific	110 S Microfluidizer
Shaker	Eppendorf	Thermo mixer comfort
	Scientific Industries	Vortex Genie 2
	New Brunswick Scientific	Excelle E24 Incubater Shaker Series"
	Multitron Pro	INFORS HT
Utility	3D printed, inhouse	48-pin head replicator
	Biorad	Trans-Blot Turbo Transfer System
		Agarose Electrophoresis and Casting Systems
	Custom made	SDS-Page Electrophoresis and Casting System
	Eppendorf	Multichannelpipette(10-100 µL) Research plus
		Xplorer electronic pipettor
	Heidolph	Magnet stirrer MR 3000
		Automatic pump SP Quick

Purpose	Manufacturer	Product
	Mettler Toledo	pH-meter FE20 FiveEasy
	Nanotemper	Prometheus
	Satorius	Analytical balance PT1200
	Sharp	Microwave 800W
	Schott	Glassware
	Stuart	Roller mixer SRT6D
	Thermo	Herasafe™ KSP

PRIMER

Table 8 Primer sequences from 5' to 3'. Degenerated positions are label as **N**: A, T, C, G; **V**: A, C, G; **W**: A, T; **S**: G, C; **M**: A, C; **K**: G, T; **R**: A, G; **Y**: C, T.

ID	Oligo Name	sequence
P1N	CobB_rv	GCGCAGAGGTCTCACTGCGGCGCGAAAGGTACGAATACCTG ATTCCGCAGAAATTCCTGCCCCTGTCAGTACGAGTACTCTTG
P1	CobBA76**NNK**fw-new	GCGCAGGAAAGGTCTCAGGAAGAACATCGGGTTGAAGATGT G**NNK**ACGCCGGAAGGTTTCGATCGCGATC
P2	CobBa49F60**MNN**rv	GCGCAGAGGTCTCACTGCGGCGCG**MNN**GGTACGAATACCTG ATTCCGCAGAAATTCC**MNN**CCCTGTCAGTACGAGTACTCTTG
P3	CobBV187**NNK**fw	GCGCAGGAAAGGTCTCACCGCAC**NNK**GTGTGGTTTGGCGAA ATGCCAC
P4	CoBBV187rv	GCGCAGAGTAGGTCTCAGCGGGCGCAAGGGTGCCGGAAAC
P5	CobBI131**NNK**fw	GCGCAGGAAAGGTCTCACAGAAT**NNK**GACAACCTGCATGAA CGCGCAG
P6	CoBLib3rev	GCGCAGAGTAGGTCTCATCTGCGTCACCAGCAAAAAGCGATC
P7	CobB_cheak_rv	CCAGTCGAGAACCTGACCAC
P8	CobB_cheak_fw	CGCGCGCGCCACGGTGATG
P9	crPyrFPAM_Bsalfw	AAACAAGGTCGGCAAAGAGATGTTTACATTGTTTG
P10	crPyrPam_Bsalrv	AAAACAAACAATGTAAACATCTCTTTGCCGACCTT
P11	PyrFedit_fw	CAGGTCGGCAAAGAGATGTTTACATTGTAAGCTTAACAGTTTG TGCGCGAACTTCAACAGCGTG
P12	PyrFedit_rv	CACGCTGTTGAAGTTCGCGCACAAACTGTTAAGCTTACAATG TAAACATCTCTTTGCCGAGGTTC
P13	CobBY92R95**NNK**_fw	GCGCAGGAAAGGTCTCACGATCCTGAACTGGTGCAAGCGTTT **NNK**AACGCC**NNK**CGTCGACAGCTGCAGCAGCCAG
P14	CobBF76**NNK**_rv	GCGCAGAGTAGGTCTCAATCGCGATCGAAACCTTCCGGCGT **MNN**CACATCTTCAACCCGATGTTCTTC
P15	pCRISP_PAM_seq	TGAGTGAGCTGATACCGCTC
P16	PyrFCheak_fw	GACGTTAACTGCTTCATCTTC
P17	PyrFCheak_rev	GCATGAACATTCACCATCCAC
P18	crCobBPAM_BasI_fw	AAACTGGAAAAACCAAGAGTACTCGTACTGACAGG
P19	crCobBPAM_BasI_rev	AAAACCTGTCAGTACGAGTACTCTTGGTTTTTCCA
P20	pBKseq_rev	GCCTACAAAAGCACGCAA
P21	CobBbp32edit-fw	TGGAAAAACCAAGAGTACTCGTACTGACATAAGCTTAAATTTC TGCGGAATCAGGTATTCGTACCT
P22	CobBbp32edit-rev	AGGTACGAATACCTGATTCCGCAGAAATTTAAGCTTATGTCAG TACGAGTACTCTTGGTTTTTCCA
P23	M241_**NNK**_fw	GCGCAGAGGTCTCATGGAACGT**NNK**GGCATTAACAACGACA CCGA
P24	M241_**NNK**_rev	GCGCAGAGGTCTCATCCACATATTCCGCCGGAATCAGAATCG GGC
P25	Y349_**MNN**_rev	GCGCAGAGGTCTCAGTTCCAGATCGCCATGCATAATATCCAG GGTATCGCC**MNN**CACCATGCAGCTATCGC
P26	V370_L372_D373_I378_**NNK**_F w	GCGCAGAGGTCTCAGAACTGAGCAGCGCGGTGGTGGGTCC G**NNK**AGC**NNKNNK**CGTGAATGG**NNK**ATTGATAAACCGTGGA TTGG
P27	SpecR_PAM_fw	AAACCGTTGTTTCATCAAGCCTTAG
P28	SpecR_PAM_rev	AAAACTAAGGCTTGATGAAACAACG
P29	seq_primer_CAS9_Pam	GATGAAGATTATTTCTTAATA
P30	I-SceI_pCRISPER_fw_1	GCCTATTTTTATTAGGGATAACAGGGTAATTAATGGTTTCTTA GACGTCGGAATTG
P31	I-SceI_pCRISPER_rev_1	GAAACCATTAATTACCCTGTTATCCCTAATAAAAATAGGCGTA TCACGAGGCCCTT
P32	I-SceI_pCRISPER_fw_2	CACTAGTCATGATAGGGATAACAGGGTAATGAGTTTTCGTTC CACTGAGCGTCAGACC

ID	Oligo Name	sequence
P33	I-SceI_pCRISPER_rev_2	AACGAAAACTCATTACCCTGTTATCCCTATCATGACTAGTGCTTGGATTCTCACCAA
P34	PyrF_CRMAGE_gRNA_fw	GAGCACAAAGAGATGTTTACATTGTTGTTTTAGAGCTAGAAAT
P35	PyrF_CRMAGE_gRNA_rev	CTAAAACAACAATGTAAACATCTCTTTGTGCTCAGTATCTCT
P36	CobB_CRMAGE_gRNA_fw	GAGCACCCAAGAGTACTCGTACTGACGTTTTAGAGCTAGAAAT
P37	CobB_CRMAGE_gRNA_rev	CTAAAACGTCAGTACGAGTACTCTTGGGTGCTCAGTATCTCT
P38	pMAZ-SK_uni_fvw	AGCTAGAAAUAGCAAGTTAAAATAAGGC
P39	pMAZ-SK_uni_rev	AGTATCTCUATCACTGATAGGGATGTCA
P40	pREDTAI_seq	CACAAAGCATCTTCTGTTGAGT
P41	pACBB-TetT-LVA_seq	CATCCTGAACTTATCTAGACC
P42	pMAZ-SK_seq (useless)	TTTCAGAAACAACTCTGGCG
P43	pMA7CR_2.0_seq	ATGCCATAGCATTTTTATCC
P44	pMAZ-SK_seq_new	TTCAGGCGCTTTTTAGACTG
P45	pCRISPER_I-Sec-seq	GAGCTCGCTTGGACTCC
P46	HDAC8_C153**NNK**_fw	GCGCAGGAAAGGTCTCAGATGAAGCAAGCGGTTTT**NNK**TATCTGAATGATGCAGTTC
P47	HDAC8_N136_**NNM**_W141_**SVW**_rev	GCGCAGAGGTCTCACATCTTTTTTCGCATGATG**SVW**ACCACCGCTCC**NNM**TAATCGCAACTTTACACAT
P48	HDAC8_Q263_**NNK**_fw	GCGCAGGAAAGGTCTCATCCGAAAGCCGTTGTTCTG**NNK**CTGGGTGCAGATACCATTGCCGGTGATC
P49	HDAC8_Q263_rev	GCGCAGAGGTCTCACGGATTAAATGCCTGATAAACTTCTTTCAGCACGCTCTCGCA
P50	HDAC8_L301_NNM_rev	GCGCAGAGGTCTCAGCCAGATTATAACCACCACCACCNNMAATCAGGGTTGCCAGCTG
P51	HDAC8_L301_NNM_fw	GCGCAGGAAAGGTCTCATGGCAAATACCGCACGTTGTTGGACCTATCTGACC
P52	PylS_Y349_**MNN**_rev_new	GCGCAGAGGTCTCATTCCAGATCGCCATGCATAATATCCAGGGTATCGCC**MNN**CACCATGCAGCTATCGCCCACAAT
P53	PylS_V366_L372_I378_**NNK**_Fw_new	GCGCAGGAAAGGTCTCAGGAACTGAGCAGCGCG**NNK**GTGGGTCCGGTTAGC**NNK**GATCGTGAATGGGGC**NNK**GATAAACCGTGGATTGGCGCGG
P54	PylS_M241_**MNN**_rev_new	GCGCAGAGTAGGTCTCAGCGGAAAATTTGTTTGCTCAGTTCGGTGTCGTTGTTAATGCC**MNN**ACGTTCCACATATTCCGCCGGAATCA
P55	PylS_A302_**NNK**_fw_new	GCGCAGGAAAGGTCTCACCGCGTGGATAAAAACCTGTGCCTGCGTCCGATGCTG**NNK**CCGACCCTGGCTAACTATATGC
P56	Sirt1_fw_primer_NcoIn	ATCGTTATAAGGAGATATACCATGGGCAGCA
P57	Sirt1_rev_Stop_XbaI	ATCGTTTCTAGATTAAAAACAGATACTGATTACCATCAAGCCGCCTACTAA
P58	Sirt2_NcoI_His6_TEV_fw	ATCGTTCCATGGCTCATCATCACCATCACCACGAGGATCTGTACTTTCAGAGCCGTCTGCTGGACGAGCTGACCTTGGAAGGGGTGGCCCGGTACATGCAGAGCGAAC
P59	Sirt2_Stop_XbaI_rev	ATCGTTTTGGTTTCTAGATTACGACTGGGCATCTATGCTGGCGTGCTCCCTCCGGACAAGGTCCTCCAGCTCCTTC
P61	Sirt3_rev_XbaI	ATCGTTTCTAGATTATTTGTCTGGTCCATCAAGCTTCCCAGTTTCCCGCTGCACAAGGTCCCGCATC
P62	Sirt3_new_BSPHI_His6_TEV_fw	TCATGAATGCATCATCACCATCACCACGAGGATCTGTACTTTCAGAGTGACAAGGGGAAGCTTTCCCTGCAGGATGTAGCTGAGCTGATTCGGGCCAG
P64	CobB_NcoI_fw	ATTAACCATGGGCAGCAGCCATCACC
P65	CobB_XhoI_rev	CTTAACTCGAGTTAGGCAATGCTTCCCGCTTTTAATCC
P66	Sirt7_NcoI_fw	AACTTTAAGAAGGAGATATACCATGGG
P67	Sirt7_XbaI_rev	GTATCTAGATTAGGTCACTTTTTTACGTTTGGT
P68	Sirt6_NcoI_R2G_fw	GAAATTACCTATGGGTGGATCGCATCACCATCACC
P69	Sirt6_XbaI_rev	ATGTCTAGATCAGCTGGGGACCGCCTTG
P70	Sirt5_BspHI_fw	ATATATCATGAGCAGCAGCCATCATCATCAT
P71	Sirt5_rmBspHI_GtoC_XbaI_rev	CGTATCTAGATTAAGAAACAGTTTCATTTTCGTGACAGGCAAGGGCTTC
P72	Sirt4_BspHIR2S_fw	TAATCATGAGCGGATCGCATCACCATCACC
P73	Sirt4_XbaI_rev	GTACTCTAGATCAGCATGGGTCTATCAAAGGC
P74	Sirt2_L103WDS_fw	GTAAGGTCTCACGCTCTCCATCCACCGGCWDSTATGACAACCTAGAGAAGTACC
P75	Sirt2_A85NYT_I93DYG_rev	GTAAGGTCTCAAGCGAAAGTCGGGCRHGCCTGCGGATGTGGAGATTCCARNTCCCACCAAACAGATGAC
P76	Sirt2_N168HHT_I169NYT_D170VHT_fw	GTAAGGTCTCCCCTGCGCTGCTACACGCAGHHTNYTVHTACCCTGGAGCGAATAGCCGG

ID	Oligo Name	sequence
P77	Sirt2_rev	GTAAGGTCTCACAGGAGTAGCCCCTTGTCCTTCAGCAGGC
P78	Sirt1_NheI+His_fw	ACTCGCTAGCATGGGCAGCAGCCATCACC
P79	Sirt1_XhoI_deATT_rev	CAGACTCGAGGACGTCATCTTCAGAGTCTGAATATACC
P80	sirt1_fw_Nhe_ATG_-His_fw	TCTGGCTAGCATGAGCCAAGGATCCTGTGAAAGTGA
P81	sirt1_fw_Nhe_ATG_--Hi+c-mycs_fw	TCTGGCTAGCATGGAGCAGAAACTCATCTCTGAAGAGGATCTGAGCCAAGGATCCTGTGAAAGTGATGAGGAG
P82	Sirt1_NheI_fw	CAGATCCGCTAGCATGGCGGACGAGGCGGC
P83	Sirt1_SacI_rev	AGCTTGAGCTCGAGTGATTTGTTTGATGGATAGTTCATGTCTGTTAC
P84	PyrF_K72_amber_MAGE_fw	G*C*GCGAACTTCAACAGCGTGGTTTTGATATCTTTCTTGACCTGTGATTCCACGATATCCCCAACACTGCAGCGCACGCTGTCGCTGCTGCAGCTG
P85	PyrF_K72_amber_MAGE_rev	C*A*GCTGCAGCAGCGACAGCGTGCGCTGCAGTGTTGGGGATATCGTGGAATCACAGGTCAAGAAAGATATCAAAACCACGCTGTTGAAGTTCGCGC
P86	lacZ_off_MAGE_con	ATGATTACGGATTCACTGGCCGTCGTTTTACAACGTCGTGACTGAGAAAACCCTGGCGTTACCCAACTTAATCGCCTTGCAGCACATCCC
P87	CobB_QC_F60W_W67F_fw	GTACCTGGCGCGCCGCAGATGGCCTGTTTGAAGAACATCGGGTTGAAG
P88	CobB_QC_F60W_W67F_rv	GTTCTTCAAACAGGCCATCTGCGGCGCGCCAGGTACGAATACCTGATTCC
P89	CobB_QC_F60Y_fw	ATTCGTACCTATCGCGCCGCAGATGGC
P90	CobB_QC_F60Y_rv	GCGGCGCGATAGGTACGAATACCTGATTC
P91	Sirt5_QC_A82W_fw	AAAATGGCAATGGCAGGACCTGGCGACTCC
P92	Sirt5_QC_A82W_rv	CCAGGTCCTGCCATTGCCATTTTCTCCAATAACC
P93	Ura3_K93TAG_fw	GAAGACAGATAGTTTGCTGACATTGGTAATACAGT
P94	Ura3_K93TAG_rv	AATGTCAGCAAACTATCTGTCTTCGAAGAGTAAAAAATTG
P95	LM-92__BspHI_ATG_highGC_fw	TGTCTCATGAATGTCGGGGGACCCCGCTG
P96	LM-92_EcoRI_highGC_histaged_fw	GCTTAGGAATTCTCGGGGGACCCCGCTG
P97	LM-92_XhoI_rm_secondT7_rev	TTAGCTCGAGTTACATGATGCTGCAGTTCTGGGAG
P98	LM-92_NotI_ coexp_rev	TTATAGCGGCCGCTTACATGATGCTGCAGTTCTGGGAG
P99	Sirt7_Y119F_fw	ATTCCGGATTTTCGTGGTCCGAATGGTG
P100	Sirt7_Y119F_rv	GGACCACGAAAATCCGGAATGCTTGC
P101	Sirt7_C189I_fw	TAGCCAGAATATCGATGGTCTGCATCTGCG
P102	Sirt7_C189I_rv	GCAGACCATCGATATTCTGGCTAACAACATGC
P103	Sirt7_C189V_fw	TAGCCAGAATGTGGATGGTCTGCATCTGCG
P104	Sirt7_C189V_rv	GCAGACCATCCACATTCTGGCTAACAACATGC
P105	Sirt1_Nctrunk_His6_NdeI_fw	TTAGTCATATGGGCAGCAGCCATCAC
P106	Sirt1_Nctrunk_XhoI_rev	CAGACTCGAGTTAGACGTCATCTTC
P107	Sirt5_Iso3_del_189-206_fw	TGCCTCTTCACAACCTTTTCCTGATAAAGCTGGACAAATTG
P108	Sirt5_iso3_del_189-206_rv	TCAGGAAAAGGTTGTGAAGAGGCAGGCTGCGGG
P109	Sirt5_T194TAG_fw	AGAACCTGGATAGCAAGATGCCAGCATCCC
P110	Sirt5_T194TAG_rv	TGGCATCTTGCTATCCAGGTTCTGGAGCACC
P111	pGFP_Sirt1_Full_BamH1_fw	CTTGCGGATCCATGGCGGACGAGGCGGCCCTC
P112	Sirt1_Full_SalI_rev	TGACTGTCGACCTATGATTTGTTTGATGGATAGTTCATGTCTGTTACTTCC
P113	pGFP_Sirt1_Full_delTAG_rev	TGACTGTCGACTGATTTGTTTGATGGATAGTTCATGTCTGTTACTTCC
P114	pGFP_Flag-Sirt1_Full_BamHI_fw	CTTGCGGATCCATGGACTACAAGGACGATGACGATAA
P115	pCDF_Sirt1_Full_NdeI_fw	CTTGCCATATGGCGGACGAGGCGGCCCTC
P116	pCDF_Flag-Sirt1_Full_NdeI_fw	CTTGCCATATGGACTACAAGGACGATGACGATAA
P117	Sirt1_Nctrunks_-His6_NdeI_fw	TTAGTCATATGAGCCAAGGATCCTGTGAAAGTG
P118	pCDF_seq_2ndIns_rev	GTTCAAATTTCGCAGCAGC
P119	pCDF_seq_1stIns_rev	ATTATGCGGCCGTGTACA
P120	pCDF_seq_2ndIns_fw	GTACACGGCCGCATAATC
P121	pCDF_seq_1stIns_fw	ATGCGACTCCTGCATTAGG
P122	QC_insertG_LM92_fw	CCAGGATCCGGAATTCTCGGGGGACCCC
P123	QC_insertG_LM92_rev	CCCGAGAATTCCGGATCCTGGCTGTGGTG
P124	CobB-pfGFP_delTAA_KpnI_rev	TCCGTGGTACCGGCAATGCTTCCCGCTTTTAATC
P125	CobB_pGFP_ATG_NLS_XhoI_fw	TGATTGCTCGAGATGGCTCCAAAGAAGAAGCGTAAGGTAAGCCAGGATCCAAAACCAAG
P126	Sirt6_L7_**NNK**_fw	CTGCAGGTCTCAACGCGGCGGGG**NNK**TCGCCGTACGCGGACAAGGGCAA

ID	Oligo Name	sequence
P127	Sirt6_L7_rev	CTGCAGGTCTCAGCGTAATTCACCGACATGGATCCGTG
P128	Sirt6_V113**NNK**_fw	CTGCAGGTCTCAGTCAGCCAGAAC**NNK**GACGGGCTCCATGT GCGCTCAG
P129	Sirt6_V113_rev	CTGCAGGTCTCATGACCAGGAAGCGGAGGAGGCCCAC
P130	Sirt6_I183**NNK**_fw	ATGCAGGTCTCAAGGCAAGGGGGCTGCGAGCCTGCAGGGG AGAGCTGAGGGACACC**NNK**CTAGACTGGGAGGACTCCCT
P131	Sirt6_M155**NNK**_rev	CTGCAGGTCTCAGCCTTAGCCACGGTGCAGAGCCGGCCCGT GGCCTTCAGGCC**MNN**GGTGCCCACGACTGTGTCTCG
P132	Sirt6_V68**NYC**_fw	CTGCAGGTCTCATCCCCGACTTCAGGGGTCCCCACGGA**NYC** TGGACCATGGAGGAGCGAGGTC
P133	Sirt6_A51**GRN**_rev	CTGCAGGTCTCAGGGATGCCAGAGGCAGTGCTGATGCC**GRN** ACCCGTGTGGAACACCACATTG

PEPTIDES

Table 9: Amino acid sequence of histone peptides form the N to the C terminus; chemical acetylation (Ac), butyrylation (Bu), crotonylation (Cr) or allylation (Alloc) are denoted as subscript.

Peptide	Sequence	Source
H4K16Ac	NH_2-KGGAK$_{Ac}$RHRKIL-COOH	Sascha Gentz, DPF, Dortmund
H4K16Bu	NH_2-KGGAK$_{Bu}$RHRKIL-COOH	Sascha Gentz, DPF, Dortmund
H4K16Cr	NH_2-KGGAK$_{Cr}$RHRKIL-COOH	Sascha Gentz, DPF, Dortmund
H4K16Alloc	NH_2-KGGAK$_{Alloc}$RHRKIL-COOH	Sascha Gentz, DPF, Dortmund
H3K18Ac	NH_2-GKAPRK$_{Ac}$QLATK-COOH	Sascha Gentz, DPF, Dortmund

SOFTWARE

Table 10: Software used to create illustrations or analyze date.

Software	Version	Link
Adobe Illustrator	16.0.4	https://www.adobe.com/de/products/illustrator.html
CCP4	6.5.020	http://www.ccp4.ac.uk/
ChemDraw	17.1	https://www.perkinelmer.com/uk/category/chemdraw
Coot	0.8.2	https://www2.mrc-lmb.cam.ac.uk/personal/pemsley/coot/
GraphPad	8.3.1	https://www.graphpad.com/
JLigand	1.0.40	http://www.ysbl.york.ac.uk/mxstat/JLigand/
Microsoft Excel	15.29.1	https://support.office.com/de-de/excel
Phaser	2.5.6	https://www.phaser.cimr.cam.ac.uk/
Phenix	1.9-1692	https://www.phenix-online.org/
PRODRG	See CCP4	https://www.sites.google.com/site/vanaaltenlab/prodrg
SciDavis	1.22	http://scidavis.sourceforge.net/
XDS	Version 2020	http://xds.mpimf-heidelberg.mpg.de/
XSCALE	Version 2020	http://xds.mpimf-heidelberg.mpg.de/html_doc/xscale_program.html

METHODS

Some methods described in this section were published in similar form previously but described here in more detail, including the unpublished data and negative results. Please consult the original publications if needed, methods originally published in Spinck et. al (2018) are marked with an asterisk (*) and methods from Spinck et. al (2020) with two asterisks (**).

All reactions were prepared on ice unless otherwise stated. All buffers and solutions were sterile filtered and water, glycerol, LB medium and M9 medium were sterilized by autoclaving.

METHODS FOR PLASMID ISOLATION, DNA PURIFICATION AND CLONING

Plasmid Isolation and purification were done using the commercial kit. For small scale plasmid isolation, the GeneJET™ Plasmid-Miniprep-Kit (Thermo Fischer), or the Plasmid Miniprep Kit I, peqGOLD (Peqlab) were use. Large scale plasmid isolation was preformed using a Midi or Maxi Plasmid Prep Kit (QIAGEN). Plasmid Isolation from 96-deep well plates were done using the vacuum system and E-Z 96® FastFilter Plasmid DNA Kit from omega. DNA or PCR products were purified using the QIAquick PCR Purification Kit (QUIAGEN) for samples in solution and QIAquick Gel Extraction Kit (QUIAGEN) for purifications form agarose/TAE gels. Restriction digests was preformed using the commercial restriction enzymes from NEB or Thermo Fischer according to manufacturer information.

COMPETENT CELLS AND TRANSFORMATION PROTOCOL

Competent cells were created using the protocols by Sambrook et al., (1989).

Chemical Competent Cells and Heat Shock Protocol

Briefly, cells were grow overnight in 5 mL LB at 37°C and 200 rpm, antibiotic was added when the cells contained a plasmid. 100 mL LB were inoculated with 1 mL ONC and grown to an OD_{600} between 0.3 and 0.5 in the absence of antibiotic at 37°C and 200

rpm. The cells were cooled on ice for 10 min and harvested by centrifugation at 4000 rpm for 5 min. The pellet was suspended in 25 mL TFB1-buffer (100 mM RbCl, 50 mM $MnCl_2$, 30 mM KAc, 10 mM $CaCl_2$, 15% Gycerol, pH 5) and incubated on ice for 90 min. The cells were collected as before and suspended in 2 mL TFB2 (10 mM MOPS, 10 mM RbCl, 75 mM CaCl2, 15% Glycerol, pH 8). Cells were aliquoted, flash frozen in liquid nitrogen and stored at -80°C (134).

Plasmid were transformed by mixing 1 μL plasmid DNA (ca. 100 ng) with 20 μL competent cells. The mixture was incubated on ice for 30 min and then heated to 42°C for 1 min 15 s, imminently chilled on ice and 180 μL LB medium was added. The cells were left to recover for 1 h and plated on LB agar petri dish containing the appropriated antibiotic.

Electro Competent Cells and Electroporation Protocol

The cells were grown and harvested as described for the chemical competent cells. The harvest cell pellet was washed 2-3 times with 25 mL ice cold, sterile filtered ddH_2O. After the last washing step, the finely dispersed cells were collected by centrifugation with 3000 rpm for 5 min. The supernatant was discarded and the excess water removed by knocking it out on a paper towel. The remaining water (ca. 200 μL) was collected by centrifugation 1000 rpm for 30 s and used to suspend the cells. The cells were not stored and used directly for electroporation.

4 μL plasmid (ca. 1000 ng/μL) was premixed with 40 μL competent cells and incubated on ice for 1 min. 40 μL were transferred to a 2 mm, ice cold electroporation cuvette. The cells were knocked to the bottom of the cuvette, the cuvette dried with a paper towel and for the actual electroporation, current applied using the following settings on a Gene Pulser Xcell Electroporation Systems (BioRad): 2500 V, 25 μF, 200 Ω. Imminently after the electric shock, 1 mL LB medium was added to the cuvette and the cells transferred to a 1.5 mL microreaction tube. The cells were left to recover for 1 h

at 37°C and either plated on LB agar plates or grown in culture, containing the appropriated antibiotic.

EXPRESSION OF KDACS

Depending on the individual KDAC, different *E.coli* cells were used. If the KDAC had to be fully purified *E. coli* BL21 DE3 RIL was used, when the KDAC was used within a lysate, crude Ni-NTA purified protein the expression was performed in DH10B Δ*pyrF* Δ*cobB* pPylT-URA3 (+15 μg/mL tetracycline in all cultures) to prevent contamination with endogenous CobB. The expression in *E. coli* BL21 DE3 RIL, which was transformed with the respective pBK plasmids for CobB, HDAC8, Sirt1 Sir2 or Sirt3 is described here. When preparing KDAC for crystallisation, 10 μM $ZnCl_2$ was added to the expression culture and lysis buffer, as the initial crystals of CobB wt obtained without the addition showed incomplete saturation of the Zn-binding motive.

CobB, Sirt2/3 and HDAC8 */**

A preculture was prepared in 10 mL LB medium (50 μg/mL kanamycin) 37°C overnight, used to inoculate 1 L LB medium (50 μg/mL kanamycin) and cells were grown to an OD_{600} of 0.3. The temperature was reduced to 30°C for 1 h before expression was induced by addition of arabinose to a final concentration of 0.2%. Cells were harvested after 16 h at 30°C incubation by centrifugation (20 min, 6000 rpm, 4°C). The cell pellets were washed with PBS and stored at –20°C.

SirT1**

BL21(DE3) cells were transformed with wild-type or mutant pCDF-His_6-SirT1-NcatC plasmid. An ONC was prepared in 10 mL LB (50 μg/mL spectinomycin) and incubated at 37°C while agitating at 200 rpm. The expression culture was inoculated with the ONC and grown at 37°C and 200 rpm to an OD_{600} of 0.8. The expression was induced by addition of 0.5 mM IPTG and the culture shifted to 18°C. The cells were harvested by centrifugation the next day, washed with PBS and stored at –20°C.

PURIFICATION OF KDACS

In general, the purification for mutant variants is the same as for the wt, thus, only the purification of the wt KDAC is describe here. After Ni^{2+}-NTA- purification, the buffer of the eluate was always exchanged to the gel filtration buffer using a Amicon® Ultra Centrifugal Filters. It should be noted that the purification was optimized to do multiple purification in parallel and all volumes given are for 1 L expression culture.

CobB and HDAC8**

The cell pellet was thawed on ice and resuspended in 25 mL Ni-NTA wash buffer (20 mM HEPES pH 7.5, 200 mM NaCl, 20 mM imidazole, 1 mM DTT) supplemented with lysozyme (~0.5 mg/mL), DNase (1 mg) and protease inhibitor (1 mM PMSF). The cell suspension was lysed by passing through a pneumatic cell disintegrator, debris was removed by centrifugation (20 min, 20,000 rpm, 4°C) and 500 µL HisPur™ Ni^{2+}-NTA resin (250 µL if the eluate is used for a reaction) was added to the supernatant. After 1 h at 4°C, the beads were collected by passing the suspension over a plastic column with frit (BioRad, Munich) and washed with 40 mL Ni-NTA wash buffer. Protein was eluted in 4 mL Ni-NTA wash buffer supplemented with 200 mM imidazole. The eluate was concentrated and the buffer exchanged to gelfiltration buffer (20 mM HEPES pH 7.5, 100 mM NaCl, 10 mM DTT) before loading on a HILoad™ 26/60 Superdex™ 200 size-exclusion chromatography column (GE healthcare, UK) preequilibrated with gel filtration buffer. Fractions containing protein were analysed on an SDS-PAGE, pooled and concentrated in a microfiltration (Amicon Ultra-15 Centrifugal Unit, 10 kDa, Merck Millipore). The protein was aliquoted, flash frozen in liquid nitrogen and stored at –80°C.

Sirt1/3/***

The cell pellet was resuspended in Sirtuin wash buffer (20 mM Tris pH 8, 200 mM NaCl, 20 mM Imidazole) supplemented with 0.2 mM PMSF, lysozyme (0.5 mg/mL) and

DNase (ca 1 mg). The protein was purified as described above using the Sirt1 wash buffer and the Sirtuin gel filtration buffer (20 mM Tris pH 8, 50 mM NaCl, 10 mM DTT).

Sirt2*

The purification was essentially preformed as the Sirt1/3 purification but purification of Sirt2 required overnight incubation with the Ni-NTA resin, which greatly improves the yield. Also, the use of a Superdex^{TM} 75 is recommended over a Superdex^{TM} 200, to better separate a common degradation product of Sirt2.

EXPRESSION AND PURIFICATION OF THE LAMIN A PEPTIDE (LM-92)

BL21(DE3) RIL cells was transformed with the pCDF LM-92 plasmid. Transformants were used to inoculate 10 mL LB medium (50 μg/mL spectinomycin) and grown overnight at 37°C while shacking with 200 rpm. The overnight culture was used to inoculate 1 L LB (50 μg/mL spectinomycin) and grown to an OD_{600} of 1. The expression of LM-92 was induced by addition of 1 mM IPTG and cells were harvested after 2 h by centrifugation (4°C, 10 min, 20.000 rpm). It is critical that all the following steps are done as quickly as possible, since the LM-92 peptide is rapidly degraded in *E.coli* cells and the lysate. The cell pellet was immediately lysed by resuspension in 25 mL boiling hot water. The hot cell suspension was kept boiling for 30 min by heating the suspension in regular intervals in a microwave (800 W) in an open container, the volume should be kept at 30 mL by addition of hot water if necessary. The solution was then chilled on ice and the LM-92 buffer components (final concentration: 20 mM Bis-Tris pH 6.8, 300 mM KAc, 10 mM Imidazole, 1 mM DTT) were add from a stock solution as the lysate cooled. The cell debris was removed by centrifugation (20 min, 20,000 rpm, 4°C) and 200 µL Ni-NTA resin was added to the supernatant. The suspension was agitated at 4°C for 2 h before the resin was separated by gravity filtration over a plastic column with frit (BioRad, Munich). The resin was washed with 50 mL LM-92 wash buffer (20 mM Bis-Tris pH 6.8, 300 mM KAc, 10 mM Imidazole, 1 mM DTT) and

eluted in 3 mL LM-92 wash buffer supplemented with 200 mM Imidazole. The elution was concentrated in a microfiltration (Amicon Ultra-15 Centrifugal Unit, 3 kDa, Merck Millipore) and the buffer exchanged to LM-92 gelfiltration buffer (20 mM Bis-Tris pH 6.8, 50 mM KAc, 10 mM DTT). The solution was concentrated until it became slightly cloudy. The cloudy solution was transferred to a 2 mL microreaction tube, diluted with 0.5 volumes LM-92 gelfiltration buffer and heated to 60°C for 5 min. The now clear LM-92 peptide solution was fractionated over a Superdex 75 16/60 gelfiltration column. Fractions containing protein were identified by mixing 20 µL 2x Bradford reagent with 20 µL fraction in a PCR stripe. Fraction containing protein showed a deep blue color change and were separated on an 18% SDS-Gel. All fractions showing the full length LM-92 peptide were pooled and concentrated as before. The LM-92 is not soluble at high concentration (>>50 µM) and tends to become turbid upon concentration. Freezing the concentrated stock at -80°C or storage on ice for extended periods can also cause the solution to becoming cloudy. The cloudy LM-92 solution is inactive and does not activate Sirt1 efficiently. Activity can be restored by heating the solution to 60°C for 10 min before use, this should cause the solution to clear up.

DUAL-LUCIFERASE BASED DEACYLATION ASSAY

E.coli DH10B Δ*pyrF* Δ*cobB* was transformed with pPylT DLR-TAG (135), pBK His_6-CobB and pCDF PylS or AcKRS3. The transformants were picked and grown in 750 µL LB medium (25 µg/mL spectinomycin, 25 µg/ml kanamycin and 7.5 µg/mL tetracycline) and grown in triplicates for 8 h in a 96 deep-well block at 37°C, shaking with 200 rpm. The expression was induced by addition 250 µL LB medium (25 µg/mL spectinomycin, 25 µg/ml kanamycin, 7.5 µg/mL tetracycline, 0.8% arabinose and 40 mM acetyl lysine or 4 mM for other modifications) and the temperature was reduced to 30°C. The cells were harvested by centrifugation (4000 rpm, 5 min) and the supernatant removed. The

luciferase signal was developed using the commercial Dual-Luciferase® Reporter Assay System (Promega). Briefly, the cells were lysed by addition of 100 µL 1x passive lysis buffer (Promega) supplemented with DNase (ca. 1 mg), lysozyme (1 mg/mL) and 0.2 mM PMSF to each well. The cells were resuspended in the lysis buffer by vortexing the block, followed by incubation at RT for 10 min. The cell debris was collected by centrifugation and 20 µL of the supernatant was transferred to a 96 well microwell plate. To each well with lysate, 50 µL LARII reagent was added and the firefly signal measured using a FluoStar Omega Microplate Reader (BMG Labtech). Afterwards, 50 µL Stop & Glo® Reagent was added and the *Renilla* luciferase activity was measured as before. The firefly luciferase signal of each well was normalized one the Renilla luciferase signal.

DUAL LUCIFERASE ASSAY USING PURIFIED COBB

The luciferase was expressed using transformants not containing the pBK His_6-CobB plasmid, following the same protocol at a 100 mL scale. The cells were harvested and lysed for 30 min at RT with a concentration of 62 OD_{600}/mL in passive lysis buffer. The reaction was set up in triplicates using 6.2 OD_{600}/mL lysate, 20 µM CobB, 1 mM NAD^+ and ±50 mM NAM in a 20 µL volume. The reaction without nicotinamide were stopped by addition of NAM to a final concentration of 50 mM after 1, 3, 5, 10, 20, 30 and 45 min. The luciferase signal was measured as described above.

EXPRESSION OF FIREFLY LUCIFERASE K529MOD*/**

E. coli BL21 DE3 RIL were transformed with plasmids pCDF-PylT-FLuc(opt)-His_6 K529TAG and pBK-AcKRS3opt (for FLuc K529ac) or pBK-PylS (136) (for other acylations or protection groups). Cells were grown in LB medium (50 µg/ml spectinomycin and 50 µg/ml kanamycin) to an OD_{600} of 0.3 ($Fluc_{other}$) or 0.8 ($Fluc_{Ac}$) at 37°C, shaking with 200 rpm. The culture was supplemented with 50 mM NAD^+, modified lysine (10 mM Acetyl lysine or 1 mM for lsysins carrying other modifications)

and expression was induced by addition of 1 mM IPTG. $Fluc_{Ac}$ was harvested after 3 h at 37°C, while for other expressions, the culture was cooled to 30°C and the expression prolonged overnight. The harvested cell pellet was washed with NAM (20 mM) supplemented PBS and pelleted by centrifugation. The pellets were stored at -20°C or used directly for purification.

PURIFICATION OF FIREFLY LUCIFERASE K529MOD*/**

The cell pellet was suspended in luciferase wash buffer (20 mM Tris/HCl pH 8, 10 mM imidazole, 200 mM NaCl, 10 mM DTT), supplemented 2 mM PMSF, 0.5x Roche Protease Inhibitor cocktail, 20 mM NAM, DNAse and lysozyme. The homogeny cell suspension was lysed using a pneumatic cell disintegrator and debris was removed by centrifugation (20 min, 50,000 g, 4°C). The supernatant was incubated with 500 µl Ni-NTA-beads/ 1 L of expression for 2 h with agitation at 4°C. The suspension was separated by gravity filtration over a frit and the beads washed with 30 ml Ni-NTA wash buffer. The bound luciferase was eluted in Ni-NTA wash buffer supplemented with 200 mM imidazole. Eluates were dialyzed against luciferase storage buffer (20 mM Tris pH 8, 50 mM NaCl, 10 mM DTT or 1 mM TCEP), aliquoted and flash frozen in liquid nitrogen before storage at -80°C. The different substrates were used in KDAC assays in appropriate dilution. The dilution level of Fluc carrying different lysine modifications was determined by titrating the luciferase to the point where it equals the signal of 30 nM $Fluc_{Ac}$ in a luciferase endpoint assay using 20 µM CobB and 1 mM NAD^+. Final dilution used in this work were the following 1:1500 Ac, 1:500 Bu, 1:125 Boc, Alloc, Cr and Pr. It should be noted that the $Fluc_{alloc}$ must be stored at 4°C over the duration of 2-3 days before usage. Using the $Fluc_{alloc}$ directly after thawing or purification will yield no measurable activity for an unknown reason.

LUCIFERASE-BASED KDAC ASSAY (FLUC ASSAY) *

Two variants of the KDAC assay exist, an endpoint assay or an continuous assay. A typical endpoint deacylation reaction contains: Diluted Firefly Luciferase K529mod (30 nM $Fluc_{Ac}$, for other modifications see purification, $Fluc_{alloc}$ note), 1 mM NAD^+, 10-100 nM Sirtuin in 50 µl Sirtuin buffer (25 mM Tris/HCl pH 8.0, 137 mM NaCl, 2.7 mM KCl, 1 mM $MgCl_2$, 1 mM DTT, 1 mg/ml BSA). For the COMAS screening and the validation of the compounds, the BSA was omitted from the Sirtuin buffer and DTT was replaced by 1 mM GSH. For reactions with HDAC8, the Sirtuin buffer was replaced with HDAC8 buffer (137) (50 mM HEPES pH 7.4, 100 mM KCl, 0.001% Tween-20, 5% DMSO, 0.25 mM TCEP and 0.1 mM $ZnCl_2$). The reactions were incubated for 2 h at 30°C, but were reduced to 30 min at 30°C for the COMAS-screening of compounds. An equal amount of 2x luciferin buffer (138) (40 mM Tricine, 200 µM EDTA, 7.4 mM $MgSO_4$, 2 mM $NaHCO_3$, 34 mM DTT, 0.5 mM ATP and 0.5 mM luciferin, pH 7.8) was added to the reaction. The luminescence was quantified using a FluoStar Omega Microplate Reader (BMG Labtech).

The continuous assay was set up by premixing all components of the endpoint reaction omitting NAD^+. NAD^+ was added to initiate the reaction and the luminescence was recorded after 2 min preincubation at a rate of one data point every minute over a period of 30 min. The reaction velocity was calculated from the slope of the linear phase of the reaction.

KINETIC OF SIRT1 USING THE CONTINUOUS FLUC ASSAY.

The reaction kinetics of the Sirtuin 1 inhibitors were determined by preparing the continuous Fluc assay using 100 nM Sirt1 and 0, 100, 200 or 400 nM of a compound in COMAS reaction buffer. All components were first prepared on ice and premixed omitting the NAD^+. The NAD^+ concentration was titrated from 500 µM to 0 µM in a 1:1 dilution series and added to the reaction one ice. The reaction was warmed up to RT

before the kinetic measurement was started by determining the luminescence over a period of 60 min taking a data point every minute. The reaction velocity was calculated from the slop of the reaction, and kinetic parameters were calculated using Lineweaver–Burk straight line extrapolation (139) of the plotted experimental data.

FLUOR-DE-LYS KDAC ASSAY*

The reaction composition and conditions of the Flour-de-lys assay are identical to the Fluc assays but replacing the luciferase with 10 µM Fluor-de-Lys peptide (Ac-Gly-Gly-Lys(ac)-AMC). The reaction was stopped by addition of an equal volume of 2x trypsin (0.1 mg/mL in Sirtuin Buffer) and the coumarin fluorescence (ex. 355 nm, em. 460 nm) was quantified on a FluoStar Omega Microplate Reader (BMG Labtech)

LIBRARY CREATION**

The active site mutant library for the different KDACs was designed based on the following crystal structure: CobB: 1S5P (140), HDAC8: 5DC6 (141), Sirt1: 4KXQ (142) and Sirt6: 3ZG6 (49) . The codons at the target site were replaced by site saturated mutagenesis using reduced codons designed with AA-Calculator (143). The replacement was performed by iterative rounds of PCR using the Expand™ High Fidelity PCR System (Roche). One PCR reaction contained 1x Buffer 2, 0.2 mM dNTPs, 1 µM forward and reverse primer (Table 8), 100 ng pBK-KDAC plasmid DNA (Table 4), 3.5 U Expand Polymerase in a 50 µL volume and run with the following program: 1 min 95°C; 10x [20 s 95°C; 30 s 65°C (-1°C/cycle); 5 min 68°C]; 25x [20 s 95°C; 30 s 55°C; 5 min 68°C]; 5 min 68°C; hold 4°C. The PCR template was removed by DpnI digested with 20 U Dpn I (NEB) for 1 h at 37°C. The reaction was purified using the QIAquick PCR Purification Kit (QIAGEN), usually the addition of 5 uL 3 M sodium acetate solution pH 5.2 was required to acidify the solution. The purified PCR product was either directly digested with 80 U HF-Bsa I (NEB) for 2 h or, if the PCR produced more than one fragment, the target fragment was first gel purified from a 1%

agarose/TAE gel using a QIAquick Gel Extraction Kit (QIAGEN). The pure, digested PCR product of two PCR reactions was combined and circularized by T4 DNA ligase in a total volume of 500 µL. All reagents had to be stored at room temperature and properly resuspended before preparing this reaction, any precipitate in this step (commonly DTT or salts) would have lead to reduced efficiency electroporating the plasmids into competent cells. The reaction is prepared in 1x T4 DNA Ligase Reaction Buffer containing, 100 µL digested and purified PCR product and 10 kU T4 DNA Ligase (NEB). If more than two PCRs had to be ligated this was scaled up accordingly and done in parallel. The reaction was incubated overnight at 16°C, centrifuged and the supernatant precipitated on ice (do not precipitate at -20°C, DTT will fall out of solution) by adjusting the precipitants concentration to a final concentration of 0.3 M sodium acetate pH 5.2 and 70% ethanol or 33% isopropanol. The precipitate was collected by centrifugation for 30-45 min at 18.000 rpm and washed twice with 70% ice cold ethanol to remove precipitated salts (color less pellet, not always visible). Once the salts were removed, the precipitate was dried for 5-10 min at 37°C and the DNA dissolved in 10 µL ddH_2O by rinsing the walls of the reaction vessel thoroughly. Pure DNA should be a thin translucent (wet, dissolves quickly) to slightly colorless (too dry, takes time to dissolve) film at the wall of the reaction vessel and lead to deliquesce of the water drop when rinsing the wall. Rinsed until no deliquesce of the drop could observed anymore, and the DNA concentration was between 500 – 2000 ng/µL. To test the efficiency of the ligation, 100 ng DNA was digested with HindIII (1 site in plasmid) and analyzed on a 1% agarose/TAE gel; if the reaction showed more than the expected band (1 site in the pBK plasmid) the ligation was evaluated incomplete.

The ligated plasmid was electroporated into MAX Efficiency™ DH10B™ Competent Cells (ThermoFisher). Transformation efficiency was determined from the colony count

of a dilution series (10^{-4} to 10^{-7}) on LB agar plates (50 μg/mL kanamycin) for every round of mutagenesis. Coverage was calculated using the GLUE-IT web tool for each round of mutagenesis, and the plasmid DNA was purified and used in the next round of mutagenesis when it covered >95% of all possible amino acid combinations (143). To isolate the plasmid DNA from the mutant pool, the Plasmid Maxi Kit was used (QIAGEN).

The number of mutants of the final KDAC was determined by a dilution series and coverage was calculated using GLUE-IT (143). Number of mutants (theoretical coverage) in the final KDAC libraries: CobB 1.0 x 10^8 (99.6%), SirT1 1.8 x 10^7 (85.0%), Sirt6 1.5 x 10^8 (98.3%) and HDAC8 4.0 x 10^7 (99.6%)

INITIAL DESIGN OF THE KDAC SELECTION SYSTEM**

To test the selection strategy *E. coli* DB6656 (Δ*pyrF*) were transformed with pPylT-URA3, pPylT-URA3-K93TAG-PylS or pPylT-URA3-K93TAG-AcKRS3 and grown overnight in LB-medium (15 μg/mL tetracycline). The culture was replicated using a pinhead replicator in tenfold dilutions with M9 minimal medium (10^0 to 10^{-7}) onto M9 selection plates (M9 minimal medium, 0.2% arabinose, 1% glycerol, 0.1 mM tryptophan, 50 μg/mL kanamycin, 15 μg/mL tetracycline, ± 0.1 mM uracil, ± 10 mM acetyl-lysine and 1 mM boc-lysine, ± 0.1% 5-fluoroorotic acid, ± 50 mM Nicotinamide). Plates were imaged after incubation for 48 h at 37°C.

CREATION OF E. COLI DH10B ΔPYRF ΔCOBB WITH CRISPR/CAS9

The genes encoding PyrF and CobB were disrupted in E. coli DH10B by inserting each a stop codon shortly after the start codon of the respective gene in two sequential rounds of genome engineering using CRISPR/Cas9 following established protocols (144). The primers used for targeting and editing are listed in Table 8. To confirm successful mutagenesis, individual colonies were tested by PCR. One PCR was run in

a 20 µL volume of 1x HF buffer containing 0.5 mM dNTPs, 1 µM forward and revers Primer, 0.2 U Phusion High-Fidelity DNA Polymerase (Thermo Fisher) and 5 µL diluted cell suspension. The PCR was run using the following program: 10 min 98°C; 30x [15 s 98°C; 30 s 55°C; 30 s 72°C]; hold 8°C. The PCR product was purified and 200 ng DNA restriction digest with HindIII to test for the introduced restriction site. The Cas9 plasmid was cured by overnight growing in LB medium containing 60 µg/mL promazine at 37°C and 200 rpm (145). Of the treated culture, 1000 cells were plated on LB agar plates and the single colonies were replicated using a cloth on LB agar plates containing 34 µg/mL chloramphenicol. Colonies showing no growth on chloramphenicol containing agar were picked and grown as before in a 96 deep-well block and retested for antibiotic resistance. The successfully cured cells were retested for the knockout by colony PCR and stored in 25% glycerol/LB medium at -80°C.

GENERAL KDAC SELECTION SYSTEM**

To create a general applicable KDAC selection system, the *E. coli* DH10B Δ*pyrF* Δ*cobB* strain was created using CRISPER/Cas9 (see above). The selection has been tested for HDAC8, Sirt1, Sirt2, Sirt3, Sirt6 and Sirt7 by transforming the *E. coli* DH10B Δ*pyrF* Δ*cobB* with pPylT-URA3-K93TAG-PylS or pPylT-URA3-K93TAG-AcKRS3 and with either pBK-His_6-HDAC8, pBK-His_6-Sirt1cat, pBK-His_6-TEV-SirT2cat, pBK-His_6-TEV-SirT3cat, pBK- His_6-Sirt6 or pBK- His_6-Sirt7. The transformation was usually done in two steps by creating competent cells of cells containing one of the two pPylT plasmids, due to the low transformation efficiency of the knockout strain. Transformants were grown overnight in 4 mL LB (50 µg/mL kanamycin, 15 µg/mL tetracycline) and replicated in a tenfold dilution series onto M9 selection plates (M9 minimal medium, 0.2% arabinose, 1% glycerol, 0.4% glucose, 0.1 mM tryptophan, 80 mg/L valine, 80 mg/L isoleucine, 80 mg/L leucine, 50 µg/mL kanamycin, 15 µg/mL

tetracycline, ± 0.1 mM uracil, ± 10 mM acetyl-lysine or 1 mM butyryl-lysine (Sirt7) and ± 0.1% 5-fluoroorotic acid). Plates were imaged after incubation for 48 h at 37°C for Sirt1-3 and HDAC8, Sirt6-7 required 3-4 days of growth.

LIBRARY SELECTION**

Freshly prepared electrocompetent *E. coli* DH10B Δ*pyrF* Δ*cobB* containing pPylT-URA3-K93TAG-PylS or pPylT-URA3-K93TAG-AcKRS3 were electroporated with the KDAC mutant library, the efficiency determined by a dilution series to cover >95% of library diversity and the remaining cells were grown in 100 mL LB (50 μg/mL kanamycin, 15 μg/mL tetracycline) at 37°C overnight shaking with 200 rpm. Before plating the cells, the pool was diluted 1:50 in 50 mL LB (50 μg/mL kanamycin, 15 μg/mL tetracycline) and incubated at 37°C and 200 rpm. The growth was monitored by measuring the OD_{600}, and when the cells grew exponentially, they were used in the next step. Usually after 3 h the cells were growing exponentially and had reached a OD_{600} between 0.3 and 0.5.Then an amino acid (10 mM acetyl-lysine or 1 mM for other modified lysines) and 0.2% arabinose (final concentration) was added to the culture. After 3 h, 1 mL cells were harvested by centrifugation (8000 rpm, 2 min) and washed twice with 1 mL PBS to remove the amino acid and uracil. The washed cells were resuspended and adjusted to an OD_{600} of 1 in PBS. 100 μL cell suspension (approximately 10^8 cells) was plated on the selection plate (positive selection: M9 selection plate +amino acid, –uracil, –5-FOA or negative selection: M9 selection plate +amino acid, +uracil, +5-FOA) and a control plate (M9 selection plate, –amino acid, –uracil, –5-FOA). After no fluid film on petri dishes derived from plating was visible anymore (shortly dried), plates were incubated for at least 48 h at 37°C. Colonies were washed off the plate using 2-5 mL LB medium and a drigalski spatula, plasmid DNA was isolated and used to transform *E. coli* cells for subsequent selections.

CobB Selection**

To obtain CobB mutants with preference for deacetylation over decrotonylation, three rounds of selection on the CobB active site library were performed. Starting with a positive selection for deacetylation followed by negative selection against decrotonylation and a final positive selection for deacetylation. Single colonies were picked from the third-round selection plate, grown in a 96-deep well block containing LB medium (1 mL, 50 μg/mL kanamycin), plasmid DNA was isolated, retransformed in DH10β by heat shock using a 96 well PCR plate and PCR program: (hold 4°C, 1 min 15 s 42 °C, hold 4°C), and once more plasmid DNA isolated and sequenced.

In parallel to this selection, any combination of deacylation and deprotection activity was selected for in two rounds for and against all possible combinations of deacylation and/or deprotection activities. If colonies were obtained, 8-24 mutants were grown in a 96-deep well block containing LB medium (1 mL, 50 μg/mL kanamycin). Plasmid DNA was isolated from the culture and send for sequencing.

Sirt1 selection**

The selection for Sirt1 was identical to the selection for the acetyl selective CobB mutants. The only difference was instead of retransforming the individual clones, the pool was retransformed in DH10β before individual mutants were picked.

HDAC8

One round of positive selection for different deacylation activities was preformed, 10 colonies were picked and send for sequencing.

Sirt6

In the case of Sirt6, one round of positive selection for deacetylation was preformed and monitored constantly for growth of colonies. Since the wt took 3-4 days to show colonies, individual clones were picked after 2- and 3-days. The colonies picked after 2 days were send for sequencing while the colonies obtained after 3 days were picked

into a 96-deep well plate and retested by 6-AU selection before individual colonies were sequenced.

ACTIVITY PLATE ASSAY USING 6-AZAURIDINE (6-AU)**

Individual plasmid isolates were used to transform *E. coli* DH10B Δ*pyrF* Δ*cobB* containing pPylT-URA3-K93TAG-AcKRS3 and grown in a 96-deep well block containing 1 mL LB (50 μg/mL kanamycin, 15 μg/mL tetracycline). Cells were replicated using a 48-pin head replicator onto LB agar plates (50 μg/mL kanamycin, 15 μg/mL tetracycline), M9 selection plates containing increasing amounts of 6-AU (positive selection: M9 selection plate ±10 mM acetyl-lysine, –uracil, –5-FOA). The necessary 6-AU concentration range was determined beforehand by titration of 6-AU with the wt KDAC and differed for different lysine acylation of Ura3 K93. Here, 0-2 mM was used for CobB and 0-0.8 mM for Sirt6, plates were imaged after 48 h and 72 h respectively.

SIRTUIN REACTION ON HISTONE EXTRACT AND WESTERN BLOT ANALYSIS**

Isolation of histones: HEK293 GnTI$^-$ cells were grown in Freestyle medium (supplemented with 2% FBS at 37°C in an orbital shaker with 8% CO_2 to a density of 2-3 × 10^6 cells/ml. The cells were incubated for further 8 h at 37°C with 8% CO_2 before addition of 10 mM sodium butyrate to inhibit deacylation. The flask was shifted to 30°C with 8% CO_2 while shaking at 130 rpm and the cells harvested 40 h after addition of the butyrate. The pellet was resuspended in HEK293 lysis buffer (25 mM Tris pH 8, 300 mM NaCl, 10% glycerol, 1 mM TCEP, 1 mM EDTA, 5 µg/ml AEBSF, 5 µg/ml aprotinin, 5 µg/ml leupeptin) and passed through a microfluidizer. Cell debris was collected by centrifugation at 15.000 g for 5 min at 4°C. The histones were extracted from the debris according to the acidic extraction protocol of Sechter et al. (146). The

TCA precipitated histone pellet was suspended in water and diluted to a concentration of 1 mg/mL which was used as substrate stock.

A typical histone deacylation reaction was performed in KDAC buffer (25 mM Tris/HCl pH 8.0, 137 mM NaCl, 2.7 mM KCl, 1 mM $MgCl_2$, 1 mM DTT, 1 mg/ml BSA) and contained 250 ng histone extract, Sirtuin (64 nM to 4 µM) and 2 mM NAD^+. The reaction mix was incubated for 2 h at 30°C and stopped by adding 10 µL 3x SDS-sample Buffer followed by denaturation at 90°C for 10 min. 5 µL were loaded on a 15% SDS-PAGE and histone modifications analyzed by Western blot. The H4 K16ac modification was detected using a monoclonal antibody (Abcam, ab109463, 1:15000 in 3% skimmed milk/TBS) and lysine crotonylation was detected using a pan-specific anti-CrK antibody (PTM Biolabs, PTM501, 1:2000 in 5% % skim milk/TBST).

PATCH DROP ACYLATION SELECTIVITY ASSAY

All mutants from a 96 micro well plate were retransformed into E*. coli* DH10B Δ*pyrF* Δ*cobB* containing pPylT-URA3-K93TAG-AcKRS3 or pPylT-URA3-K93TAG-PylRS by mixing 1 µL plasmid with 10 µL chemical competent cells in a 96 well PCR plate. The heat shock was performed in a PCR cycler with the following program: hold 4°C, 1 min 15 s 42 °C, hold 4°C. 100 uL LB medium was added to each well and the culture transferred to a 96-deep well block. The cells could recover for 1 h at 37°C shaking at 200 rpm before 900 uL LB medium (50 µg/mL kanamycin, 15 µg/mL tetracycline) was added. The next day, the cells were replicated with a 48-pin head replicator onto positive selection plate for different acylation or protection groups and a LB agar plate (50 µg/mL kanamycin, 15 µg/mL tetracycline). The growth of the selection plates was monitored for growth over the next 2-4 days, the LB plate was removed after 1 day. The growth of the different mutants was compared to the wt reference and the selectivity determined by comparing growth on different plates.

DEMODIFICATION REACTIONS OF MYOGLOBIN K4MOD**

Modified myoglobin $K4_{mod}$ was expressed and purified according to published protocols (136). The reactions were performed in a 50 µL volume of 40 mM Tris buffer pH 8 containing 50 mM NaCl, 1 mM DTT, 0.1 mM $ZnCl_2$, 3 mM NAD^+, 30 µM myoglobin $K4_{mod}$ and purified CobB (4 µM wildtype, 16 µM $CobB_{ac2}$, 48 µM $CobB_{ac3}$ and 36 µM $CobB_{ac6}$). The reactions incubated for 16 h at 30°C and were stopped by cooling them to 4°C. 12 µL of each reaction mix was injected on a HPLC (Agilent 1100, Agilent Technologies) and desalted by on C4 column. The proteins were eluted with a gradient of 20-80% acetonitrile in water (0.1% TFA) and analyzed by ESI-MS (LCQ Advantage MAX, Thermo Finnigan). Protein mass was calculated by MagTran and myoglobin peaks were normalized the maximal peak intensity (147).

SDS-GEL ELECTROPHORESIS

SDS samples were prepared by mixing 15 µL sample and 5 µL 4x SDS-sample buffer. The sample was heated for 10 min at 80°C and 10 µL were loaded on a discontinuous Tris-Glycine SDS gel (1: 37.5 Bis-/Acrylamide; 4%/10%, 4%/15% or 4%/18% gels; pH 6.8/8.8; 0.1% SDS). The gel was run in SDS running buffer (25 mM Tris, 192 mM Glycine, 0.1% SDS pH 8.3) with 150 V for 90 min. The gel was either stained by InstantBlue® Protein Gel Stain (expedeon) or used for western blot analysis.

SEMI-DRY WESTERN BLOT FOR HISTONE ANALYSIS

An SDS-Gel was placed on top of Towbin-transfer buffer (25 mM Tris, 192 mM Glycine, 20% methanol, pH 8.3) soaked whatman filter paper (two) and placed in a cassette of the Trans-Blot Turbo Transfer System (Biorad). A methanol soaked PVDF membrane was placed on the gel followed by two Towbin-transfer buffer whatman filter paper. The cassette was sealed, and excess buffer was removed. The transfer was run with 1 A for 30 min. The SDS-gel was stained using InstantBlue® Protein Gel Stain (expedeon) and the PVDF membrane with 0.1% Ponceau S Staining Solution (Sigma) in 1%

acetic acid. The membrane was then blocked for 1-2h using the appropriate blocking reagent (See Table 5). The blocking solution was discarded, and the membrane washed with TBST and five times with TBS over 15 min. The antibody was diluted (See Table 5) in blocking solution and incubated with the membrane at 4°C overnight while agitated. The washing step was repeated and the membrane incubated for 1 h with the secondary antibody in 5% skim milk/TBS (See Table 5) at RT. After repeating the washing step once more the antibody signal was developed using either ECL™ Select Western Blotting Detection Reagent (GE Healthcare). The blot was imaged for 10 s to 5 min using the Imager Celvin® S 320 (Biostep)

DOT BLOT**

200 ng acylated myoglobin $K4_{mod}$ (Acetylated, Butyrylated or Crotonylated) was spotted on a nitrocellulose membrane and let dried for 2 min. The membranes were developed using the general procedure described for western blots after the transfer of samples. The blocking agents used in this experiment were: panKac-101: 5% BSA/TBS, panKcr-501: 5% skim milk/TBST, panKbu-301: 5% BSA/TBST, PTM Biolabs. The blocking buffer was also used to dilute the antibodies: panKac-101 1:2000, panKcr-501 1:2000 and panKbu-301 1:2000.

IMMUNE FLUORESCENCE**

HeLa cells were maintained in 5% CO_2, 37°C in DMEM+GlutaMAX™-I medium (Gibco life technologies) supplemented with 10% heat-inactivated fetal calf serum. For microscopy, Hela cells were seeded in 6-well plates on glass coverslips to a 1.5 $x10^5$ cells/ml density 24 h prior to transient transfection of CobB-GFP constructs with Lipofectamine 2000 (Thermo Fisher Scientific). As indicated in the text, cells were either fixed 24 h p. transfection (or after additional treatment with 2 mM sodium

crotonate pH 7.2 for 2 h) for 15 min with 4% paraformaldehyde. Staining with pan-KAc pan-KCr and pan-KBu antibodies in blocking buffer (3% BSA, 0.1% TritonX-100 in PBS; antibody dilution 1:1000, panKac-101, panKcr-501, panKbu-301 PTM Biolabs) lasted 2 h at 37°C and the secondary antibody anti-rabbit-Cy3 conjugate (1:1000 Jackson Immuno Research,111-165-144) together with 1 µg/ml DAPI was done for 1 h at 37°C. Thereafter, the coverslips were dried, mounted and analyzed by LSM (Zeiss LSM800/510, 40x or 63x oil objective). The level of acylation was quantified using Fiji, comparing the mean intensity of DAPI to the intensity of the antibody in transfected and untransfected cells (148). The data of >50 cells from at least 3 different field of views was plotted using GraphPad prism (version 8.3.1 for windows OS).

SYPRO ORANGE THERMAL STABILITY ASSAY.

The reaction was set up in COMAS reaction buffer with a final volumn of 20 uL containing 1 mg/mL purified Sirt1, ±100 µM Compound, ± 1 mM NAD^+, ± 1 mM H3K18ac peptide and 10x Sypro Orange. The reactions were prepared in triplicates and the melting curve was measured by detecting the change in fluorescents in a CFX96 rtPCR (BioRad) with the following settings: 20°C 10 min, 360x [20 °C, 10 s, FRET Mode, + 0.2 °C/Cycle], hold 8 °C. The T_m was determined by fitting the experimental data with a Boltzmann equation using SciDavis (version 1.22).

PROMETHEUS THERMAL SHIFT ASSAY

The protein and peptides were premixed on ice in a 3x20 uL volume COMAS reaction buffer with a final concentration of 0.5 mg/mL purified protein and ± 1 mM modified H3K18 peptide. The solution was incubated for 20 min on ice, transferred to a capillary and placed in the Prometheus (Nanotemper). The fluorescent signal of each capillary was detected at 10% beam intensity and the beam intensely adjusted if necessary to give a signal of 4000-5000 point. The following program was run: 20-90 °C, + 1.5°C/min while measuring the fluorescent ratio at 350/330. The data was analyses using the

integrated software and the melting point (Tm) determined using the first derivative of the data.

CRYSTALLIZATION OF COBB AND COBB MUTANTS

The crystallization of CobB, $CobB_{ac2}$, $CobB_{ac3}$ and CobB F7 were set up as reported for CobB (140).

CobB/$CobB_{ac2}$**

Crystals were obtained after 1 day from hanging drop crystallization with 100 mM Bis-Tris, 30 mM HCl, 22% PEG 3350 ($CobB_{ac2}$ 23% Ac and Cr, 24% Bu) as precipitant and 10 mg/mL CobB (10.5 mg/mL $CobB_{ac2}$) preincubated with 1 mM H4 $K16_X$ (X: Ac, Bu, Cr) peptide. Crystals were flash frozen in liquid nitrogen with 20% PEG400 as cryoprotectant containing 1 mM H4 $K16_X$ (X: Ac, Bu, Cr).

$CobB_{ac3}$**

Crystals were obtained after 1 week from hanging drop crystallization with 100 mM Bis-Tris, 10 mM HCl, 22% PEG 3350 as precipitant and 7.2 mg/mL $CobB_{ac3}$ preincubated with 1 mM H4 $K16_{Ac}$ peptide. Crystals were flash frozen in liquid nitrogen with 20% glycerol as cryoprotectant containing 1 mM H4 $K16_{Ac}$.

$CobB_{ac2}$-H4K16$_{Cr}$-NAD^+**

This complex was obtained after 16 h hanging drop crystallization with 100 mM Bis-Tris, 20 mM HCl, 22% PEG 3350 as precipitant and 11.1 mg/mL $CobB_{ac2}$ preincubated on ice with 1 mM NAD^+ and 1 mM H4 $K16_{Cr}$ peptide. Crystals were flash frozen in liquid nitrogen with 20% PEG400 as cryoprotectant containing 1 mM NAD^+ and 1 mM H4 $K16_{Cr}$.

For the soaked complex, $CobB_{ac2}$-H4K16Cr crystals were transferred, using a nylon loop, to a 1 µL hanging drop supplemented with 1 mM H4K16Cr peptide and 1 mM NAD^+. The drop was placed over the same conditions the $CobB_{ac2}$-H4K16Cr crystals originated from for 2 h or 36 h. Crystals were flash frozen in liquid nitrogen using 20%

PEG400 as cryoprotectant supplemented with 1 mM NAD^+ and 1 mM H4 K16Cr peptide.

CobB F7-H4K16$_{Alloc}$

Crystals from CobB F7 (unpublished) were obtained after 1 day from hanging drop crystallization with 100 mM Bis-Tris, 50 mM HCl, 24% PEG 3350 as precipitant and 10 mg/mL CobB F7 preincubated with 1 mM H4 K16aloc peptide. Crystals were flash frozen in liquid nitrogen with 20% PEG400 as cryoprotectant containing 1 mM H4 K16aloc.

Data acquisition and refinement

Data collection was performed at beamline PXII X10SA at the Suisse Light Source, Villigen, Switzerland. The data was processed with XDS and scaled using XSCALE (149). Molecular replacement was performed with Phaser (150) and the data was refined using Refmac5 (151) initially and Phenix.refine (152) in the final steps. The ligand geometry file was created using JLigand (153) for coordinates and PRODRG (154) for calculation of restraints. Model building was done with Coot (155). For the data collection and refinement statistic see S. Table 7.

SUPPLEMENTARY INFORMATION

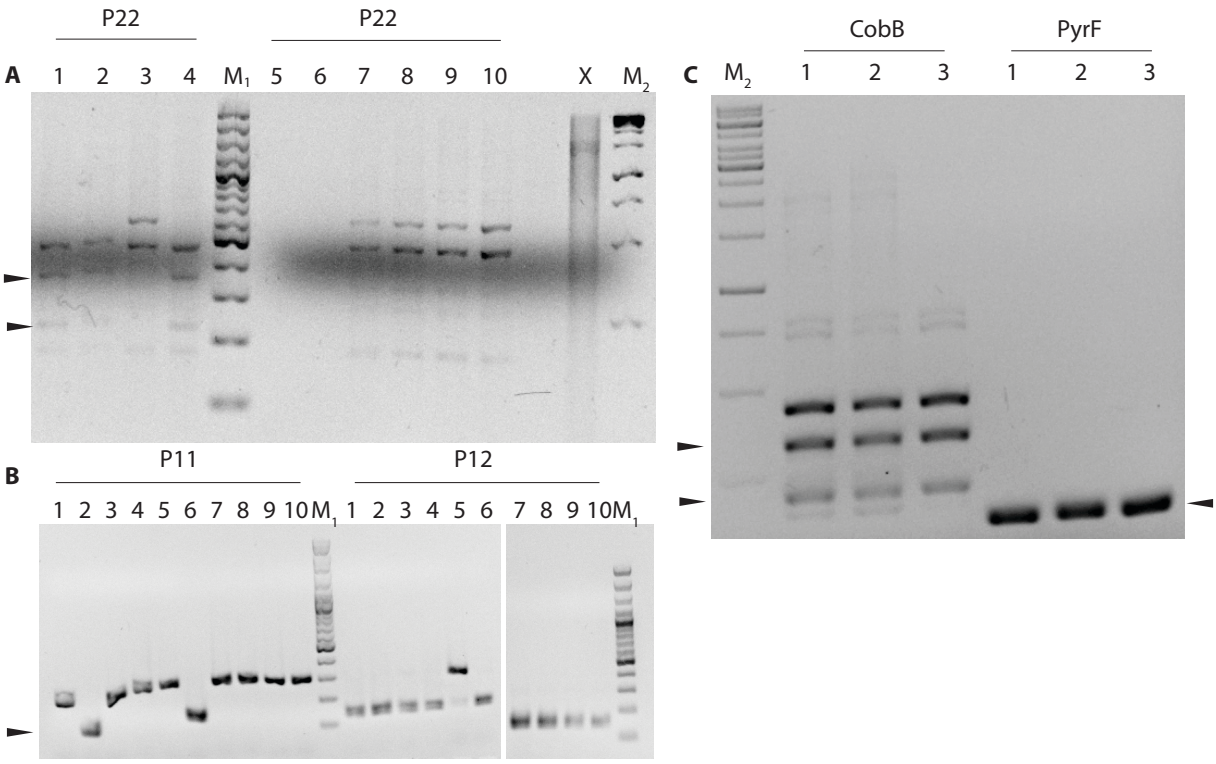

S. Figure 1: **Colony PCR from CobB (A) and PyrF (B) knockout after HindIII digest, useing repair primer P22 (CobB) and P11 or P12 (PyrF) seperated on a 2% agarose/TAE gel.** Arrow indicates the height of the expected cleavage product (CobB 347 bp + 223 bp, PyrF 139 bp + 148 bp) upon successful Cas9/CRISPR mutagenesis. C) Repetition of the colony PCR after curing of all Cas9/CRISPR plasmid confirming the knockout of CobB and PyrF. Introduction of primer P22 and P11 was also confirmed by sequencing *of* the PCR product. M_1= 100 bp ladder, M_2 1kb ladder, Thermo Fischer

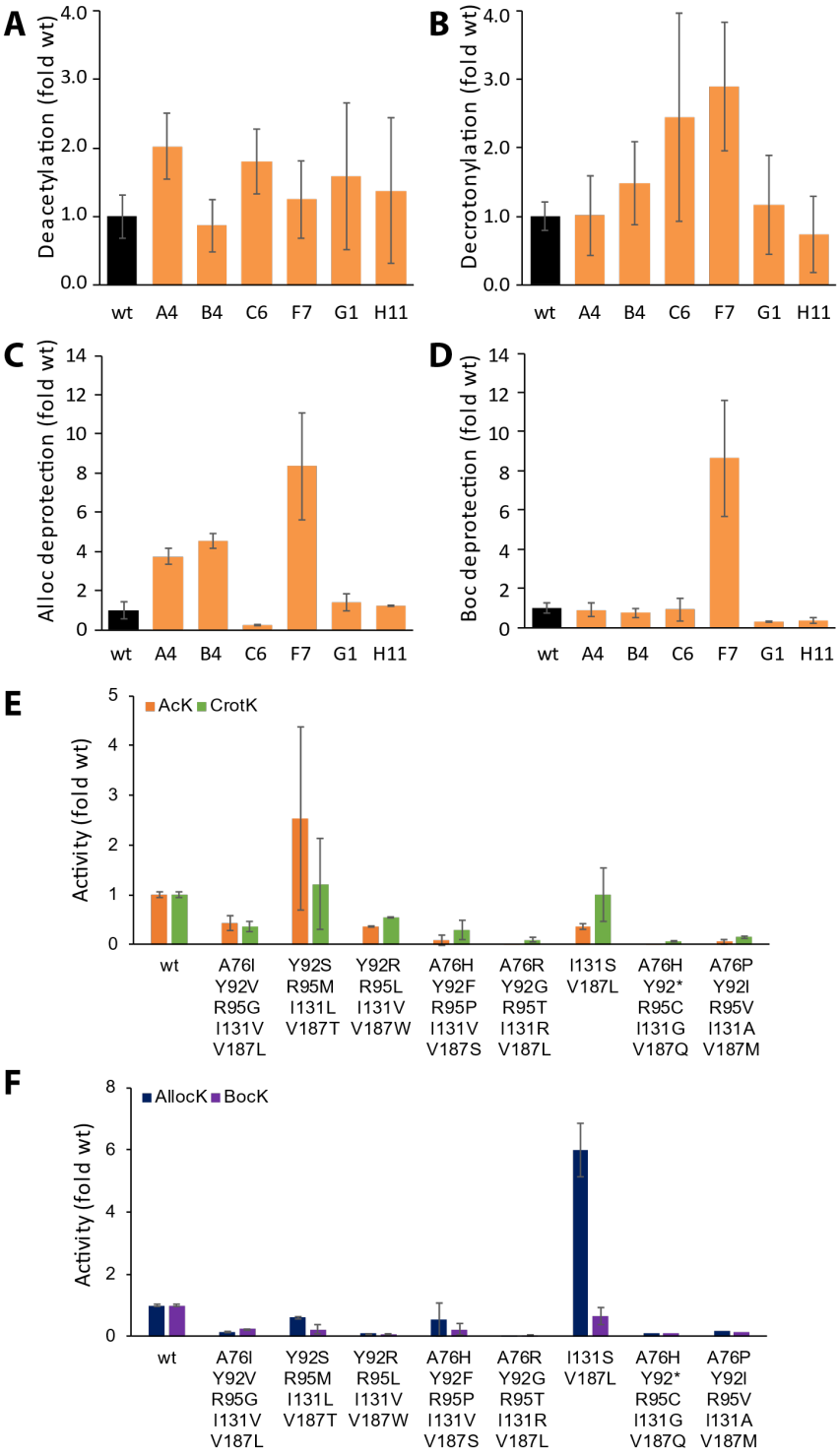

S. Figure 2: Dual-Luciferase measurement for deacylation and deprotection of the modified K529X (Ac, Cr, Alloc or Boc) by coexpression of various mutants from plate 1 and plate 2 (See . Error! Reference source not found. **and** Error! Reference source not found.**).** A-D) Renilla-Firefly K529X (X: Ac, Cr, Boc, Alloc) luciferase fusion was coexpressed over 16 h together with all mutants picked from the boc positive selection plate. The firefly luciferase signal was normalized to the renilla luciferase signal and the activity is shown as fold wt activity. E-F) 7 mutants were selected from plate 2 and tested as in A-D for deacylation and deprotection. The error bars shown are the standard deviation of 2-3 measurements preformed in triplicates.

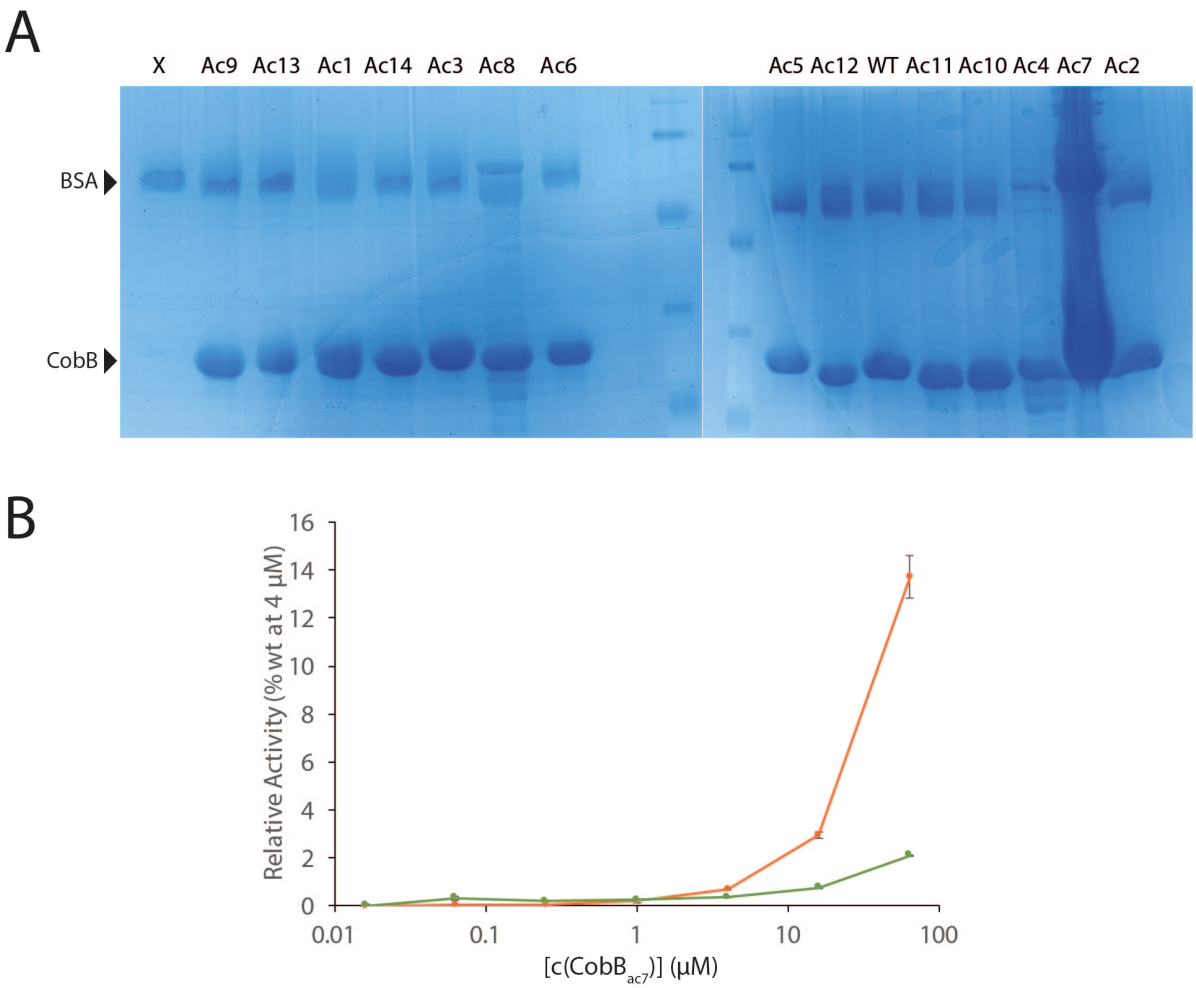

S. Figure 3: Extended data for Figure 7.A) Full SDS-gel loading control for the Figure 5B. B) Deacetylation (orange) and decrotonylation (green) activity for $CobB_{Ac7}$ relative to the activity of CobB at 4 µM.

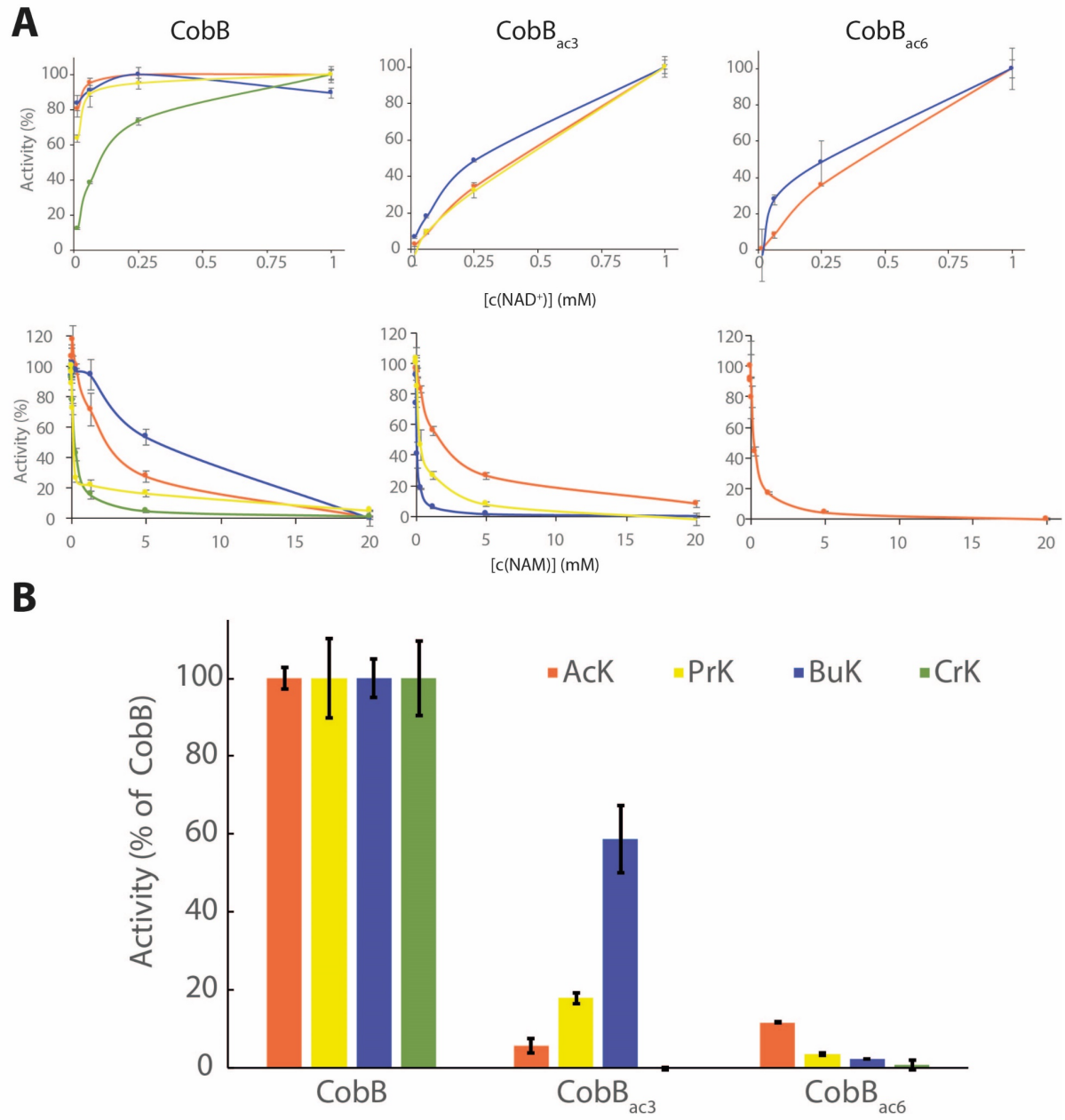

S. Figure 4: Catalytic rates of acetyl-selective CobB variants in dependence of NAD, NAM concentration and FLuc acylation. A) FLuc with the indicated modification was incubated with CobB (64 nM), CobB$_{ac3}$ (2 µM) or CobB$_{ac6}$ (2 µM) and luminescence assayed in endpoint format. 2 mM NAD^+ was present in the NAM titrations. B) CobB variants were assayed on purified FLuc carrying the indicated modification on K529. Experiments were performed in triplicates; error bars are standard deviation of the mean.

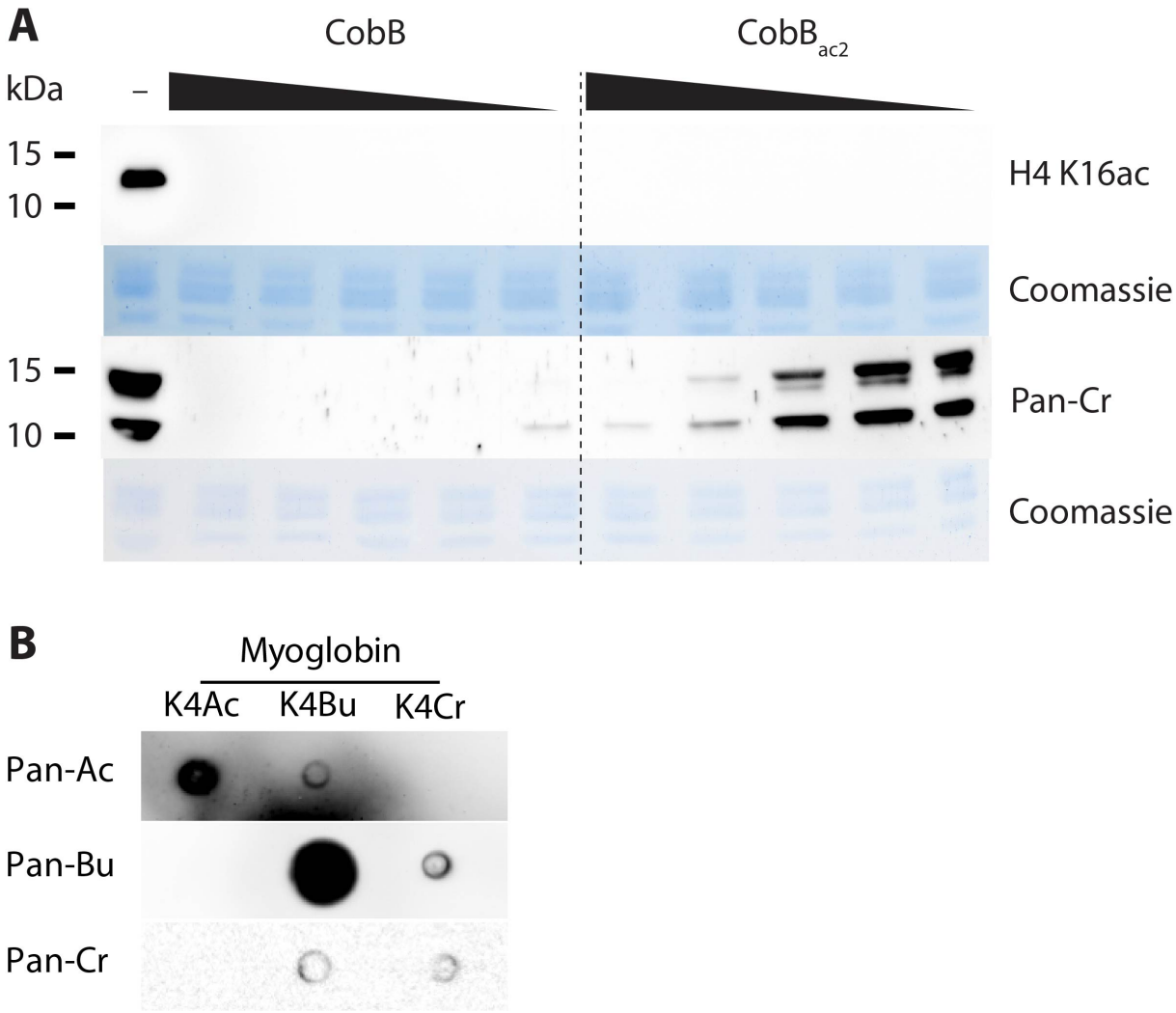

S. Figure 5: Deacylation of histone extract by CobB and CobB$_{ac2}$ analysis by western blot and dot blot to test the antibody specificity of the pan-specific antibodies. A) Purified human histones were incubated with CobB or CobB$_{ac2}$ (63 nM to 1 µM) for 2 h at 30°C in the presence of 2 mM NAD^+. The modification state of the histones was analyzed by Western blot using anti-H4 K16ac and anti-crotonyl-lysine antibodies. B) Dot-blot spotted with 200 ng spotted myoglobin carrying an acetyl, butyryl or crotonyl group at lysine 4 to test the selectivity of different pan-acyl antibodies.

A

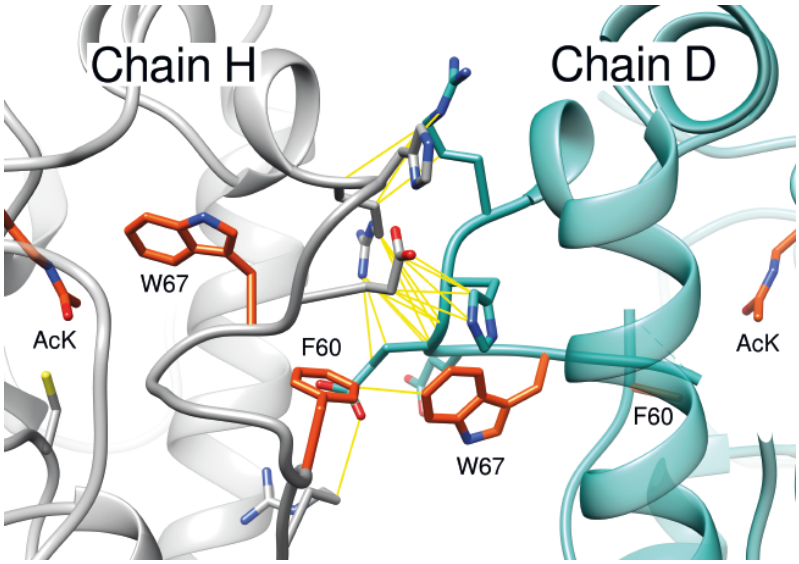

B

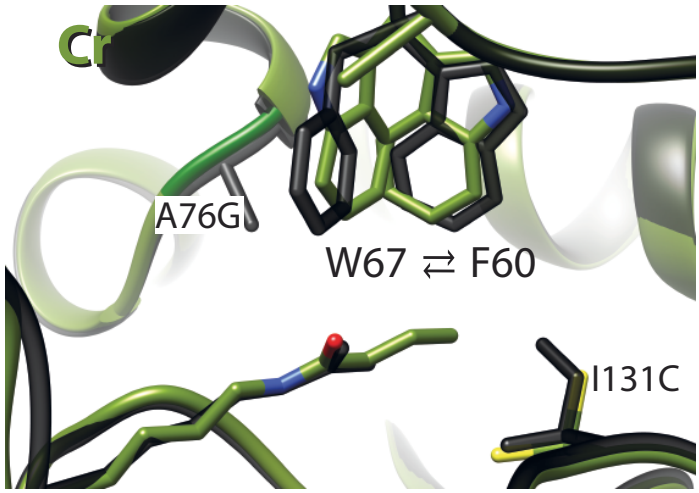

S. Figure 6: Omitted chains from overlay of CobB and CobB$_{ac2}$ A) Crystal chains omitted from overlay of CobB$_{ac2}$ acetyl bound state (Figure 3C), due to contact (yellow lines) between the substrate binding loops of both chains. Acetyl-lysine, W60 and F60 of both chains (H, grey, D, opal) are highlighted in orange. B) Second molecule (Chain A) of CobB$_{ac2}$ in unit cell of H4 K16cr co-crystal. Chain A shows a mixture of conformations with W67 switching positions between the alternative and native state; F60 unresolved.

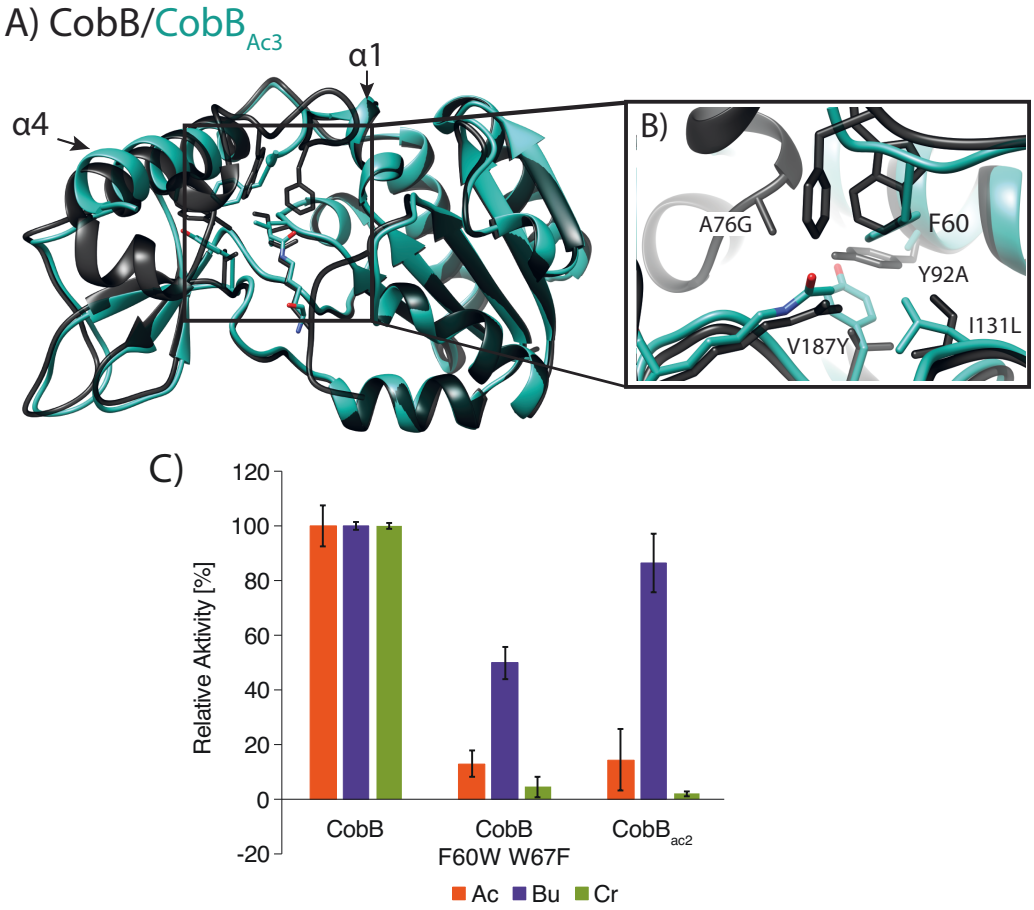

S. Figure 7: Structure of CobB$_{ac3}$ and activity of the CobB F60W W67F mutant. A) Overlay of H4 K16ac bound structures of CobB (black) and CobB$_{ac3}$ (A76G, Y92A, I131L, V187Y, opal). CobB$_{ac3}$ shows major distortions of cofactor binding loop and helix α2 and α3 following residue F60 until the beginning of helix α4. B) Close-up of the active site. The 4 mutations in CobB$_{ac3}$ allow F60 to bind the hydrophobic pocket previously held by W67. C) Selectivity of designed mutant (2 μM**)** towards different lysine modifications relative to CobB and CobB$_{Ac2}$ measured by Firefly luciferases KDAC assay for acetyl- (Ac) butyryl- (Bu) and crotonyl-lysine (Cr). Swapping F60 with W67 in CobB leads to acyl selectivity comparable to CobB$_{ac2}$. Error bars are standard deviations of the means of three biologically independent replicates performed in triplicates.

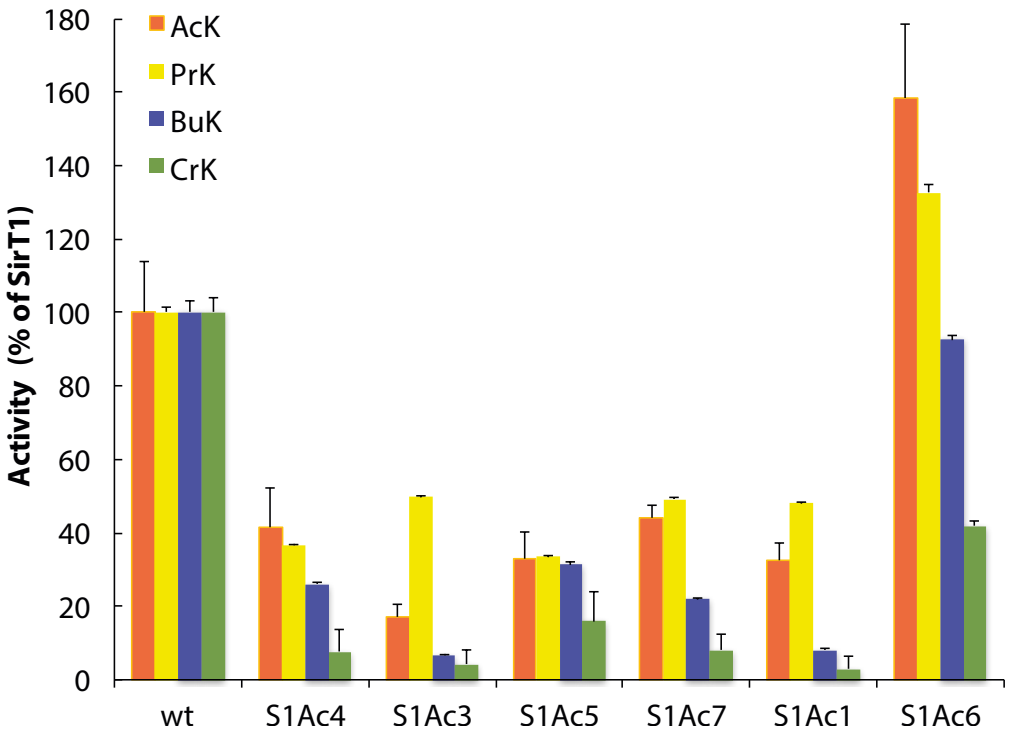

S. Figure 8: Acyl selectivity of Sirt1 variants. Crude purified Sirt1 variants assayed on FLuc K529ac/pr/bu/cr. Error bars are standard deviations of the means of three replicates.

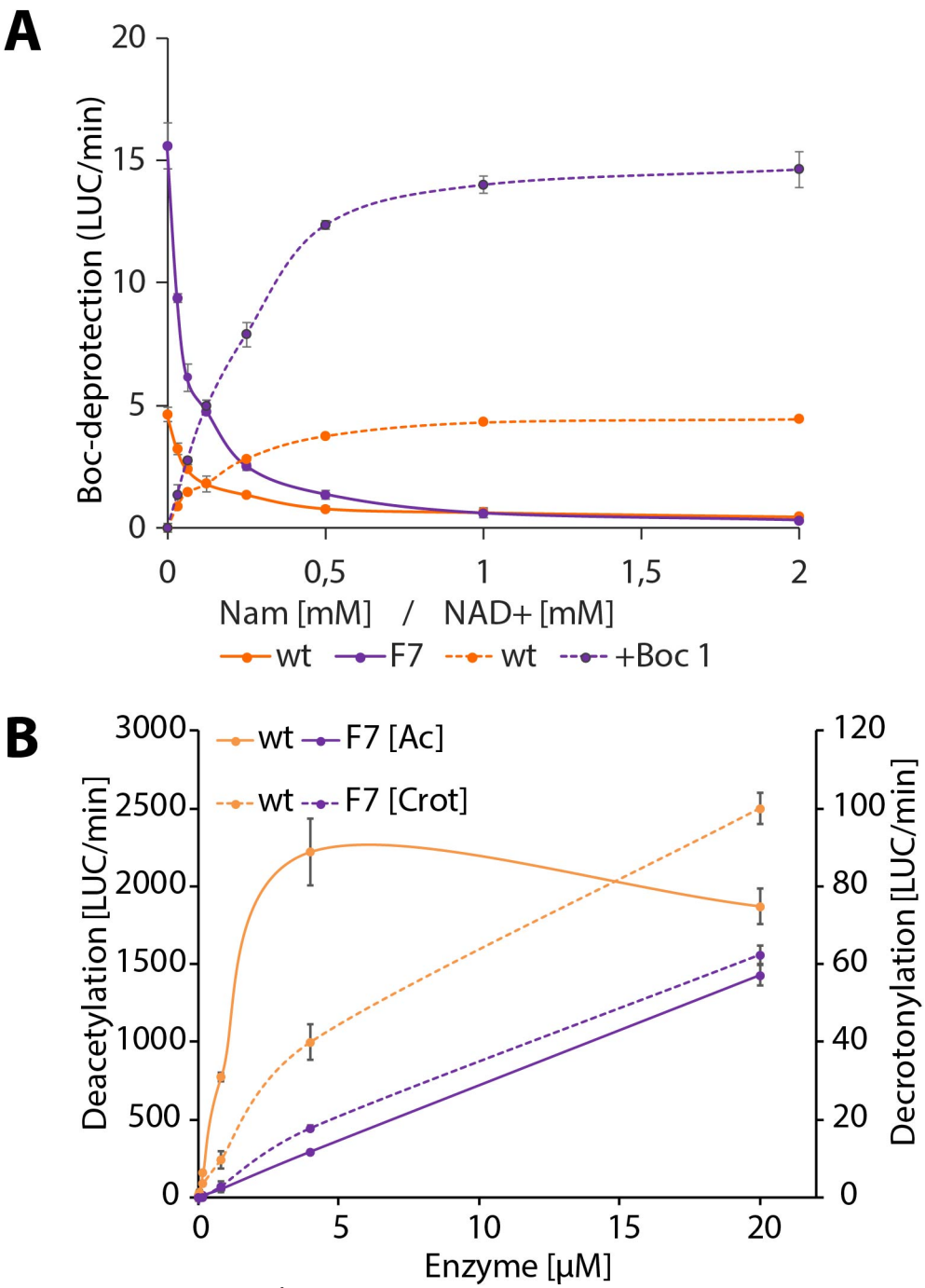

S. Figure 9: Effect of NAD^+ and Nicotinamid (NAM) on the CobB and CobB F7 boc deprotection reaction and their activity for deacetylation and debutyrylation. A) Boc deprotection reaction of 4 µM CobB or CobB F7 with increasing amounts of NAD^+ or Nicotinamid (NAM, NAD^+ 2 mM). B) Deacetylation and decrotonylation activity of CobB and CobB F7 measured by the Fluc assay.

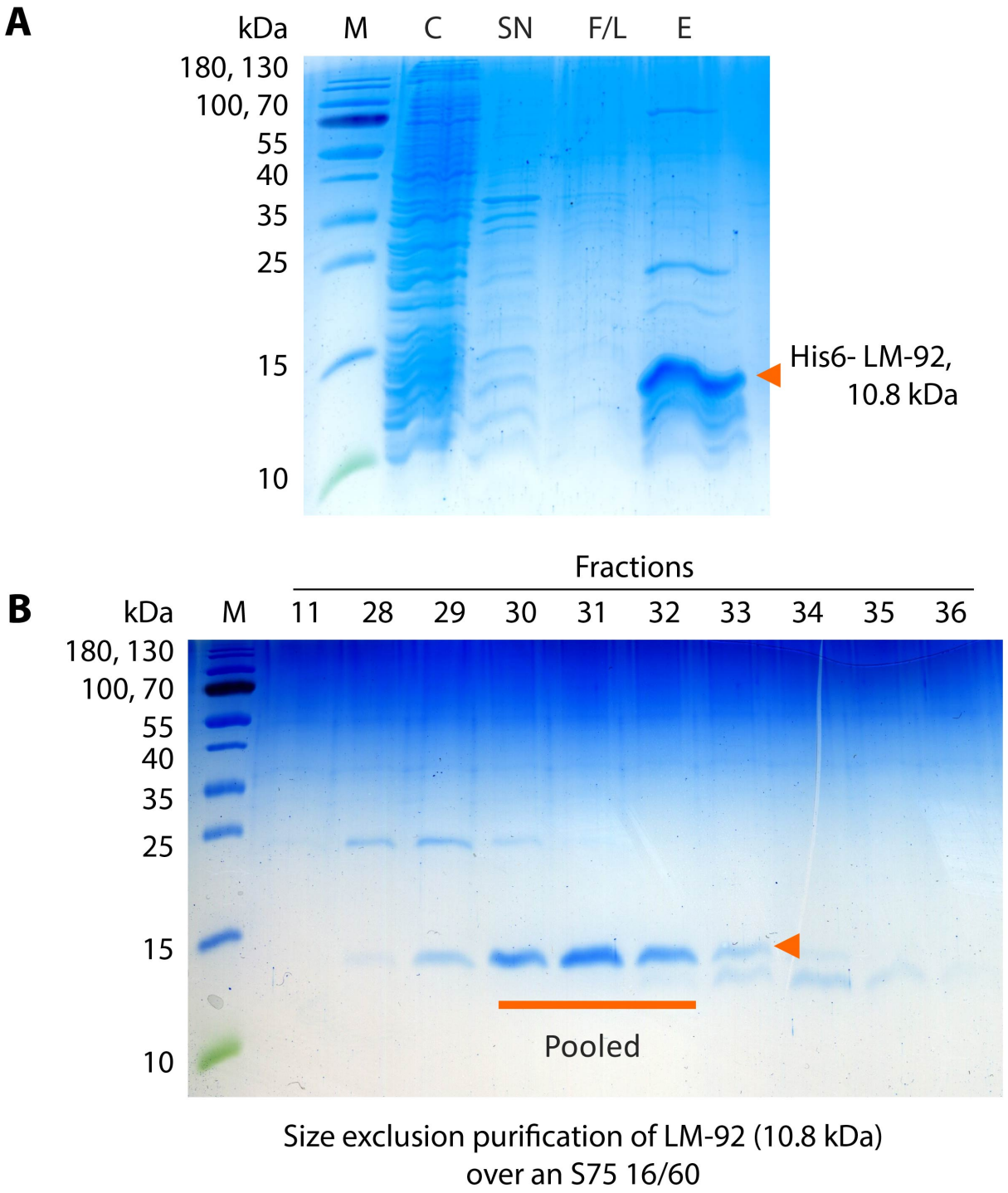

Size exclusion purification of LM-92 (10.8 kDa)
over an S75 16/60

S. Figure 10: SDS-Gels of the LM-92 peptide (10.8 kDa, including the His_6-tag, orange arrow) purification from *E.coli*. A) Coomassie stained 18% SDS-Gel, shows the cell lysate after lysis by boiling for 30 min (C), supernatant (SN) after centrifugation of C, loading and washing fraction of the SN after running it over Ni-NTA beads (F/L) and the elution (E). B) The elution was applied to an S75 16/60 gel filtration column for further purification. All fractions containing protein were identified using Bradford reagent since LM-92 has no UV-absorption and analyzed on an 18% SDS gel as before. The indicated fractions (30-32) were pooled and used in the further biochemical assays.

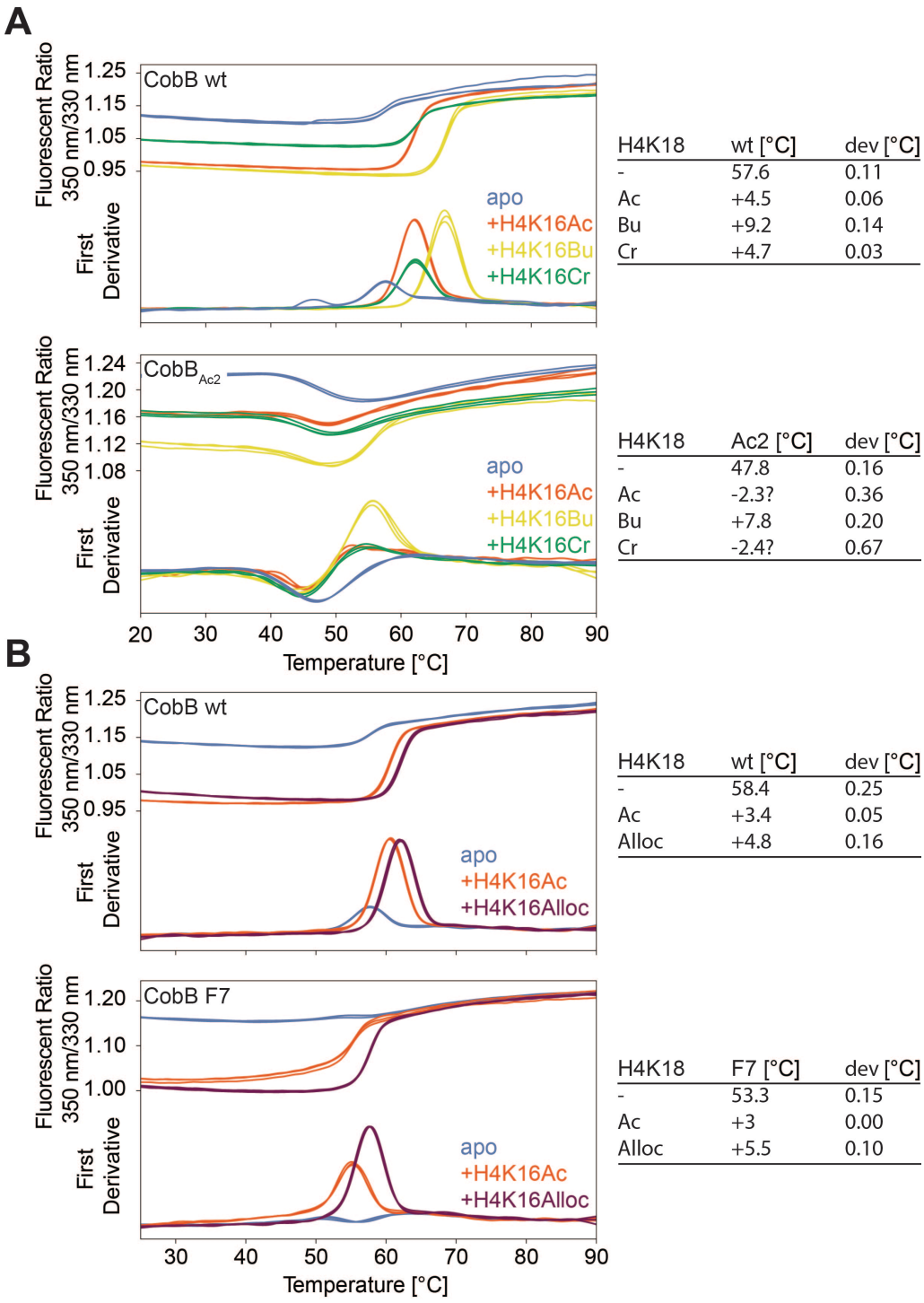

H4K18	wt [°C]	dev [°C]
-	57.6	0.11
Ac	+4.5	0.06
Bu	+9.2	0.14
Cr	+4.7	0.03

H4K18	Ac2 [°C]	dev [°C]
-	47.8	0.16
Ac	-2.3?	0.36
Bu	+7.8	0.20
Cr	-2.4?	0.67

H4K18	wt [°C]	dev [°C]
-	58.4	0.25
Ac	+3.4	0.05
Alloc	+4.8	0.16

H4K18	F7 [°C]	dev [°C]
-	53.3	0.15
Ac	+3	0.00
Alloc	+5.5	0.10

S. Figure 11: Melting curves of CobB wt, F7 and Ac2 in complex with modified H4K16 peptides. The melting temperature was determined by measuring the fluorescent ration of tryptophan at 350 nm to 330 nm at slowly increasing temperature (20-90°C, +1.5°C/min). The first derivative was calculated from the plotted fluorescent ratios to determine the inflection point of the curve (Tm). A) CobB and CobB$_{Ac2}$ melting curve and Tm for the apoprotein and the complex with acylated H4K16 peptide (Ac: Acetyl, Bu: Butyryl, Cr: Crotonyl). The melting point of CobB$_{Ac2}$ for Acetyl and Crotonyl complex is not clearly defined (?), most likely due to the difference in W67 positioning. B) Melting curve and Tm of CobB and CobB F7 as apoprotein or in complex with modiefied H4K16 (Ac: Acetyl, Alloc: Allyloxycarbonyl). The measurements were performed in triplicates and the error (dev) is given as standard deviation of the mean.

S. Table 1: Sequencing results after one round positive selection (+) for the ability to cleave the indicated lysine modification (Alloc, Boc or Crotonylation). Colonies were retested in a patch drop assay on positive selection plates (BocK, AllocK, CrK), good growth was indicated with an x. n.t: no transformants

Plate1	+	BocK	AllocK	CrK	long
A04	AllocK	x	x	x	I131M V187A
A05	AllocK		x	x	A76A Y92W R95Y I131M V187L
A12	AllocK				R95V I131G V187L
B04	AllocK		x	x	Y92F R95L I131A V187L
B05	AllocK				I131L V187C
B06	AllocK		-	x	I131M V187L
B11	AllocK				A76S Y92W R95C I131G
B12	AllocK		x	-	A76S Y92W R95L I131M V187L
C05	AllocK		x	x	R95L I131G V187G
C06	AllocK	x			I131V V187M
C11	AllocK		x	x	A76V I131G V187L
D12	AllocK		x	x	I131G
H12	AllocK				I131A V187L
H11	AllocK		x		A76S R95V I131V V187L
G11	AllocK		x		I131G V187E
G05	AllocK		x		I131A V187A
E11	AllocK			x	A76S Y92W R95K I131W V187L
A07	BocK		-	-	I131W V187G
B07	BocK	?	?	?	Y92F I131M V187L
D07	BocK	x	x	x	A76S Y92W R95W I131V V187V
H07	BocK		x		Y92Q I131L V187Q
E07	BocK				R95P I131R V187G
F07	BocK	x	x	x	I131V V187L
A01	CrK		(X)	x	I131V V187P
A02	CrK			x	A76L Y92T R95F I131V V187S
A03	CrK				A76L Y92F R95? I131A
A10	CrK				Y92V R95C I131R V187R
B01	CrK		-	-	Y92F I131V V187C
B02	CrK				A76V Y92T R95F V187L
B03	CrK		x	x	A76C Y92D R95M I131L V187S
B10	CrK			-	A76T Y92N R95L I131L V187L
C01	CrK		x	x	A76L I131M V187G
C02	CrK		-	x	A76S Y92N R95C I131L V187V
C03	CrK			x	A76C Y92W R95T I131N
C10	CrK			x	A76L Y92S R95F I131N V187M
D01	CrK				A76Y Y92L R95V I131V
D02	CrK			x	A76L Y92I R95V I131M V187L
D03	CrK			x	A76C Y92V R95M I131F V187L
D09	CrK			x	Y92V R95S I131L V187M
E02	CrK	n.t	n.t	n.t	A76L Y92A R95I V187F
E03	CrK	-		x	A76V Y92F R95F V187L
H10	CrK				A76V Y92C R95C V187L
H03	CrK		x		A76C Y92F R95G I131A
G10	CrK		x		I131G V187E
G09	CrK				I131A V187A
G03	CrK				A76L Y92L I131Y V187L
F10	CrK			x	Y92M R95V I131L V187L
F09	CrK			x	Y92M R95V I131L V187L
G01	CrK		x	x	A76T R95G I131V V187L
F03	CrK				A76N Y92F R95L I131M V187L
F02	CrK				I131L V187S
E10	CrK		x	x	I131W V187G
E09	CrK			x	A76V I131M V187M

S. Table 2: Sequencing for various combinations of positive (+) and negative (+) selection for or against the indicated lysine modifications (AcK, BocK, AllocK or CrK). Mutants were retested on positive selection plates for the ability to cleave AcK, BocK, AllocK, or CrK, growth was judged from good (++) to non (-). *amber codon, %frameshift, ? not sequenced, 7.1/6.1 Library containing NNK at A49 and F60 instead of Y92 and R95, not further used.

Plate2	+	-	AcK	BocK	AllocK	CrK	Mutations
A01	AcK	no	+	-	-	-	A76P Y92W R95L I131Y V187A
A02	AcK	no	+	-	-	-	A76P Y92L R95M I131V V187L
B01	AcK	no	+	-	-	0	I131V V187M
B02	AcK	no	+	-	-	-	A76P Y92W R95L I131Y V187A
C01	AcK	no	+	-	-	-	A76L Y92L R95G I131W V187L
D01	AcK	no	+	-	-	-	A76C Y92K R95M I131L V187M
E01	AcK	no	+	-	-	-	A76L Y92A R95L I131C ?
F01	AcK	no	+	-	-	-	A76L R95V I131V V187N
G01	AcK	no	+	-	-	-	I131A V187L
H01	AcK	no	+	-	-	-	A76F Y92W R95I V187S
A08	AcK	Crot	+	-	-	-	???????
A11	AcK	Crot	+	-	-	-	???????
B08	AcK	Crot	+	-	-	-	?????I131V V187L
B11	AcK	Crot	+	(-)	-	+	A76S Y92H R95V V187T
C08	AcK	Crot	+	-	-	-	A76X Y92X R95X I131V ?
C09	AcK	Crot	+	-	-	-	A76H Y92F R95P I131V V187S
D08	AcK	Crot	+	-	-	-	A76I Y92V R95G I131V V187L
D09	AcK	Crot	+	-	-	-	???????
E09	AcK	Crot	+	-	-	-	A76I Y92V R95G I131V V187L
E10	AcK	Crot	+	(-)	-	-	Y92R R95L I131V V187W
F09	AcK	Crot	+	-	-	-	???????
F10	AcK	Crot	+	-	-	-	A76I Y92V R95G I131V V187L
G07	AcK	Crot	0	-	(+)	+	Y92S R95M I131L V187T
G09	AcK	Crot	+	-	-	-	A76I Y92V R95G I131X V187L
G10	AcK	Crot	+	-	-	-	A76I Y92V R95G I131V V187L
H07	AcK	Crot	0	-	-	-	??A76I Y92V R95G I131V V187L
H09	AcK	Crot	+	n.t	n.t	n.t	???????
H10	AcK	Crot	+	-	-	-	???????
A06	AcK_7.1	no	+	-	-	-	A49C F60T A76C I131L V187L
B06	AcK_7.1	no	+	-	+	0	A49S F60* A76* V187L
E05	AcK_7.1	no	+	-	-	-	I131V
F05	AcK_7.1	no	+	-	-	-	A49C F60W A76L ?
G05	AcK_7.1	no	+	-	+	0	A49S F60* A76* V187L
H05	AcK_7.1	no	+	-	+	0	A49S F60R A76C V187G
C06	AcK	no	+	-	+	0	A76L Y92R R95L I131L V187W
D06	AcK	no	+	-	+	-	Y92V R95L I131H V187M
E06	AcK	no	+	-	+	0	???????
F06	AcK	no	+	-	-	0	???????
G06	AcK	no	+	-	+	0	A76L Y92R R95L I131L V187W
H06	AcK	no	+	-	+	0	Y92T R95F I131W V187L
A04	Ac+Alloc	no	+	+	+	+	I131G V187L
B04	Ac+Alloc	no	+	-	-	-	A76M Y92S R95L I131A V187T
C04	Ac+Alloc	no	+	-	0	-	I131A V187T
D04	Ac+Alloc	no	+	-	0	0	I131L V187M
E04	Ac+Alloc	no	+	-	0	-	A76X Y92X I131L V187Q
F02	Ac+Alloc	no	+	+	+	+	V187L
F04	Ac+Alloc	no	+	-	0	0	Y92F R95L I131A V187S
G02	Ac+Alloc	no	+	-	+	-	A76C Y92V R95Q I131Y V187L
H02	Ac+Alloc	no	+	+	+	-	V187L
A05	Ac+Crot	no	+	-	-	-	A76M Y92G R95A I131F V187L
B05	Ac+Crot	no	+	-	-	-	Y92W I131L V187D
C02	Ac+Crot	no	+	-	-	+	I131V V187M
C05	Ac+Crot	no	+	-	-	0	A76T Y92G R95L I131F V187W
D02	Ac+Crot	no	+	-	-	+	I131V V187M
D05	Ac+Crot	no	+	-	-	-	R95X I131L V187M
E02	Ac+Crot	no	+	-	-	+	I131V V187M
G04	Ac+Crot	no	+	-	-	-	A76C Y92N R95C I131W

Plate2	+	-	AcK	BocK	AllocK	CrK	Mutations
H04	Ac+Crot	no	+	-	-	-	A76L Y92W R95Q I131V V187L
E12	Alloc	no	+	(-)	-	++	A76S Y92W R95K I131W V187L
A09	Alloc	Ac	-	-	+	+	A76P Y92I R95V I131A V187M
B09	Alloc	Ac	-	(-)	-	+	I131S V187L
C10	Alloc	Ac	-	(-)	+	+	A76R Y92G R95T I131R V187L
D07	Alloc	Ac	-	(-)	+	+	Y92X R95G I131S ?
D10	Alloc	Ac	-	(-)	-	+	A76R Y92G R95T I131R V187L
E07	Alloc	Ac	0	(-)	+	+	A76R Y92G R95T I131R V187L
F07	Alloc	Ac	-	(-)	+	+	A76R Y92G R95T I131R V187L
F11	Alloc	Ac	-	(-)	-	+	A76H Y92* R95C I131G V187Q
G11	Alloc	Ac	-	(-)	++	+	I131S V187L
H08	Alloc	Ac	-	(-)	+	+	A76R Y92G R95T I131R V187L
H11	Alloc	Ac	-	(-)	+	+	R95X I131S V187L
A03	Alloc_6.1	no	+	+	+	-	V187T
B03	Alloc_6.1	no	+	(+)	+	-	I131L V187S
C03	Alloc_6.1	no	+	(+)	+	+	V187T
D03	Alloc_6.1	no	+	-	0	-	F60L A76C V187T
B12	Boc	no	-	-	+	-	Y92% R95P I131R V187G
G12	Boc	no	+	(-)	+	+	I131V V187L
A12	Crot	no	+	-	-	-	Y92M R95V I131L V187L
C12	Crot	no	+	(-)	+	+	A76N Y92F R95L I131M V187L
D12	Crot	no	0	(-)	-	-	I131L V187S
F12	Crot	no	+	-	(+)	-	I131W V187G
H12	Crot	no	+	(-)	(+)	++	A76T R95G I131V V187L
A07	Crot	Ac	+	(-)	+	+	?????I131V V187S
A10	Crot	Ac	-	-	+	+	A76H Y92F R95P I131V V187S
B07	Crot	Ac	-	(-)	+	+	A76H Y92F R95P I131V V187S
C07	Crot	Ac	0	(-)	+	+	A76H Y92F R95P I131V V187S
C11	Crot	Ac	-	(-)	-	+	A76H Y92F R95P I131V V187S
D11	Crot	Ac	-	(-)	-	+	A76H Y92F R95P I131V V187S
E08	Crot	Ac	-	(-)	+	++	A76H Y92F R95P I131V V187S
E11	Crot	Ac	-	(-)	-	+	A76H Y92F R95P I131V V187S
F08	Crot	Ac	-	-	+	+	A76H Y92F R95P I131V V187S
G08	Crot	Ac	-	-	0	-	???????
E03	Crot_6.1	no	+	-	-	-	F60W A76*
F03	Crot_6.1	no	+	-	-	-	F60W A76*
G03	Crot_6.1	no	+	-	-	0	F60W A76*
H03	Crot_6.1	no	+	+	-	+	V187L
B10	WT	Ac	-	(-)	-	+	?????

S. Table 3: Summary of the sequencing results for CobB after three rounds of selection, alternating positive selection for deacetylation and negative selection against decrotonylation.

Mutant	A76	Y92	R95	I131	V187	Other	n
$CobB_{ac1}$	C	S	G	V	C		8
$CobB_{ac2}$	G			C		V161A	7
$CobB_{ac3}$	G	A		L	Y		4
$CobB_{ac4}$	L	A	E	L	A	P36S, V45A, A203T	4
$CobB_{ac5}$	L	K	W	L	I		5
$CobB_{ac6}$	L	S	S	L	W		4
$CobB_{ac7}$	S	G	K		L	S206P	18
$CobB_{ac8}$	S	I	A		V		3
$CobB_{ac9}$	L	G	M	M	P		2
$CobB_{ac10}$	L	A		L	P		1
$CobB_{ac11}$	L		V	M			1
$CobB_{ac12}$	L	M	T	V	Y	E103G, V161A	1
$CobB_{ac13}$	L	W	N	W	Q	E79G, K192R, M202I	1
$CobB_{ac14}$	V	V	N	W	Q	Q105R, D172G	1
SUM							60

S. Table 4: Detailed Sirt1 sequencing results after the third selection round separated by the acylation (BuK: Butyrylation CrK: Crotonylation, PrK: Propylation) encoded during the counter selection.

Name	Mutation	BuK	CrK	PrK	total
S1Ac1	A313V I316A I347F F366L I411M	13	17	15	45
S1Ac2	A313V I316C F366T I411V	9	7	6	22
S1Ac8	A313V I316H I347V F366L I411V	2	1	2	5
S1Ac3	I316M I347L F366L	1	1	1	3
S1Ac4	A313V I347F F366L I411L	1			1
S1Ac5	A313L I347V F366M		1		1
S1Ac6	F366P			2	2
S1Ac7	I347M F366M			3	3
	Sum	26	27	29	82

S. Table 5:IC50 (μM) and deivation of the mean (Dev.) of the 124 compounds identified in the initial screening for Sirt1, Sirt2 and Sirt3. Compounds chosen for further analysis are highlighted in green.

#	Cpd Id	Sirt1	Dev.	Sirt2	Dev.	Sirt3	Dev.	Luc	dev
1	169631	1.193	0.152	0.857	0.159	0.758	0.170	inactive	-
2	173318	1.901	0.267	2.281	0.663	2.138	1.101	inactive	-
3	174405	2.608	0.435	2.611	0.898	1.666	0.778	inactive	-
4	174597	0.631	0.118	0.509	0.170	0.306	0.129	inactive	-
5	176066	0.909	0.168	0.567	0.099	0.411	0.164	inactive	-
6	177388	0.569	0.163	0.587	0.131	0.431	0.213	inactive	-
7	177409	4.638	0.922	3.624	1.063	1.865	0.724	inactive	-
8	179659	1.000	0.194	0.798	0.210	0.526	0.256	inactive	-
9	183236	0.502	0.158	0.324	0.061	0.197	0.078	inactive	-
10	186636	1.249	0.319	0.847	0.209	0.630	0.155	inactive	-
11	186878	0.590	0.078	0.565	0.060	0.278	0.078	9.934	-
12	191061	0.362	0.060	0.241	0.017	0.147	0.065	9.204	-
13	191192	0.047	0.012	0.059	0.019	0.048	0.020	inactive	-
14	201971	0.731	0.152	0.729	0.115	0.485	0.147	inactive	-
15	202640	2.493	0.180	3.714	0.824	0.885	0.334	inactive	-
16	208923	3.365	0.127	2.869	0.271	1.214	0.278	inactive	-
17	209000	2.669	0.225	2.555	0.534	0.661	0.151	inactive	-
18	217191	1.410	0.083	1.208	0.249	0.417	0.098	inactive	-
19	217473	0.108	0.024	0.174	0.038	0.084	0.007	inactive	-
20	217652	0.443	0.045	0.528	0.049	0.191	0.068	8.653	0.667
21	218728	1.926	0.151	2.529	0.451	1.416	0.497	inactive	-
22	223290	0.088	0.004	0.490	0.091	0.472	0.248	2.718	0.362
23	224014	2.177	0.048	2.497	0.612	2.735	0.255	inactive	-
24	224024	2.697	0.157	1.812	0.344	1.804	0.378	inactive	-
25	224577	0.704	0.148	0.653	0.180	0.604	0.202	inactive	-
26	224691	4.047	0.166	1.888	0.388	1.447	0.305	inactive	-
27	224951	0.710	0.166	0.666	0.141	0.636	0.195	inactive	-
28	229790	1.345	0.055	0.747	0.169	0.656	0.173	inactive	-
29	238456	4.214	0.466	2.684	0.854	2.392	0.543	inactive	-
30	247163	0.215	0.029	0.555	0.151	0.506	0.181	inactive	-
31	247163	0.125	0.013	0.335	0.075	0.306	0.113	inactive	-
32	280728	2.767	0.282	4.888	0.866	4.080	0.448	inactive	-
33	280784	0.066	0.004	inactive	-	inactive	-	inactive	-
34	280813	1.613	0.242	1.703	0.198	1.093	0.186	inactive	-
35	280813	1.273	0.075	1.168	0.242	0.704	0.120	inactive	-
36	280927	inactive	-	inactive	-	inactive	-	inactive	-
37	337148	3.927	0.172	inactive	-	inactive	-	inactive	-
38	351058	3.187	0.248	5.207	0.391	2.379	0.651	inactive	-
39	392472	0.191	0.012	0.144	0.005	0.086	0.020	3.498	0.328
40	407082	2.612	0.348	2.120	0.324	1.078	0.171	inactive	-
41	407082	2.572	0.234	2.418	0.232	1.126	0.222	inactive	-
42	407091	0.654	0.263	0.898	0.424	0.919	0.095	0.155	0.015
43	280964	0.854	0.054	1.229	0.105	0.739	0.222	6.848	0.216
44	409511	0.031	0.001	1.295	0.053	6.967	-	inactive	-
45	149684	5.730	0.697	5.578	0.868	4.881	0.537	inactive	-
46	163077	7.168	0.431	4.524	0.755	6.487	1.778	inactive	-
47	141147	6.692	0.358	4.012	0.652	6.354	0.926	inactive	-
48	166054	5.149	0.066	3.798	0.473	4.060	0.613	inactive	-
49	161752	9.368	-	6.816	1.594	4.574	0.933	inactive	-
50	168005	5.609	0.433	6.914	-	6.186	3.311	inactive	-
51	134463	inactive	-	inactive	-	inactive	-	inactive	-
52	140045	3.794	0.080	3.622	0.577	2.532	0.415	inactive	-
53	114696	0.356	0.052	0.799	0.166	0.570	0.073	inactive	-
54	124840	2.584	0.080	2.782	0.393	1.753	0.091	inactive	-
55	115502	1.232	0.071	3.758	1.822	2.282	0.476	inactive	-
56	139884	2.109	0.161	3.177	0.676	1.536	0.227	inactive	-
57	157183	0.037	0.005	0.061	0.012	0.042	0.005	9.851	-
58	121082	2.354	0.193	3.389	0.259	1.341	0.173	inactive	-
59	161998	1.564	0.093	1.288	0.051	0.458	0.090	inactive	-
60	149769	0.140	0.012	0.325	0.016	0.123	0.028	4.789	0.158
61	112967	2.946	0.155	2.376	0.324	0.732	0.300	inactive	-
62	138866	1.235	0.085	0.711	0.026	0.239	0.060	9.633	-
63	162027	2.256	0.043	2.347	0.185	0.695	0.170	inactive	-

#	Cpd Id	Sirt1	Dev.	Sirt2	Dev.	Sirt3	Dev.	Luc	dev
64	158345	2.477	0.200	2.101	0.041	0.878	0.219	inactive	-
65	141175	6.474	0.285	9.958	-	8.860	0.062	inactive	-
66	123399	1.011	0.089	2.341	0.813	0.934	0.256	inactive	-
67	134845	5.269	0.321	2.851	0.255	4.175	0.936	inactive	-
68	139281	2.768	0.153	inactive	-	inactive	-	inactive	-
69	127147	1.591	0.057	1.860	0.148	1.609	0.073	inactive	-
70	106904	1.621	0.056	1.587	0.142	1.162	0.193	inactive	-
71	153268	0.107	0.005	0.091	0.013	0.060	0.003	1.500	0.139
72	166436	2.767	0.110	2.534	0.249	2.080	0.448	9.182	-
73	107136	0.880	0.019	1.049	0.203	0.858	0.046	inactive	-
74	153532	2.152	0.060	2.954	0.260	2.465	0.187	inactive	-
75	142678	6.871	0.143	4.719	0.350	4.175	0.117	inactive	-
76	160871	3.048	0.171	2.459	0.309	1.988	0.175	inactive	-
77	140037	0.911	0.055	0.966	0.153	0.623	0.033	inactive	-
78	144303	4.906	0.543	4.763	1.025	3.139	0.193	inactive	-
79	154002	0.017	0.001	0.051	0.008	0.036	0.007	0.116	0.030
80	118618	0.252	0.018	0.380	0.096	0.182	0.032	6.009	0.138
81	109090	3.603	0.285	2.656	0.387	1.680	0.095	inactive	-
82	155594	0.278	0.029	0.780	0.276	0.475	0.111	inactive	-
83	133874	1.049	0.224	2.068	0.580	1.607	0.176	inactive	-
84	133004	1.588	0.205	1.270	0.202	0.603	0.083	inactive	-
85	144638	2.259	0.353	2.826	0.544	1.260	0.241	inactive	-
86	126631	1.928	0.194	1.960	0.448	1.029	0.109	inactive	-
87	280964	0.979	0.122	1.483	0.257	0.756	0.123	7.147	0.384
88	409511	0.028	0.002	1.304	0.197	8.726	1.026	inactive	-
89	101084	2.093	0.214	4.754	0.915	7.400	2.135	inactive	-
90	106872	1.608	0.187	8.117	1.932	inactive	-	inactive	-
91	106879	1.959	0.138	7.132	1.773	4.880	-	inactive	-
92	106885	1.258	0.121	6.824	2.497	7.333	2.450	inactive	-
93	106893	2.000	0.088	7.888	1.838	7.023	3.098	inactive	-
94	106869	2.141	0.016	7.264	2.145	4.539	1.850	inactive	-
95	109376	0.487	0.046	1.505	0.655	1.427	0.539	inactive	-
96	110991	0.943	0.054	0.828	0.245	0.508	0.143	6.834	0.007
97	128841	1.924	0.085	2.654	1.322	2.034	1.212	inactive	-
98	129211	3.036	0.164	inactive	-	inactive	-	inactive	-
99	129723	1.344	0.075	inactive	-	inactive	-	inactive	-
100	130355	1.114	0.151	0.685	0.086	9.402	-	6.483	0.122
101	132497	1.486	0.115	5.452	1.118	3.127	1.632	inactive	-
102	138139	2.107	0.115	2.570	0.374	1.775	0.503	inactive	-
103	142138	0.395	0.026	0.666	0.327	0.574	0.379	inactive	-
104	149107	0.271	0.014	inactive	-	inactive	-	inactive	-
105	151088	1.489	0.083	8.844	0.694	inactive	-	inactive	-
106	154428	1.252	0.034	0.876	0.142	0.981	0.405	inactive	-
107	168625	2.232	0.035	inactive	-	inactive	-	inactive	-
108	198249	1.973	0.278	3.809	0.686	1.880	0.825	inactive	-
109	206490	0.088	0.025	inactive	-	0.502	0.162	inactive	-
110	211041	1.115	0.145	inactive	-	inactive	-	inactive	-
111	216090	1.410	0.212	2.827	0.603	4.936	1.352	inactive	-
112	216101	0.519	0.131	1.257	0.314	1.050	0.200	inactive	-
113	216107	1.532	0.309	1.451	0.335	1.498	0.179	inactive	-
114	224468	0.668	0.166	1.182	0.397	0.837	0.254	inactive	-
115	225079	5.684	0.589	6.387	1.727	5.322	1.048	inactive	-
116	226187	3.549	0.458	5.845	2.093	6.135	1.549	inactive	-
117	226427	1.674	0.205	0.974	0.022	1.140	0.051	inactive	-
118	247163	0.351	0.098	0.997	0.240	0.899	0.234	inactive	-
119	247163	0.228	0.053	0.750	0.172	0.608	0.163	inactive	-
120	247163	0.113	0.031	0.392	0.096	0.307	0.058	6.659	0.679
121	280728	4.109	0.274	9.101	0.744	7.795	-	inactive	-
122	382437	1.357	0.079	1.842	0.105	2.304	0.440	inactive	-
123	280964	0.990	0.150	2.166	0.705	1.509	0.309	8.190	0.448
124	Ex527	0.027	0.002	1.367	0.065	8.819	1.147	inactive	-

S. Table 6: Km and v_{max} calculated from linear fit of the Lineweaver-Burk plot of the date shown in **Figure 17**.

Ex527 [nM]	Km [nM]	v_{max} [Luc/min]	149107 [nM]	Km [nM]	v_{max} [Luc/min]
0	53	434.8	0	53.4	333
100	21.2	188.7	100	43.8	263
200	10.8	96.2	200	36.7	208
400	7.5	66.6	400	18.7	120

S. Table 7: Data collection and refinement statistics

	$CobB_{ac3}$-H4K16Ac	**CobB-H4K16Ac**	**CobB-H4K16Bu**	**CobB-H4K16Cr**	**$CobB_{ac2}$-H4K16Bu**
Space group	C121 (5)	C2221(20)	P41212 (92)	P41212 (92)	P212121 (19)
Cell parameters (Å)	90.25, 79.10, 39.90	131.10, 131.26, 58.54	92.73 92.73 58.62	93.96, 93.96, 58.54	60.49, 92.44, 94.45
(°)	90, 110.77, 90	90, 90, 90	90, 90, 90	90, 90, 90	90, 90, 90
Wavelength (Å)	0.978	1	1	1	1
Resolution (Å)	50-1.6 (1.66-1.60)	50-1.6 (1.66-1.60)	50-1.35 (1.38-1.35)	50-2.3 (2.38-2.3)	50-1.95 (2.02-1.95)
Unique reflections	34254 (2536)	66812 (4841)	57070 (4152)	12129 (881)	39338 (2868)
Multiplicity	6.5 (6.9)	13.0 (13.2)	25.2 (25.6)	25.6 (25.7)	13.1 (13.2)
CC 1/2	99.8 (86.3)	99.9 (64.4)	97.8 (77.5)	99.9 (81.6)	99.9 (75.3)
Completeness (%)	98.9 (99)	100 (99.5)	100 (99.9)	100 (100)	100 (100)
I/σ_I	17.6 (3.1)	18.8 (1.6)	19.0 (1.6)	23.9 (2.5)	18.0 (1.7)
R_{merge} (%)	10.1 (70.4)	6.7 (158.1)	9.0 (261)	9.8 (164.1)	7.9 (163.7)
R_{work}/R_{free} (%)	17.9 / 20.5	17.2/18.7	16.9/18.8	21.1/25.0	19.7/21.5
Wilson B ($Å^2$)	14.7	27.8	18.4	53	39.3
Mean isotropic B factor ($Å^2$)	24.4	36.27	25.5	59.1	47.9
Bond length r.m.s.d. (Å)	0.010	0.008	0.012	0.003	0.004
Bond angle r.m.s.d. (°)	1.290	1.16	1.42	0.76	0.861
Ramachandran favoured (outliers)	100 (0)	100 (0)	98.0 (0)	99 (0)	98.6 (0)
Number of atoms	3773	7800	4129	1931	4020
No H	1771	3707	2224	0	0
Water	220	294	287	27	187
Ligand (CIF)	Acetyl-Lysine (aly)	Acetyl-Lysine (aly)	Butyryl-Lysine (btk)	Crotonyl-Lysine (kcr)	Butyryl-Lysine (btk)
Pdb accession code	6RXS	6RXJ	6RXK	6RXL	6RXO

	CobBac2-H4K16Ac	CobBac2-H4K16Cr	CobBac2-H4K16Cr-Int3-36h	CobBac2-H4K16Cr-Int3-16h	CobB F7
Space group	P212121 (19)	P212121 (19)	P1211 (4)	C121 (5)	P41212 (92)
Cell parameters (Å)	92.30, 95.38, 168.83	57.56, 91.89, 95.90	61.38, 94.07, 94.06	132.9, 132.95, 57.99	92.73, 92.73, 58.62
(°)	90, 90, 90	90, 90, 90	90, 90.03, 90	90, 90.04, 90	90, 90, 90
Wavelength (Å)	1	1	1	1	0.978
Resolution (Å)	50-1.92 (1.99-1.92)	50-1.8 (1.86-1.80)	50-1.7 (1.76-1.70)	50-2.0 (2.07-2.00)	50-1.4 (1.44-1.40)
Unique reflections	114176 (8343)	47854 (3481)	117292 (8604)	62989 (5013)	50773 (3704)
Multiplicity	12.9 (12.4)	12.6 (12.4)	6.7 (6.9)	6.9 (7.0)	25.7 (25.3)
CC 1/2	99.8 (67.9)	99.9 (83.5)	100 (63.9)	100 (68.5)	100 (45.5)
Completeness (%)	100 (100)	100 (99.9)	100 (99.9)	99.9(100)	100 (100)
I/σI	13.9 (2.1)	15.3 (2.1)	20.1 (1.3)	19.6 (1.8)	23.0 (0.92)
Rmerge (%)	12.0 (133.0)	8.5 (134.4)	4.7 (142.5)	4.3 (109.0)	8.5 (346.6)
Rwork/Rfree (%)	20.4/24.3	19.2/23.4	19.9/22.8	22.3 /25.9	16.07 / 19.02
Wilson B (Å2)	32.3	30.7	32.9	48	20.56
Mean isotropic B factor (Å2)	41.6	38.9	44.1	59.6	30.1
Bond length r.m.s.d. (Å)	0.010	0.007	0.007	0.004	0.014
Bond angle r.m.s.d. (°)	1.300	1.120	1.380	1.04	1.509
Ramachandran favoured (outliers)	99 (0.2)	99.0 (0.2)	97.0 (0.1)	97.0 (0)	99.59 (0)
Number of atoms	12180	4166	8316	8133	3944
No H	0	0	0	0	2070
Water	879	335	582	235	144
Ligand (CIF)	Acetyl-Lysine (aly)	Crotonyl-Lysine (kcr)	Cr-Int.3 (2I3)	Cr-Int.3 (2I3)	Alloc-Lysine (LN2)
Pdb accession code	6RXM	6RXP	6RXQ	6RXR	Xxx

REFERENCES

1. Spinck M, Neumann-Staubitz P, Ecke M, Gasper R, & Neumann H (2020) Evolved, Selective Erasers of Distinct Lysine Acylations. *Angewandte Chemie International Edition* n/a(n/a).
2. Spinck M, Ecke M, Sievers S, & Neumann H (2018) Highly Sensitive Lysine Deacetylase Assay Based on Acetylated Firefly Luciferase. *Biochemistry* 57(26):3552-3555.
3. Albrecht A & Willand M (2018) Homunculus. *Faust-Handbuch: Konstellationen – Diskurse – Medien*, eds Rohde C, Valk T, & Mayer M (J.B. Metzler, Stuttgart), pp 535-543.
4. Leeuwenhoek AV (1677) Observationes D. Anthonii Lewenhoeck, de natis'e semine genitali animalculis. *Philosophical Transactions of the Royal Society of London* 12(142):1040-1046.
5. Bowler PJ (1971) Preformation and Pre-Existence in the Seventeenth Century: A Brief Analysis. *Journal of the History of Biology* 4(2):221-244.
6. Cobb M (2017) 60 years ago, Francis Crick changed the logic of biology. *PLOS Biology* 15(9):e2003243.
7. International Human Genome Sequencing C (2004) Finishing the euchromatic sequence of the human genome. *Nature* 431(7011):931-945.
8. Mandal S & Badhe BA (2012) Malignant transformation in a mature teratoma with metastatic deposits in the omentum: a case report. *Case reports in pathology* 2012:568062-568062.
9. Greenberg JA & Clancy TE (2008) Fetiform teratoma (homunculus). *Reviews in obstetrics & gynecology* 1(3):95-96.
10. Berdasco M & Esteller M (2010) Aberrant Epigenetic Landscape in Cancer: How Cellular Identity Goes Awry. *Developmental Cell* 19(5):698-711.
11. Van Speybroeck L (2002) From Epigenesis to Epigenetics. *Annals of the New York Academy of Sciences* 981(1):61-81.
12. Gerstein MB*, et al.* (2007) What is a gene, post-ENCODE? History and updated definition. *Genome Research* 17(6):669-681.
13. Van Speybroeck L, de Waele D, & Van de Vijver G (2002) Theories in Early Embryology. *Annals of the New York Academy of Sciences* 981(1):7-49.
14. Kornberg RD (1977) Structure of Chromatin. *Annual Review of Biochemistry* 46(1):931-954.
15. Luger K, Mäder AW, Richmond RK, Sargent DF, & Richmond TJ (1997) Crystal structure of the nucleosome core particle at 2.8 Å resolution. *Nature* 389(6648):251-260.
16. Campos EI & Reinberg D (2009) Histones: Annotating Chromatin. *Annual Review of Genetics* 43(1):559-599.
17. Bird AP (1986) CpG-rich islands and the function of DNA methylation. *Nature* 321(6067):209-213.
18. Allfrey VG, Faulkner R, & Mirsky AE (1964) ACETYLATION AND METHYLATION OF HISTONES AND THEIR POSSIBLE ROLE IN THE REGULATION OF RNA SYNTHESIS. *Proceedings of the National Academy of Sciences of the United States of America* 51(5):786-794.
19. Strahl BD & Allis CD (2000) The language of covalent histone modifications. *Nature* 403(6765):41-45.

20. Rothbart SB & Strahl BD (2014) Interpreting the language of histone and DNA modifications. *Biochimica et biophysica acta* 1839(8):627-643.
21. Andrey G & Mundlos S (2017) The three-dimensional genome: regulating gene expression during pluripotency and development. *Development* 144(20):3646.
22. Wang Z*, et al.* (2008) Combinatorial patterns of histone acetylations and methylations in the human genome. *Nature Genetics* 40(7):897-903.
23. Wang M*, et al.* (2010) Structural genomics of histone tail recognition. *Bioinformatics (Oxford, England)* 26(20):2629-2630.
24. Day JJ (2014) New approaches to manipulating the epigenome. *Dialogues in clinical neuroscience* 16(3):345-357.
25. Szyf M (2009) Epigenetics, DNA Methylation, and Chromatin Modifying Drugs. *Annual Review of Pharmacology and Toxicology* 49(1):243-263.
26. Shah K, Liu Y, Deirmengian C, & Shokat KM (1997) Engineering unnatural nucleotide specificity for Rous sarcoma virus tyrosine kinase to uniquely label its direct substrates. *Proceedings of the National Academy of Sciences* 94(8):3565.
27. Baud MGJ*, et al.* (2014) A bump-and-hole approach to engineer controlled selectivity of BET bromodomain chemical probes. *Science* 346(6209):638.
28. Han Z, Chou C-w, Yang X, Bartlett MG, & Zheng YG (2017) Profiling Cellular Substrates of Lysine Acetyltransferases GCN5 and p300 with Orthogonal Labeling and Click Chemistry. *ACS Chemical Biology* 12(6):1547-1555.
29. Zengerle M, Chan K-H, & Ciulli A (2015) Selective Small Molecule Induced Degradation of the BET Bromodomain Protein BRD4. *ACS Chemical Biology* 10(8):1770-1777.
30. Rousseaux S & Khochbin S (2015) Histone Acylation beyond Acetylation: Terra Incognita in Chromatin Biology. *Cell journal* 17(1):1-6.
31. Inoue A & Fujimoto D (1969) Enzymatic deacetylation of histone. *Biochemical and Biophysical Research Communications* 36(1):146-150.
32. Seto E & Yoshida M (2014) Erasers of histone acetylation: the histone deacetylase enzymes. *Cold Spring Harbor perspectives in biology* 6(4):a018713-a018713.
33. Gregoretti I, Lee Y-M, & Goodson HV (2004) Molecular Evolution of the Histone Deacetylase Family: Functional Implications of Phylogenetic Analysis. *Journal of Molecular Biology* 338(1):17-31.
34. Lombardi PM, Cole KE, Dowling DP, & Christianson DW (2011) Structure, mechanism, and inhibition of histone deacetylases and related metalloenzymes. *Current opinion in structural biology* 21(6):735-743.
35. Frye RA (1999) Characterization of Five Human cDNAs with Homology to the Yeast SIR2 Gene: Sir2-like Proteins (Sirtuins) Metabolize NAD and May Have Protein ADP-Ribosyltransferase Activity. *Biochemical and Biophysical Research Communications* 260(1):273-279.
36. Sauve AA (2010) Sirtuin chemical mechanisms. *Biochimica et biophysica acta* 1804(8):1591-1603.
37. Shi Y, Zhou Y, Wang S, & Zhang Y (2013) Sirtuin Deacetylation Mechanism and Catalytic Role of the Dynamic Cofactor Binding Loop. *The journal of physical chemistry letters* 4(3):491-495.
38. Wang Y*, et al.* (2017) Deacylation Mechanism by SIRT2 Revealed in the 1'-SH-2'-O-Myristoyl Intermediate Structure. *Cell chemical biology* 24(3):339-345.
39. Hawse WF & Wolberger C (2009) Structure-based Mechanism of ADP-ribosylation by Sirtuins. *Journal of Biological Chemistry* 284(48):33654-33661.

40. Ahuja N*, et al.* (2007) Regulation of Insulin Secretion by SIRT4, a Mitochondrial ADP-ribosyltransferase. *Journal of Biological Chemistry* 282(46):33583-33592.
41. Bao J & Sack MN (2010) Protein deacetylation by sirtuins: delineating a post-translational regulatory program responsive to nutrient and redox stressors. *Cellular and molecular life sciences : CMLS* 67(18):3073-3087.
42. Dang W (2014) The controversial world of sirtuins. *Drug discovery today. Technologies* 12:e9-e17.
43. Chen Y*, et al.* (2007) Lysine propionylation and butyrylation are novel post-translational modifications in histones. *Molecular & cellular proteomics : MCP* 6(5):812-819.
44. Tan M*, et al.* (2011) Identification of 67 histone marks and histone lysine crotonylation as a new type of histone modification. *Cell* 146(6):1016-1028.
45. Xie Z*, et al.* (2012) Lysine succinylation and lysine malonylation in histones. *Molecular & cellular proteomics : MCP* 11(5):100-107.
46. Dai L*, et al.* (2014) Lysine 2-hydroxyisobutyrylation is a widely distributed active histone mark. *Nature Chemical Biology* 10(5):365-370.
47. Xie Z*, et al.* (2016) Metabolic Regulation of Gene Expression by Histone Lysine β-Hydroxybutyrylation. *Molecular Cell* 62(2):194-206.
48. Huang H*, et al.* (2018) Lysine benzoylation is a histone mark regulated by SIRT2. *Nature communications* 9(1):3374-3374.
49. Jiang H*, et al.* (2013) SIRT6 regulates TNF-α secretion through hydrolysis of long-chain fatty acyl lysine. *Nature* 496(7443):110-113.
50. Feldman JL, Baeza J, & Denu JM (2013) Activation of the protein deacetylase SIRT6 by long-chain fatty acids and widespread deacylation by mammalian sirtuins. *The Journal of biological chemistry* 288(43):31350-31356.
51. Teng Y-B*, et al.* (2015) Efficient Demyristoylase Activity of SIRT2 Revealed by Kinetic and Structural Studies. *Scientific Reports* 5(1):8529.
52. Kosciuk T*, et al.* (2020) NMT1 and NMT2 are lysine myristoyltransferases regulating the ARF6 GTPase cycle. *Nature Communications* 11(1):1067.
53. Hirschey MD & Zhao Y (2015) Metabolic Regulation by Lysine Malonylation, Succinylation, and Glutarylation. *Molecular & Cellular Proteomics : MCP* 14(9):2308-2315.
54. Tanabe K*, et al.* (2018) LC-MS/MS-based quantitative study of the acyl group- and site-selectivity of human sirtuins to acylated nucleosomes. *Scientific reports* 8(1):2656-2656.
55. Houtkooper RH, Pirinen E, & Auwerx J (2012) Sirtuins as regulators of metabolism and healthspan. *Nature Reviews Molecular Cell Biology* 13(4):225-238.
56. Matsushita N*, et al.* (2011) Distinct regulation of mitochondrial localization and stability of two human Sirt5 isoforms. *Genes to cells : devoted to molecular & cellular mechanisms* 16(2):190-202.
57. Feldman JL, Dittenhafer-Reed KE, & Denu JM (2012) Sirtuin catalysis and regulation. *The Journal of biological chemistry* 287(51):42419-42427.
58. Horio Y, Hayashi T, Kuno A, & Kunimoto R (2011) Cellular and molecular effects of sirtuins in health and disease. *Clinical science (London, England : 1979)* 121(5):191-203.
59. Lin Z & Fang D (2013) The Roles of SIRT1 in Cancer. *Genes Cancer* 4(3-4):97-104.
60. Wan J, Liu H, & Ming L (2019) Lysine crotonylation is involved in hepatocellular carcinoma progression. *Biomedicine & Pharmacotherapy* 111:976-982.

61. Flynn EM*, et al.* (2015) A Subset of Human Bromodomains Recognizes Butyryllysine and Crotonyllysine Histone Peptide Modifications. *Structure* 23(10):1801-1814.
62. Simithy J*, et al.* (2017) Characterization of histone acylations links chromatin modifications with metabolism. *Nature Communications* 8(1):1141.
63. Zhang Q*, et al.* (2016) Structural Insights into Histone Crotonyl-Lysine Recognition by the AF9 YEATS Domain. *Structure (London, England : 1993)* 24(9):1606-1612.
64. Liu S*, et al.* (2017) Chromodomain Protein CDYL Acts as a Crotonyl-CoA Hydratase to Regulate Histone Crotonylation and Spermatogenesis. *Molecular Cell* 67(5):853-866.e855.
65. Fu H*, et al.* (2018) Dynamics of Telomere Rejuvenation during Chemical Induction to Pluripotent Stem Cells. *Stem cell reports* 11(1):70-87.
66. Lavu S, Boss O, Elliott PJ, & Lambert PD (2008) Sirtuins — novel therapeutic targets to treat age-associated diseases. *Nature Reviews Drug Discovery* 7(10):841-853.
67. Rodriguez RM, Fernandez AF, & Fraga MF (2013) Role of sirtuins in stem cell differentiation. *Genes & cancer* 4(3-4):105-111.
68. Wei W*, et al.* (2017) Class I histone deacetylases are major histone decrotonylases: evidence for critical and broad function of histone crotonylation in transcription. *Cell research* 27(7):898-915.
69. Argiriadi MA*, et al.* (2009) Rational mutagenesis to support structure-based drug design: MAPKAP kinase 2 as a case study. *BMC structural biology* 9:16-16.
70. Smith BC & Denu JM (2006) Sir2 protein deacetylases: evidence for chemical intermediates and functions of a conserved histidine. *Biochemistry* 45(1):272-282.
71. Hawse WF*, et al.* (2008) Structural Insights into Intermediate Steps in the Sir2 Deacetylation Reaction. *Structure* 16(9):1368-1377.
72. Colak G*, et al.* (2013) Identification of Lysine Succinylation Substrates and the Succinylation Regulatory Enzyme CobB in Escherichia coli. *Molecular & Cellular Proteomics : MCP* 12(12):3509-3520.
73. Antikainen NM & Martin SF (2005) Altering protein specificity: techniques and applications. *Bioorganic & Medicinal Chemistry* 13(8):2701-2716.
74. Packer MS & Liu DR (2015) Methods for the directed evolution of proteins. *Nature Reviews Genetics* 16(7):379-394.
75. Wang XX, Cho YK, & Shusta EV (2007) Mining a yeast library for brain endothelial cell-binding antibodies. *Nature methods* 4(2):143-145.
76. Boder ET & Wittrup KD (1997) Yeast surface display for screening combinatorial polypeptide libraries. *Nature Biotechnology* 15(6):553-557.
77. Ghadessy FJ, Ong JL, & Holliger P (2001) Directed evolution of polymerase function by compartmentalized self-replication. *Proceedings of the National Academy of Sciences of the United States of America* 98(8):4552-4557.
78. Chin JW (2017) Expanding and reprogramming the genetic code. *Nature* 550(7674):53-60.
79. Hao B*, et al.* (2002) A New UAG-Encoded Residue in the Structure of a Methanogen Methyltransferase. *Science* 296(5572):1462.
80. Nguyen DP*, et al.* (2009) Genetic Encoding and Labeling of Aliphatic Azides and Alkynes in Recombinant Proteins via a Pyrrolysyl-tRNA Synthetase/tRNACUA Pair and Click Chemistry. *Journal of the American Chemical Society* 131(25):8720-8721.

81. Nguyen DP*, et al.* (2014) Genetic encoding of photocaged cysteine allows photoactivation of TEV protease in live mammalian cells. *Journal of the American Chemical Society* 136(6):2240-2243.
82. Neumann H, Peak-Chew SY, & Chin JW (2008) Genetically encoding Nε-acetyllysine in recombinant proteins. *Nature Chemical Biology* 4(4):232-234.
83. Neumann H, Neumann-Staubitz P, Witte A, & Summerer D (2018) Epigenetic chromatin modification by amber suppression technology. *Current Opinion in Chemical Biology* 45:1-9.
84. Longstaff DG, Blight SK, Zhang L, Green-Church KB, & Krzycki JA (2007) In vivo contextual requirements for UAG translation as pyrrolysine. *Molecular Microbiology* 63(1):229-241.
85. Starai VJ, Celic I, Cole RN, Boeke JD, & Escalante-Semerena JC (2002) Sir2-Dependent Activation of Acetyl-CoA Synthetase by Deacetylation of Active Lysine. *Science* 298(5602):2390.
86. Castaño-Cerezo S*, et al.* (2014) Protein acetylation affects acetate metabolism, motility and acid stress response in Escherichia coli. *Molecular systems biology* 10(11):762-762.
87. Packer MS & Liu DR (2015) Methods for the directed evolution of proteins. *Nature Reviews Genetics* 16:379.
88. Sanders BD, Jackson B, & Marmorstein R (2010) Structural basis for sirtuin function: what we know and what we don't. *Biochimica et biophysica acta* 1804(8):1604-1616.
89. Avrahami EM*, et al.* (2018) Reconstitution of Mammalian Enzymatic Deacylation Reactions in Live Bacteria Using Native Acylated Substrates. *ACS synthetic biology* 7(10):2348-2354.
90. Stefan A*, et al.* (2018) Purification of active recombinant human histone deacetylase 1 (HDAC1) overexpressed in Escherichia coli. *Biotechnology Letters* 40(9):1355-1363.
91. Miller BG, Snider MJ, Wolfenden R, & Short SA (2001) Dissecting a charged network at the active site of orotidine-5'-phosphate decarboxylase. *The Journal of biological chemistry* 276(18):15174-15176.
92. Boeke JD, Trueheart J, Natsoulis G, & Fink GR (1987) 5-Fluoroorotic acid as a selective agent in yeast molecular genetics. *Methods in enzymology* 154:164-175.
93. Pourmir A & Johannes TW (2012) Directed evolution: selection of the host organism. *Comput Struct Biotechnol J* 2:e201209012-e201209012.
94. AbouElfetouh A*, et al.* (2015) The E. coli sirtuin CobB shows no preference for enzymatic and nonenzymatic lysine acetylation substrate sites. *Microbiologyopen* 4(1):66-83.
95. Wang K, Neumann H, Peak-Chew SY, & Chin JW (2007) Evolved orthogonal ribosomes enhance the efficiency of synthetic genetic code expansion. *Nature Biotechnology* 25(7):770-777.
96. Xuan W, Yao A, & Schultz PG (2017) Genetically Encoded Fluorescent Probe for Detecting Sirtuins in Living Cells. *Journal of the American Chemical Society* 139(36):12350-12353.
97. Yang Y & Sauve AA (2016) Biochemistry and Enzymology of Sirtuins. *Sirtuins*, ed Houtkooper RH (Springer Netherlands, Dordrecht), pp 1-27.
98. Deardorff MA, Porter NJ, & Christianson DW (2016) Structural aspects of HDAC8 mechanism and dysfunction in Cornelia de Lange syndrome spectrum disorders. *Protein science : a publication of the Protein Society* 25(11):1965-1976.

99. Porter NJ, Christianson NH, Decroos C, & Christianson DW (2016) Structural and Functional Influence of the Glycine-Rich Loop G(302)GGGY on the Catalytic Tyrosine of Histone Deacetylase 8. *Biochemistry* 55(48):6718-6729.
100. Klein MA*, et al.* (2020) Mechanism of activation for the sirtuin 6 protein deacylase. *The Journal of biological chemistry* 295(5):1385-1399.
101. Liu T, Liu PY, & Marshall GM (2009) The Critical Role of the Class III Histone Deacetylase SIRT1 in Cancer. *Cancer Research* 69(5):1702.
102. Liu B*, et al.* (2012) Resveratrol Rescues SIRT1-Dependent Adult Stem Cell Decline and Alleviates Progeroid Features in Laminopathy-Based Progeria. *Cell metabolism* 16(6):738-750.
103. Livernois AM, Hnatchuk DJ, Findlater EE, & Graether SP (2009) Obtaining highly purified intrinsically disordered protein by boiling lysis and single step ion exchange. *Analytical Biochemistry* 392(1):70-76.
104. Gertz M*, et al.* (2013) Ex-527 inhibits Sirtuins by exploiting their unique NAD+-dependent deacetylation mechanism. *Proceedings of the National Academy of Sciences of the United States of America* 110(30):E2772-E2781.
105. Hemphill J, Borchardt EK, Brown K, Asokan A, & Deiters A (2015) Optical Control of CRISPR/Cas9 Gene Editing. *Journal of the American Chemical Society* 137(17):5642-5645.
106. Luo J, Samanta S, Convertino M, Dokholyan NV, & Deiters A (2018) Reversible and Tunable Photoswitching of Protein Function through Genetic Encoding of Azobenzene Amino Acids in Mammalian Cells. *ChemBioChem* 19(20):2178-2185.
107. Reille-Seroussi M, Mayer SV, Dörner W, Lang K, & Mootz HD (2019) Expanding the genetic code with a lysine derivative bearing an enzymatically removable phenylacetyl group. *Chemical Communications* 55(33):4793-4796.
108. Luo J, Liu Q, Morihiro K, & Deiters A (2016) Small-molecule control of protein function through Staudinger reduction. *Nature Chemistry* 8(11):1027-1034.
109. Li J*, et al.* (2014) Palladium-triggered deprotection chemistry for protein activation in living cells. *Nature Chemistry* 6(4):352-361.
110. Gattner MJ, Vrabel M, & Carell T (2013) Synthesis of ε-N-propionyl-, ε-N-butyryl-, and ε-N-crotonyl-lysine containing histone H3 using the pyrrolysine system. *Chemical Communications* 49(4):379-381.
111. Kim CH, Kang M, Kim HJ, Chatterjee A, & Schultz PG (2012) Site-specific incorporation of ε-N-crotonyllysine into histones. *Angewandte Chemie (International ed. in English)* 51(29):7246-7249.
112. Xiao H, Xuan W, Shao S, Liu T, & Schultz PG (2015) Genetic Incorporation of ε-N-2-Hydroxyisobutyryl-lysine into Recombinant Histones. *ACS Chemical Biology* 10(7):1599-1603.
113. Choudhary C, Weinert BT, Nishida Y, Verdin E, & Mann M (2014) The growing landscape of lysine acetylation links metabolism and cell signalling. *Nature Reviews Molecular Cell Biology* 15(8):536-550.
114. Rardin MJ*, et al.* (2013) SIRT5 regulates the mitochondrial lysine succinylome and metabolic networks. *Cell metabolism* 18(6):920-933.
115. Jing H*, et al.* (2017) SIRT2 and lysine fatty acylation regulate the transforming activity of K-Ras4a. *eLife* 6:e32436.
116. Sohrabi C, Foster A, & Tavassoli A (2020) Methods for generating and screening libraries of genetically encoded cyclic peptides in drug discovery. *Nature Reviews Chemistry* 4(2):90-101.

117. Heo J*, et al.* (2017) Sirt1 Regulates DNA Methylation and Differentiation Potential of Embryonic Stem Cells by Antagonizing Dnmt3l. *Cell Reports* 18(8):1930-1945.
118. Bell EL*, et al.* (2014) SirT1 is required in the male germ cell for differentiation and fecundity in mice. *Development* 141(18):3495.
119. Wang H*, et al.* (2019) Sirt1 Promotes Osteogenic Differentiation and Increases Alveolar Bone Mass via Bmi1 Activation in Mice. *Journal of Bone and Mineral Research* 34(6):1169-1181.
120. Galburt EA & Tomko EJ (2017) Conformational selection and induced fit as a useful framework for molecular motor mechanisms. *Biophysical chemistry* 223:11-16.
121. Taimen P*, et al.* (2009) A progeria mutation reveals functions for lamin A in nuclear assembly, architecture, and chromosome organization. *Proceedings of the National Academy of Sciences of the United States of America* 106(49):20788-20793.
122. Scaffidi P & Misteli T (2008) Lamin A-dependent misregulation of adult stem cells associated with accelerated ageing. *Nature Cell Biology* 10(4):452-459.
123. Dell'Omo G*, et al.* (2019) Inhibition of SIRT1 deacetylase and p53 activation uncouples the anti-inflammatory and chemopreventive actions of NSAIDs. *British Journal of Cancer* 120(5):537-546.
124. Gu W & Roeder RG (1997) Activation of p53 Sequence-Specific DNA Binding by Acetylation of the p53 C-Terminal Domain. *Cell* 90(4):595-606.
125. Park EY*, et al.* (2016) Anticancer Effects of a New SIRT Inhibitor, MHY2256, against Human Breast Cancer MCF-7 Cells via Regulation of MDM2-p53 Binding. *International Journal of Biological Sciences* 12(12):1555-1567.
126. Kalle AM*, et al.* (2010) Inhibition of SIRT1 by a small molecule induces apoptosis in breast cancer cells. *Biochemical and Biophysical Research Communications* 401(1):13-19.
127. Gertman O*, et al.* (2018) Directed evolution of SIRT6 for improved deacylation and glucose homeostasis maintenance. *Scientific Reports* 8(1):3538.
128. Michishita E*, et al.* (2008) SIRT6 is a histone H3 lysine 9 deacetylase that modulates telomeric chromatin. *Nature* 452(7186):492-496.
129. Michishita E*, et al.* (2009) Cell cycle-dependent deacetylation of telomeric histone H3 lysine K56 by human SIRT6. *Cell cycle (Georgetown, Tex.)* 8(16):2664-2666.
130. Meyer H-P*, et al.* (2013) The use of enzymes in organic synthesis and the life sciences: perspectives from the Swiss Industrial Biocatalysis Consortium (SIBC). *Catalysis Science & Technology* 3(1):29-40.
131. Yao Q*, et al.* (2018) Synergistic enzymatic and bioorthogonal reactions for selective prodrug activation in living systems. *Nature communications* 9(1):5032-5032.
132. Stadtmauer EA*, et al.* (2020) CRISPR-engineered T cells in patients with refractory cancer. *Science* 367(6481):eaba7365.
133. Hanahan D & Weinberg Robert A (2011) Hallmarks of Cancer: The Next Generation. *Cell* 144(5):646-674.
134. Sambrook J, Fritsch EF, & Maniatis T (1989) *Molecular cloning: a laboratory manual* (Cold Spring Harbor Laboratory Press, Cold Spring Harbor, NY) p xxxviii + 1546 pp.
135. Neumann H, Wang K, Davis L, Garcia-Alai M, & Chin JW (2010) Encoding multiple unnatural amino acids via evolution of a quadruplet-decoding ribosome. *Nature* 464(7287):441-444.

136. Neumann H, Peak-Chew SY, & Chin JW (2008) Genetically encoding N(epsilon)-acetyllysine in recombinant proteins. *Nat Chem Biol* 4(4):232-234.
137. Schultz BE*, et al.* (2004) Kinetics and Comparative Reactivity of Human Class I and Class IIb Histone Deacetylases. *Biochemistry* 43(34):11083-11091.
138. Siebring-van Olst E*, et al.* (2013) Affordable luciferase reporter assay for cell-based high-throughput screening. *J Biomol Screen* 18(4):453-461.
139. Lineweaver H & Burk D (1934) The Determination of Enzyme Dissociation Constants. *Journal of the American Chemical Society* 56(3):658-666.
140. Zhao K, Chai X, & Marmorstein R (2004) Structure and substrate binding properties of cobB, a Sir2 homolog protein deacetylase from Escherichia coli. *J Mol Biol* 337(3):731-741.
141. Gantt SML*, et al.* (2016) General Base–General Acid Catalysis in Human Histone Deacetylase 8. *Biochemistry* 55(5):820-832.
142. Davenport AM, Huber FM, & Hoelz A (2014) Structural and functional analysis of human SIRT1. *Journal of molecular biology* 426(3):526-541.
143. Firth AE & Patrick WM (2008) GLUE-IT and PEDEL-AA: new programmes for analyzing protein diversity in randomized libraries. *Nucleic Acids Research* 36(Web Server issue):W281-W285.
144. Jiang W, Bikard D, Cox D, Zhang F, & Marraffini LA (2013) RNA-guided editing of bacterial genomes using CRISPR-Cas systems. *Nature biotechnology* 31(3):233-239.
145. Gabriella S, Annamaria M, Zsuzsanna S, Leonard A, & Derek Sharples and Joseph M (2006) The Mechanism of Plasmid Curing in Bacteria. *Current Drug Targets* 7(7):823-841.
146. Shechter D, Dormann HL, Allis CD, & Hake SB (2007) Extraction, purification and analysis of histones. *Nature Protocols* 2:1445.
147. Zhang Z & Marshall AG (1998) A universal algorithm for fast and automated charge state deconvolution of electrospray mass-to-charge ratio spectra. *Journal of the American Society for Mass Spectrometry* 9(3):225-233.
148. Schindelin J*, et al.* (2012) Fiji: an open-source platform for biological-image analysis. *Nature Methods* 9(7):676-682.
149. Kabsch W (2010) Xds. *Acta Crystallogr D Biol Crystallogr* 66(Pt 2):125-132.
150. McCoy AJ*, et al.* (2007) Phaser crystallographic software. *J Appl Crystallogr* 40(Pt 4):658-674.
151. Murshudov GN, Vagin AA, & Dodson EJ (1997) Refinement of macromolecular structures by the maximum-likelihood method. *Acta Crystallogr D Biol Crystallogr* 53(Pt 3):240-255.
152. Adams PD*, et al.* (2010) PHENIX: a comprehensive Python-based system for macromolecular structure solution. *Acta Crystallogr D Biol Crystallogr* 66(Pt 2):213-221.
153. Lebedev AA*, et al.* (2012) JLigand: a graphical tool for the CCP4 template-restraint library. *Acta Crystallogr D Biol Crystallogr* 68(Pt 4):431-440.
154. van Aalten DM*, et al.* (1996) PRODRG, a program for generating molecular topologies and unique molecular descriptors from coordinates of small molecules. *J Comput Aided Mol Des* 10(3):255-262.
155. Emsley P, Lohkamp B, Scott WG, & Cowtan K (2010) Features and development of Coot. *Acta Crystallogr D Biol Crystallogr* 66(Pt 4):486-501.

ACKNOWLEDGEMENTS

First I would like to thank Prof. Dr. Heinz Neumann for his supervision and support throughout my Ph. D. I greatly appreciated the open research atmosphere and the degree of freedom he fostered in his research group. He also supported my development as scientist beyond my Ph. D work, which I am especially thankful for.

I would also like to thank Prof. Dr. Daniel Summerer and Prof Dr. Andrea Musacchio for kindly accepting to be my first and second referee, respectively. Furthermore, I am grateful for their engagement in my work as part of my thesis advisory committee, their comments were always greatly appreciated and facilitated my progress throughout my thesis.

I would like to thank the members of the Neumann lab for creating a vibrant and fun working atmosphere, which made all the time spent in the lab so much more enjoyable. In particular, I would like to thank Petra Neumann for her involvement in my work and proof reading of my thesis. Her enthusiasms and expertise was an invaluable and always encouraged me to take my work a step further. I would also like to thank Davide Tamburini and Neha Jain for the time spent working together. Finally, I would like to thank our lab technician Petra Geue for here assistance during my thesis.

I would like to thank my master students Maria Ecke, Damian Schiller and Anto Filipovic. Maria contributed greatly to the work done on human Sirtuin 1, while Damian and Anto extended the use of the KDAC selection for development of bump-and-hole inhibitors and biorthogonal activity in human Sirtuins, respectively. I had a great time working with all of you and loved your enthusiasms and creativity.

I also want to thank all members of my department for the help and tips I got in during my time her, I always could find help if I needed some. Thank you for the great time. Further I would like to also thank the members of all other departments, in particular

Dr. Christian Schröter and his group for sharing their resources and their help and advice.

My sincere thanks also go to all members of the facilities and administration at the MPI Dortmund. In particular Dr. Sonja Sievers, Dr. Phillip Lampe and Dr. Mathias Bischoff as well as the other members of COMAS for their work on the Sirtuin 1 inhibitor screening and the help with establishing the Fluc assay. Further I would like to thank Dr. Raphael Gasper for introducing me and my master students to x-ray crystallography and his continued help with data acquisition and analysis. My thank also goes to Sascha Gentz from the DPF for synthesizing the peptides me and my master students used. I also greatly appreciated the work of Christa Hornemann and Lucia Sironi as organizers of the IMPRS Ph. D program.

I would also like to thank my cooperation partner Prof. Dr. Michael Lammers for his help during my thesis, as well as for his current work on the novel Sirt1 inhibitor. Further I would like my cooperation partner Mark Klein in the lab of John Denu for his ongoing work on Sirt6.

Last but not least, I would like to thank my family for always supporting and encouraging me to move forward and find my own way through live. Without support I would be here today, which I am more grateful for than I can express.